Ribosome dynamics during spontaneous frameshifting

Dissertation

for the award of the degree

Doctor rerum naturalium (Dr. rer. nat.)

of the Georg-August University of Göttingen

within the doctoral program International Max Planck Research School for Molecular Biology

of the Georg-August University School of Science (GAUSS)

submitted by

Panagiotis Poulis

from Athens, Greece

Göttingen, 2022

Thesis Committee

Prof. Dr. Marina V. Rodnina

Department of Physical Biochemistry, Max Planck Institute for Multidisciplinary Sciences, Göttingen, Germany

Dr. Sarah Adio

Department for Molecular Structural Biology, Institute for Microbiology and Genetics, Georg-August University of Göttingen, Göttingen, Germany

Prof. Dr. Jörg Enderlein

III. Physical Institute, Georg-August University of Göttingen, Göttingen, Germany

Dr. Alexis Casper Faesen

Research Group Biochemistry of Signal Dynamics, Max Planck Institute for Multidisciplinary Sciences, Göttingen, Germany

Members of the examination board

Reviewer: Prof. Dr. Marina V. Rodnina

Department of Physical Biochemistry, Max Planck Institute for Multidisciplinary Sciences, Göttingen, Germany

Second reviewer: Prof. Dr. Jörg Enderlein

III. Physical Institute, Georg-August University of Göttingen, Göttingen, Germany

Further members of the examination board

Dr. Sonja Lorenz

Research Group Ubiquitin Signaling Specificity, Max Planck Institute for Multidisciplinary Sciences, Göttingen, Germany

Prof. Dr. Kai Tittmann

Department of Molecular Enzymology, Schwann-Schleiden Research Center, Georg-August University of Göttingen, Göttingen, Germany

Date of oral examination: 4th of October 2022

Related publications

Poulis, P., Patel, A., Rodnina, M. V. & Adio, S. (2022). Altered tRNA dynamics during translocation on slippery mRNA as determinant of spontaneous ribosome frameshifting. *Nature Communications*, **13**, 4231, https://doi.org/10.1038/s41467-022-31852-w

Table of Contents

List of figures

List of tables

List of symbols & abbreviations

°	degrees
°C	degrees Celsius
θ_c	critical angle of incident beam for total internal reflection
Å	Ångström (10^{-10} m)
A (in RNA or DNA sequence)	adenine
A site	ribosomal aminoacyl-tRNA site
aa	amino acid
aa-tRNA	aminoacyl-tRNA
ACN	acetonitrile
acp	3-amino-3-carboxypropyl
ADP	adenosine diphosphate
AIDS	acquired immunodeficiency syndrome
Ala or A (in protein sequence)	alanine
ASL	anticodon stem loop of tRNA
ATXN3	ataxin-3
au	arbitrary units
BHQ2	Black Hole Quencher® 2
C	classic tRNA conformations A/A and P/P
C (in RNA or DNA sequence)	cytosine
^{14}C	radioactive carbon-14
CHI	chimeric tRNA conformations ap/P and pe/E
Covid-19	coronavirus disease 2019
CR	codon recognition
Cryo-EM	cryo-electron microscopy
Cy	cyanide dye
Cys or C (in protein sequence)	cysteine
Asp or D (in protein sequence)	aspartate
DC	decoding center
DETA	N1-[3-(trimethoxysilyl)propyl]diethylenetriamine
DMSO	dimethylsulfoxide
DNA	deoxyribonucleic acid
Dph	diphthamide
E_{FRET}	FRET efficiency
E site	ribosomal exit site
E. coli	*Escherichia coli*
eEF2	eukaryotic elongation factor 2
eIF	eukaryotic initiation factor
FA	fusidic acid
fMet of fM (in protein sequence)	formylmethionine
FI	fluorescence intensity (arbitrary units)
FRET	Förster resonance energy transfer
G (in RNA or DNA sequence)	guanine
GAC	GTPase activation center of the ribosome

GDP	guanosine diphosphate
GDPNP	5’-guanylylimidodiphosphate
Gly or G (in protein sequence)	glycine
Gln or Q (in protein sequence)	glutamine
GMPPCP	guanosine-5'-[(β,γ)-methyleno]triphosphate
GTP	guanosine triphosphate
GTPase	GTP hydrolase
GTPγS	guanosine 5'-O-[γ-thio]triphosphate
H	hybrid tRNA conformations A/P, A/P* and P/E
h	hour
^{3}H	radioactive tritium
HD	Huntington’s disease
His or H (in protein sequence)	histidine
HIV-1	human immunodeficiency virus type 1
HMM	Hidden Markov modeling
HPLC	high-performance liquid chromatography
HTT	huntingtin
IB	initial binding
IC	initiation complex
IF	initiation factor
IPTG	isopropyl β-D-1-thiogalactopyranoside
k	rate, s^{-1}
Leu	leucine
LSU or 50S	large ribosomal subunit
Lys or K (in protein sequence)	lysine
M	molar (mol/L)
μ	mean of Gaussian distribution
MDa	megadalton
min	minute
ml	milliliter (10^{-3} L)
µl	microliter (10^{-6} L)
mM	millimolar (mmol/L)
µM	micromolar (pmol/µl)
mnm^{5}	5-methylaminomethyl
mRNA	messenger RNA
ms	millisecond (10^{-3} s)
MV	methylviologen
mW	milliwatt (10^{-3} W)
N	non-rotated conformation of SSU body and head
N	number of smFRET traces
N (in protein sequence)	asparagine
n	number of transitions
NA	neutravidin
NHS	N-hydroxysuccinimide
nM	nanomolar (pmol/ml)

nm	nanometer (10^{-9} m)
nt	nucleotide
OD	optical density
ORF	open reading frame
Pro	proline
P site	ribosomal peptidyl-tRNA site
PCA	protocatechuic acid
PCD	*Pseudomonas* protocatechuic acid dehydrogenase
PDB	Protein Data Bank
PEG	polyethylene glycol
PEP	phosphoenol pyruvate
pept-tRNA	peptidyl-tRNA
Phe or F (in protein sequence)	phenylalanine
Pi	inorganic phosphate $H_2PO_4^-$
PK	pyruvate kinase
Pmn	puromycin
pmol	picomole (10^{-12} mol)
POST	posttranslocation
PRE	pretranslocation
PRF	programmed ribosome frameshifting
PRFdb	Programmed ribosome frameshifting database
PTC	peptidyl transferase center
R	rotated conformation of SSU body
r	donor-acceptor distance
R_0	Förster radius
RF	release factor
RNA	ribonucleic acid
rRNA	ribosomal RNA
RRF	ribosome recycling factor
S	swiveled conformation of SSU head
S (preceded by number)	Swedberg unit, sedimentation rate (10^{-13} s)
s	second
s^2	2-thio
SARS-CoV-2	severe acute respiratory syndrome coronavirus 2
SCA3	spinocerebellar ataxia type 3
SD	Shine-Dalgarno sequence
s.d.	standard deviation
Ser	serine
smFRET	single molecule Förster resonance energy transfer
Spc	spectinomycin
SRF	spontaneous ribosome frameshifting
SRL	sarcin-ricin loop
SS	slippery sequence
SSU or 30S	small ribosomal subunit
sw	switch 1 and 2 of domain 1 of EF-G

t^6	N6-threonylcarbamoyladenosine
TAKM	Tris-NH_4Cl-KCl-$MgCl_2$ buffer
TC	ternary complex
TFA	trifluoroacetic acid
TIRF microscopy	total internal reflection fluorescence microscopy
tRNA	transfer RNA
Trolox	6-hydroxy-2,5,7,8-tetramethylchroman-2-carboxylic acid
Trp	tryptophan
Ts	thermostable
Tu	thermo-unstable
U (in RNA sequence)	uridine
Val or V (in protein sequence)	valine
W	Watt
wt	wild-type

1. Abstract

During protein synthesis, the ribosome moves along the mRNA in steps of three nucleotides at a time to maintain the translational reading frame. However, on some mRNA sequences that are denoted as slippery, ribosomes may shift by one or several nucleotides to the 5' direction in a process called spontaneous –1 frameshifting. The result is the production of aberrant peptides with a different length and amino acid sequence than the 0-frame peptide. Frameshifting is a major potential source of translation errors, which compromise the fitness of the cell. It is thus important to understand the molecular mechanism that leads to spontaneous frameshifting. In this study, we use single molecule Förster resonance energy transfer (smFRET) to investigate how the tRNAs move through the ribosome during translocation on slippery mRNA. We investigate the internal motions of the ribosome (i.e. ribosome dynamics) and the role of EF-G during translocation on slippery mRNA. Our results show that uncoupling the movements of the two tRNA that are displaced during translocation is a key determinant of spontaneous frameshifting. While the deacylated tRNA moves rapidly from the P to the E site and is released from the ribosome, the translocation of the peptidyl-tRNA from the A to the P site is slow and stalled between intermediate (chimeric, CHI) and posttranslocation states. Delayed translocation in a different stage of translocation, i.e. prior to the formation of chimeric states, does not contribute to frameshifting. During slow translocation of the peptidyl-tRNA, the SSU head domain is in the swiveled conformation, further facilitating the positional uncertainty of the peptidyl-tRNA. This allows sampling of the 0- and –1-frame codons, thus shifting the reading frame. We anticipate our work to be the starting point for further investigation of spontaneous frameshifting, the effect of frameshifted peptides in the cell in physiological and pathological conditions, the respective mechanism of frameshifting in eukaryotes, as well as the emergence of spontaneous frameshifting as a therapeutic target in human disease and infection.

2. Introduction

Proteins are biological macromolecules consisting of amino acid residues that catalyze the majority of biochemical reactions in the cell, shape cellular structures and mediate cell signaling and intracellular communication. The function of a protein is defined by its three-dimensional structure, which is in turn determined by the amino acid sequence of the peptide. The templates for protein biosynthesis are messenger RNAs (mRNAs) that are produced by transcription according to the sequence of the protein-coding genes of every organism. Each mRNA has a defined ribonucleotide sequence, in which three adjacent non-overlapping nucleotides define a codon and encode for a particular amino acid in the peptide chain. The sequence of the codons in the open reading frame (ORF) serves as template for the amino acid sequence, which ensures the synthesis of proteins with defined composition and safeguards the integrity of the cellular proteome. Each codon is recognized by an adaptor transfer RNA (tRNA) molecule, which carries a three-nucleotide complementary anticodon and is charged with a specific amino acid. The sequential non-overlapping recognition of mRNA codons by tRNAs guides the collinearity of the mRNA and peptide sequences. This process is catalyzed and coordinated by the ribosome.

2.1 Structure of the bacterial ribosome

The bacterial 70S ribosome is a 2.5-MDa molecular machine that synthesizes peptides using mRNAs as template. It consists of two ribosomal subunits, the small subunit (30S or SSU, Fig. 1a) and the large subunit (50S or LSU, Fig. 1b), which contain a unique set of ribosomal proteins and ribosomal RNA (rRNA) (Ban et al., 2000; Jenner et al., 2005; Jenner et al., 2010; Wimberly et al., 2000; Yusupov et al., 2001).

The SSU consists of 16S rRNA and 21 ribosomal proteins and is divided into three super-domains, the body, platform and head, that form the mRNA entry and exit channel and the decoding center (DC, Fig. 1a) (Wimberly et al., 2000). In the mRNA entry channel, formed by proteins S3, S4 and S5, the mRNA is threaded to the decoding center, while it leaves the ribosome via the exit channel (Fig. 1a) (Takyar et al., 2005; Wimberly et al., 2000; Yusupova et al., 2006; Yusupova et al., 2001). In the highly conserved decoding center, codon-anticodon recognition takes place between mRNA and tRNAs (Fig. 1a) (Wimberly et al., 2000).

The LSU consists of 23S and 5S rRNA and 31 ribosomal proteins, which form the L7/L12 stalk, the sarcin-ricin loop (SRL) that acts as the GTPase activation center (GAC) of the ribosome, the peptidyl-transferase center (PTC), the peptide exit tunnel, and the L1 stalk (Fig. 1b) (Ban et al., 2000; Jenner et al., 2005). The L7/L12 stalk is a flexible hinge-like structure that recruits the translational factors to the ribosome (Fig. 1b) (Datta et al., 2005; Diaconu et al., 2005; Imai et al., 2020; Stark et al., 1997; Stark et al., 2000). The SRL is a universally conserved 23S rRNA sequence that promotes GTP hydrolysis of translation factors (Fig. 1b) (Clementi et al., 2010; Fischer et al., 2016; Maracci and Rodnina, 2016; Moazed et al., 1988; Mohr et al., 2002; Voorhees et al., 2010). In the PTC, the reactions of peptide bond formation and peptidyl-tRNA hydrolysis take place (Fig. 1b) (Ban et al., 2000). The peptide exit tunnel is a tube-like structure, where the nascent peptide chain is accommodated during elongation (Fig 1b). The L1 stalk is a second flexible structure consisting of 23S rRNA helices H76, H77 and H78 and protein L1 that facilitates the dissociation of tRNAs from the ribosome (Fei et al., 2009; Fei et al., 2008; Fischer et al., 2010; Mohan and Noller, 2017).

The LSU and SSU assemble into the translation-competent 70S ribosome via non-covalent rRNA-rRNA, rRNA-protein and protein-protein interactions (Fig. 1c) (Bock et al., 2015; Dunkle et al., 2011; Frank and Agrawal, 2000; Merryman et al., 1999; Schuwirth et al., 2005; Yusupov et al., 2001). These so-called intersubunit bridges contribute to ribosome complex stability and regulate the conformational rearrangements of the ribosome during translation (Bock et al.,

2015). The 70S ribosome has three tRNA-binding sites which span across the subunits (Rodnina, 2018; Schmeing and Ramakrishnan, 2009), namely the A site, where the incoming aminoacyl-tRNA (aa-tRNA) is accommodated, the P site, where the peptidyl-tRNA (i.e. carrying the nascent peptide) is accommodated, and the E site, which is a platform for tRNA dissociation (Fig. 1c) (Chen et al., 2011b; Petropoulos and Green, 2012; Robertson and Wintermeyer, 1987; Semenkov et al., 1996).

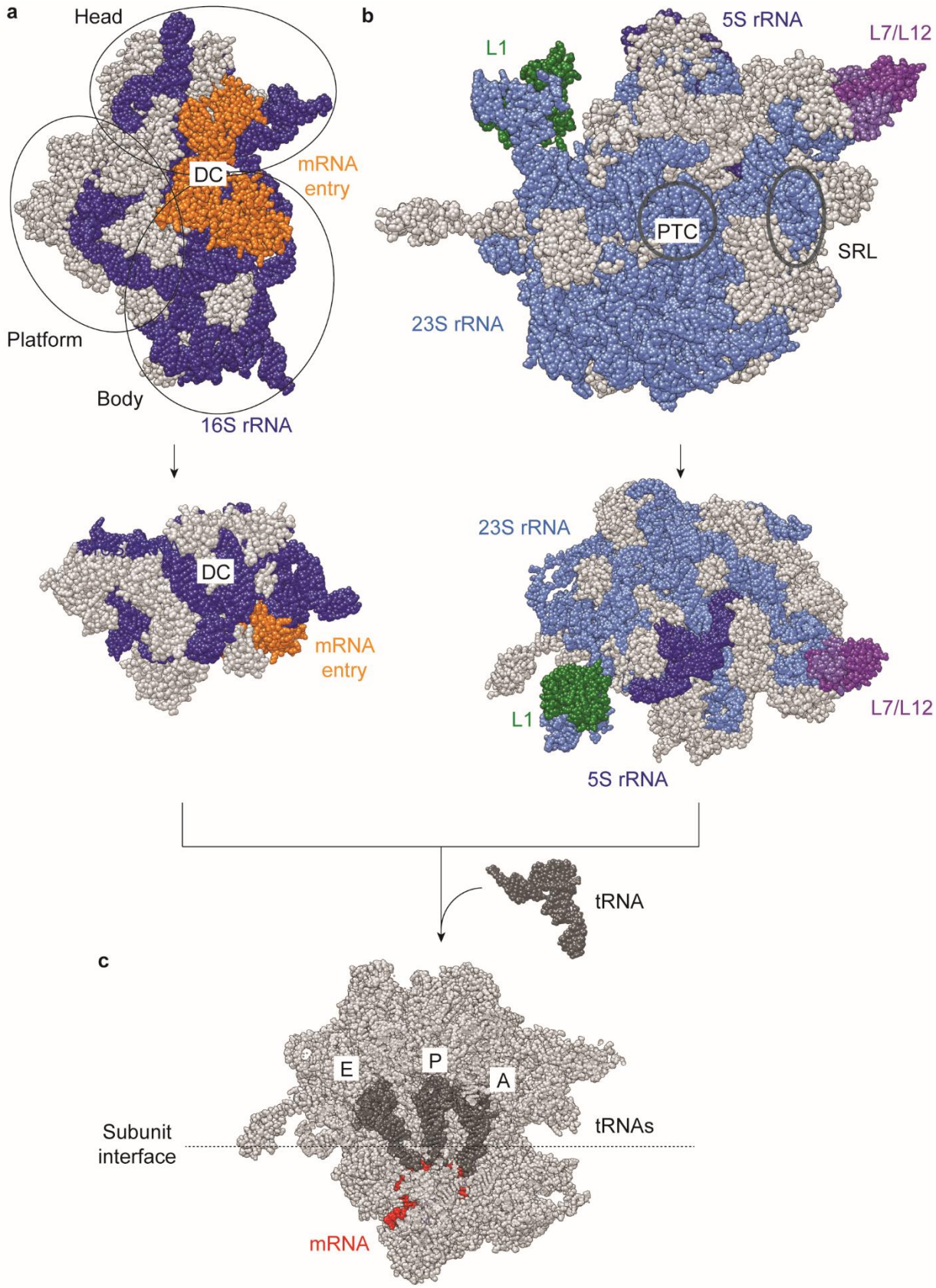
a
Head
DC
mRNA
entry
Platform
Body
16S rRNA
b
5S rRNA
L7/L12
L1
PTC
SRL
23S rRNA
DC
mRNA
entry
23S rRNA
L1
L7/L12
5S rRNA
tRNA
c
E
P
A
Subunit
interface
tRNAs
mRNA

◄**Figure 1. Structure of the bacterial ribosome.** (a) Crystal structure of the SSU from *Thermus thermophilus*. Upper view from the subunit interface. Lower view from the SSU head domain. The ribosomal proteins are depicted in grey, 16S rRNA in blue, proteins S3, S4 and S5 (mRNA entry channel) in orange. The figure is adapted from PDB 1J5E (Wimberly et al., 2000). (b) Crystal structure of the LSU from *Thermus thermophilus*. Upper view from the subunit interface. Lower view from the LSU central protuberance. The ribosomal proteins are depicted in grey, 23S rRNA in light blue and 5S rRNA in dark blue, proteins L7 and L12 in purple, protein L1 in green. The figure is adapted from PDB 4V4P (Jenner et al., 2005). (c) Crystal structure of the 70S ribosome with three tRNAs in the A, P and E sites. The ribosome is depicted in grey, mRNA in red and the tRNAs in dark grey. The figure is adapted from PDB 4V6F (Jenner et al., 2010).

2.2. The translation cycle in bacteria

A protein is synthesized during a translation cycle, which, in bacteria, is divided into four phases: initiation, elongation, termination and ribosome recycling (Fig. 2).

Initiation involves the recognition of the mRNA start codon (usually AUG) and the assembly of the elongation-competent ribosome complex on the translation start site (Allen et al., 2005; Kaledhonkar et al., 2019; Milon et al., 2007; Simonetti et al., 2008). Accurate start codon selection defines the open reading frame (ORF), i.e. the start point of the codon-by-codon progression of the ribosome along the mRNA until the stop codon (Gualerzi and Pon, 2015). Initiation is mediated by initiation factors (IFs) 1 (IF1), 2 (IF2) and 3 (IF3, Fig. 2) (Rodnina, 2018). In many, albeit not all, bacteria and mRNAs, the recruitment of the ribosome on the start codon is mediated by the base pairing between a hexameric mRNA sequence located ~9 nucleotides upstream to the start codon (Shine-Dalgarno sequence, SD) and a complementary sequence at the 3' end of the 16S rRNA (Gualerzi and Pon, 2015; Shine and Dalgarno, 1975). This interaction positions the start codon in the P site of SSU (Julian et al., 2011; Korostelev et al., 2007; Simonetti et al., 2008; Yusupova et al., 2006). After anchoring the start codon in the P site, fMet-tRNA^{fMet} (fMet is formylmethionine) is recruited by IF2 to base pair with the start codon (Milon et al., 2010), followed by GTP hydrolysis by IF2, dissociation of IFs and LSU recruitment, forming the elongation-competent 70S initiation complex (IC, Fig. 2) (Allen et al., 2005; Goyal et al., 2015; Grigoriadou et al., 2007; Kaledhonkar et al., 2019; Milon et al., 2008; Milon et al., 2012; Milon and Rodnina, 2012; Qin et al., 2009).

Elongation entails sequential steps of decoding, peptide bond formation and translocation. During decoding, the aminoacyl-tRNA (aa-tRNA) is recruited to the ribosomal A site by elongation factor Tu (EF-Tu) (Rodnina, 2018; Schmeing and Ramakrishnan, 2009). Codon recognition and accommodation of the aa-tRNA are followed by formation of the peptide bond between the nascent peptide chain and the incoming amino acid (Fig. 2) (Wohlgemuth et al., 2008); although in most cases peptide bond formation is catalyzed by the ribosome itself, in some special cases this requires an auxiliary elongation factor P (EF-P) (Doerfel et al., 2013). In the next step, the tRNA–mRNA duplexes move together from A to P and from P to E site during translocation catalyzed by elongation factor G (EF-G, Fig. 2) (Rodnina, 2018; Schmeing and Ramakrishnan, 2009). At the end of translocation, the ribosome has moved one codon to the 3' end of the mRNA and the A site is available to accommodate the next aa-tRNA, allowing the next elongation cycle to begin.

Termination occurs when ribosomes encounter a stop codon (UAG, UGA, UAA), which is not decoded by tRNAs but is recognized by release factors (RF) that catalyze the release of the nascent peptide to the cytoplasm (Fig. 2) (Rodnina, 2018; Schmeing and Ramakrishnan, 2009). Post-termination complexes carry only deacylated tRNA in the P site and are split by ribosome recycling factor (RRF) and EF-G during the recycling phase (Fig. 2) (Gao et al., 2005). After recycling, the mRNA, tRNA and ribosomal subunits are available for the next translation cycle.

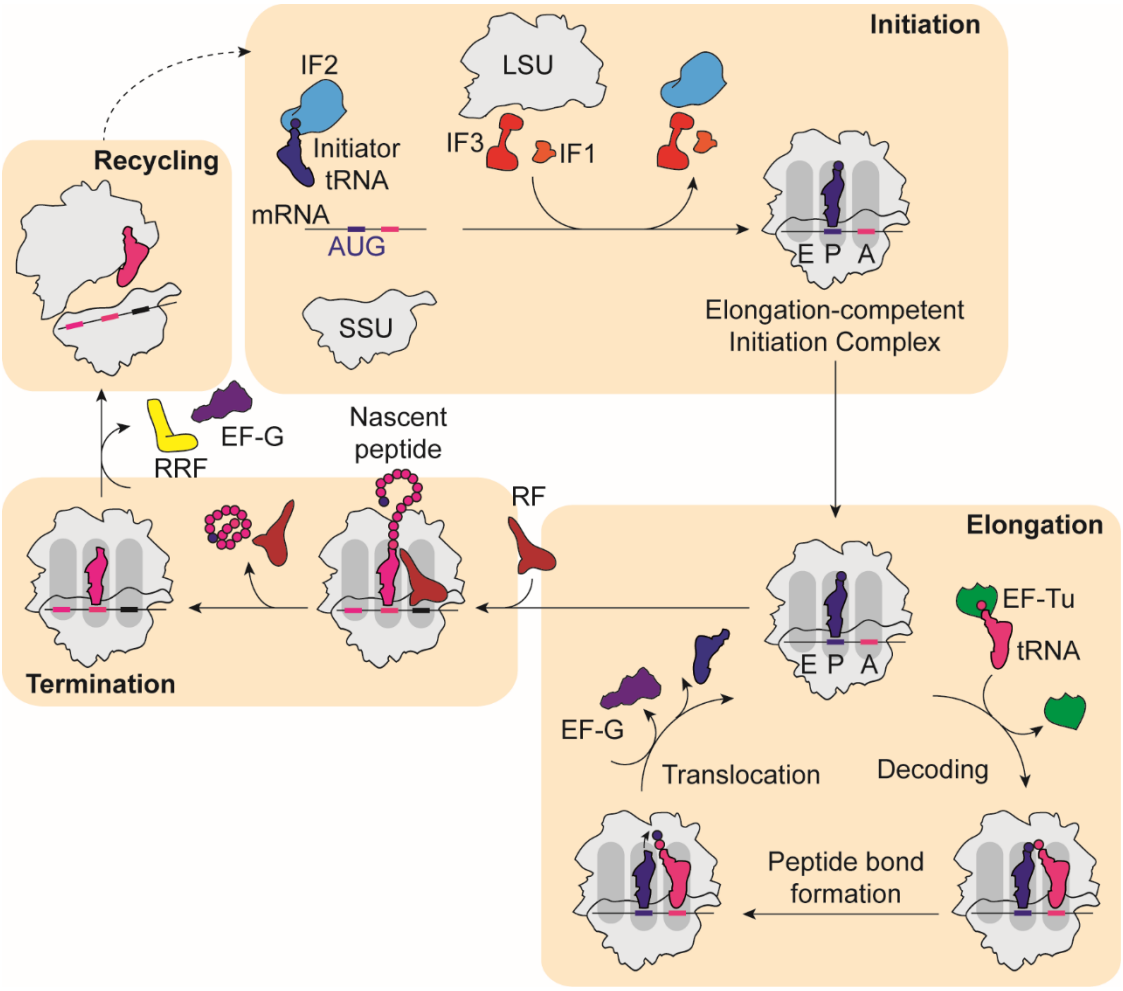

Figure 2. The bacterial translation cycle. Initiation involves IF1 (orange), IF2 (cyan) and IF3 (red), mRNA (solid line) with start codon (blue bold line), the initiator fMet-tRNA^{fMet} (dark blue) and the ribosomal subunits (grey) to form the elongation-competent initiation complex. Elongation involves repetitive cycles of decoding by EF-Tu (green) and aa-tRNA (magenta), peptide bond formation and translocation by EF-G (purple). Termination occurs on stop codons (black bold line) and involves the release of the nascent peptide by release factors (RF). Ribosome recycling is catalyzed by RRF (yellow) and EF-G. The colors of ribosome, tRNAs and translation factors are kept the same throughout the thesis.

2.3. Translation elongation in bacteria

Elongation is the phase of translation where the nascent peptide is synthesized according to the codon sequence of the mRNA. It involves three sequential steps: decoding, peptide bond formation and translocation.

The ribosome translates: decoding

The first step of elongation is the decoding of the mRNA codon and the accommodation of the aa-tRNA in the A site. The aminoacylated tRNA is recognized by the translational GTPase EF-Tu (Fig. 3a) (Nissen et al., 1995). EF-Tu consists of three domains, domain 1 (the G domain where the GTP-binding pocket is located and GTP hydrolysis takes place), 2 and 3 (Fig. 3a). Conserved residues of the three domains participate in the recognition of common elements in aa-tRNAs, such as the 3'-CCA end and the ester bond between the tRNA and the amino acid (Fig. 3a) (Nissen et al., 1995). EF-Tu delivers aa-tRNAs to the ribosome in the form of aa-tRNA—EF-Tu—GTP ternary complex (TC, Fig. 3a) (Loveland et al., 2020; Moazed et al., 1988; Stark et al., 1997).

Decoding starts with the initial binding of the TC via interactions of EF-Tu with the L7/L12 stalk in a codon-independent way (Fig. 3b) (Rodnina et al., 2017; Rodnina et al., 1996). Next, the anticodon stem loop (ASL) of the tRNA reaches towards the peptidyl-tRNA in the P site (Dunham et al., 2007; Fischer et al., 2016; Fischer et al., 2015; Loveland et al., 2017; Ogle et al., 2003; Pape et al., 1999; Pape et al., 1998; Rodnina et al., 1996; Rodnina et al., 1995; Schmeing et al., 2009; Schuette et al., 2009). The ASL is positioned in the decoding center of the SSU, base pairing with the A-site mRNA codon, while G domain of EF-Tu is still positioned away from the GAC in the LSU (A*/T state, Fig. 3b) (Loveland et al., 2020; Moazed et al., 1988; Stark et al., 1997). The geometry of the codon-anticodon mini helix is surveilled by the universally conserved 16S rRNA nucleotides A1492, A1493 and G530 of the decoding center (Ogle et al., 2001; Ogle et al., 2002). Cognate codon-anticodon duplex adopts Watson-Crick-like geometry and the 16S rRNA nucleotides flip out of their respective rRNA helices and point towards the codon-anticodon pair (A/T state, Fig. 3b), acting as a latch that pulls the beak region of the SSU head towards the SSU body, resulting in the closure of the decoding center (Fischer et al., 2016; Loveland et al., 2020; Ogle et al., 2002). At this point, the G domain of EF-Tu is in contact with SRL, which arranges the catalytic His84 of EF-Tu in an active conformation, leading to GTP hydrolysis (Fig. 3b) (Fischer et al., 2016; Maracci and Rodnina,

2016; Rodnina et al., 2017; Rodnina and Wintermeyer, 1995). In the next step, EF-Tu dissociates from the ribosome and GDP is exchanged with GTP by the nucleotide-exchanging elongation factor Ts (EF-Ts) (Burnett et al., 2013; Gromadski et al., 2002). Subsequently, the tRNA elbow moves ~80-100Å towards the A site in LSU (elbow-accommodation, EA, state, Fig. 3b) and the aminoacylated acceptor stem is positioned in the PTC (Geggier et al., 2010; Loveland et al., 2020; Pape et al., 1998; Sanbonmatsu et al., 2005).

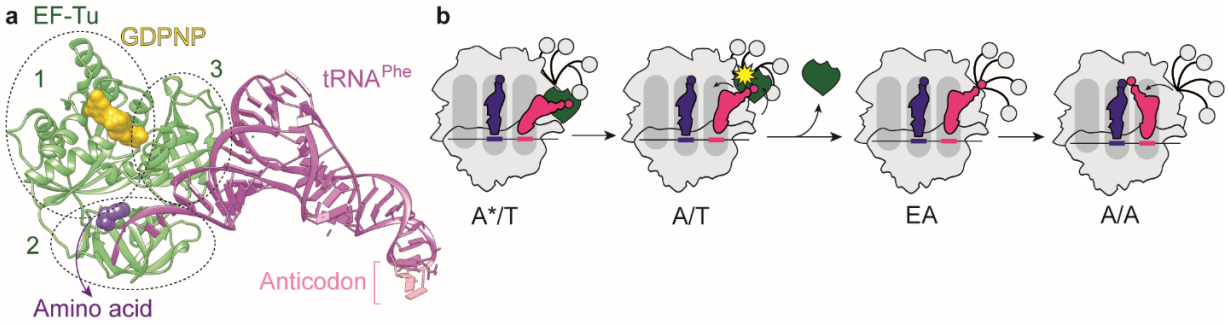

Figure 3. EF-Tu—tRNA ternary complex and the mechanism of decoding. (a) Crystal structure of EF-Tu (green) with Phe-tRNA^{Phe} (magenta) and the non-hydrolysable GTP analog GDPNP (yellow). The domains of EF-Tu are delineated in dotted circles. The amino acid phenylalanine (Phe) is shown in purple spheres and the anticodon in pink. The figure is adapted from PDB 1TTT (Nissen et al., 1995). (b) The mechanism of decoding and tRNA accommodation. GTP hydrolysis is depicted in yellow. The L7/L12 stalk is depicted as grey circles. The codons in mRNA (black solid line) and amino acids are shown in respective colors with the tRNAs. The figure is made with inputs from (Fischer et al., 2016; Loveland et al., 2017; Loveland et al., 2020).

The ribosome as a catalyst: peptide bond formation

During peptide bond formation, the new amino acid is incorporated into the growing peptide chain and the peptide is transferred from the P-site to the A-site tRNA (Fig. 4) (Rodnina, 2013). PTC consists exclusively of 23S rRNA (Ban et al., 2000; Noller et al., 1992). The mechanism of the reaction involves a two-step nucleophilic attack of the α-amino group of the amino acid of the A-site aa-tRNA to the carbonyl group of the C-terminal residue of the peptide attached to P-site peptidyl-tRNA (Fig. 4) (Hiller et al., 2011). First step involves the formation of a zwitterionic intermediate and, in the second step, the intermediate resolves into the reaction products: a P-site deacylated tRNA and A-site peptidyl-tRNA (Fig. 4) (Kuhlenkoetter et al., 2011; Moore and Steitz, 2002, 2011; Nissen et al., 2000; Polikanov et al., 2014; Rodnina, 2013; Schmeing et al., 2005). The rate of peptide bond formation depends on the amino acid and occurs rapidly and spontaneously for the majority of them (~10-100 s^{-1}) (Wohlgemuth et al., 2008). However, the reaction rate for proline is low (~0.1 s^{-1}) and ribosome stalls when consecutive proline codons are decoded (Mohammad et al., 2019; Wohlgemuth et al., 2008; Woolstenhulme et al., 2013). Stalling is resolved by elongation factor P (EF-P), an auxiliary factor that restores the optimal orientation of the substrates and accelerates peptide bond formation (Doerfel et al., 2013; Huter et al., 2017; Ude et al., 2013).

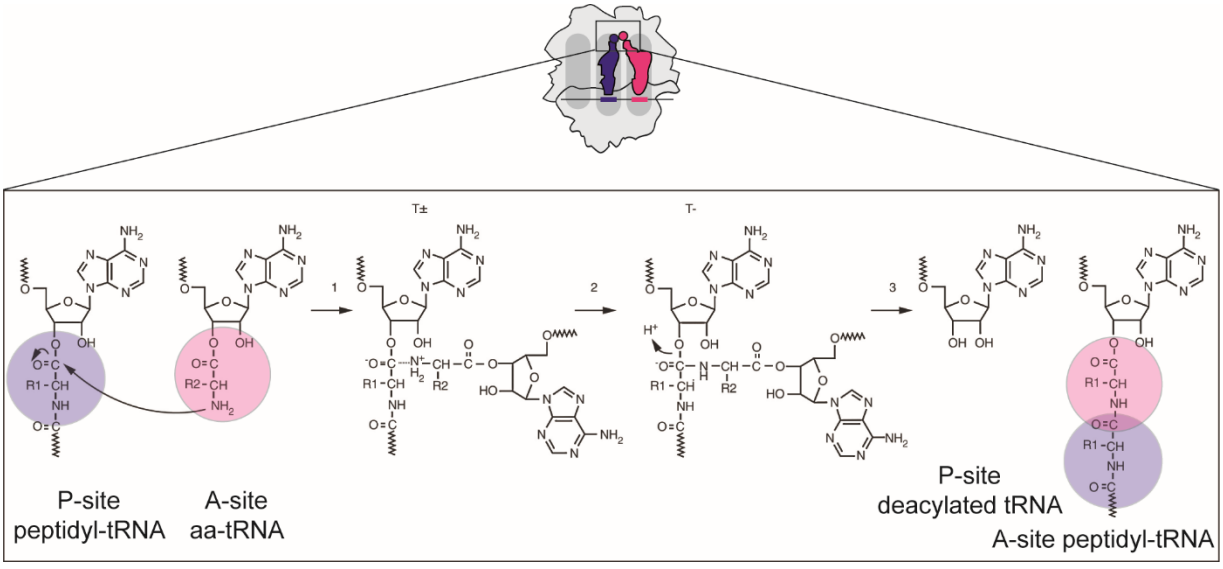

Figure 4. The reaction of peptide bond formation in the PTC. Formation of peptide bond between the A-site aa-tRNA (magenta) and P-site peptidyl-tRNA (blue). Zoom-in shows the steps in the reaction coordinate inside the PTC. Intermediate steps are shown as T. The figure is adapted from (Rodnina, 2013). Reuse/reprint with permission.

The ribosome as a molecular machine: translocation

After peptide bond formation, the pre-translocation (PRE) complex is formed, containing A-site peptidyl-tRNA and P-site deacylated tRNA. The tRNAs, the SSU body and head domains and the L1 stalk exhibit spontaneous and reversible structural rearrangements in the PRE complex (Fig. 5) (Cornish et al., 2009; Frank and Agrawal, 2000; Moazed and Noller, 1989b; Ratje et al., 2010).

The tRNAs interconvert between the classical (C, where acceptor stems and anticodon loops are located in the A and P sites in both subunits, denoted as A/A and P/P, respectively—first letter denotes the position of the anticodon loop in SSU and second letter denotes the position of the acceptor stem and tRNA elbow in LSU) and hybrid (H, where the acceptor stem and the tRNA body are located in the P and E site in LSU, respectively) conformations (Fig. 5a). The deacylated tRNA adopts a single hybrid conformation (P/E), while the peptidyl-tRNA can adopt one of the two distinct hybrid conformations, namely A/P and A/P* (Carbone et al., 2021; Petrychenko et al., 2021; Rundlet et al., 2021). In A/P conformation, only the acceptor stem moves towards the P site in LSU, while the A/P* conformation involves the additional movement of the peptidyl-tRNA body towards the P site (Fig. 5a) (Adio et al., 2015; Agirrezabala et al., 2008; Blanchard et al., 2004; Carbone et al., 2021; Chen et al., 2011a; Dunkle et al., 2011; Kim et al., 2007; Moazed and Noller, 1989b; Munro et al., 2007; Petrychenko et al., 2021; Rundlet et al., 2021; Zhang et al., 2009). Concomitantly with the tRNA movements, the SSU body performs a rotational movement ~8° in counterclockwise direction relative to the LSU across the LSU-SSU axis, thus interconverting between the non-rotated (N) and rotated (R) state (Fig. 5b) (Agirrezabala et al., 2008; Altuntop et al., 2010; Cornish et al., 2008; Ermolenko et al., 2007; Ermolenko and Noller, 2011; Fischer et al., 2010; Frank and Agrawal, 2000; Julian et al., 2008; Sharma et al., 2016; Zhang et al., 2009) The SSU head domain also swivels ~6° counterclockwise, to the direction of tRNA movement across the SSU head-body axis perpendicular to SSU body rotation axis, thus interconverting between the non-swiveled (N) and swiveled (S) state (Fig. 5c) (Belardinelli et al., 2016a; Guo and Noller, 2012; Mohan et al., 2014; Ratje et al., 2010; Schuwirth et al., 2005; Wasserman et al., 2016; Zhang et al., 2009). Finally, the L1 stalk interconverts between the open (positioned away from the E site) and closed (positioned towards the E site in contact with the elbow region of the P/E deacylated tRNA) conformations (Fig. 5d) (Cornish et al., 2009; Fei et al., 2009; Fei et al., 2008; Mohan and Noller, 2017). These four motions are stochastic, reversible and depend on the temperature and the concentration of key ions, such as Mg^{2+} (Bock et al., 2013; Fischer et al.,

2010; Munro et al., 2009). Additionally, they are kinetically loosely coupled and rarely coordinate to proceed to productive translocation spontaneously (~0.01 min^{-1}) (Konevega et al., 2007).

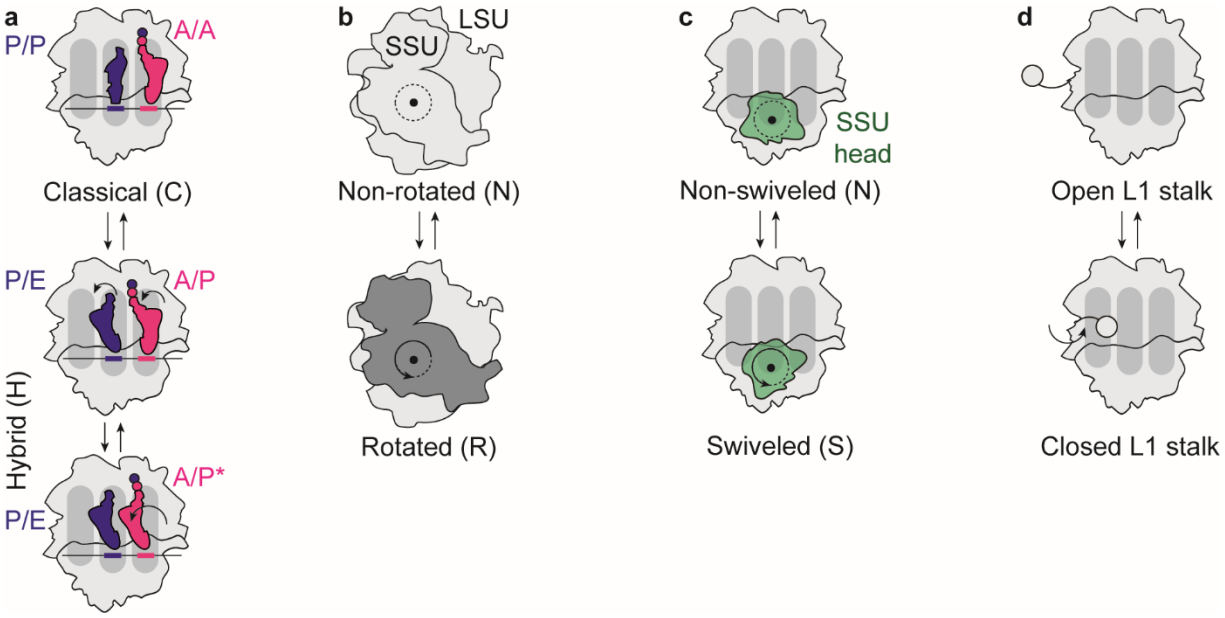

Figure 5. Structural rearrangements of the mobile elements in the PRE complex. (a) The A-site peptidyl- (magenta) and P-site deacylated (blue) tRNAs interconvert between the classical and hybrid conformations. (b) The SSU body moves to the rotated (R, dark grey) state relative to LSU and back to the non-rotated (N, light grey) state. The ribosome is shown in bottom view. (c) The SSU head domain (green) swivels to the direction of tRNA translocation across the SSU body-head axis (S) and back to the non-swiveled (N) state. In (b) and (c), dots show the axis and dotted circles and arrows the direction of rotation. (d) The L1 stalk interconverts between the open and closed conformations.

Translocation is catalyzed by EF-G, which consists of five domains, domain 1 (G domain), 2, 3, 4 and 5 (Fig. 6) (Czworkowski et al., 1994; Evarsson et al., 1994). Domain 1 contains the GTP binding pocket, where GTP hydrolysis is catalyzed by H91 (Fig. 6) (Rodnina et al., 2019). One GTP molecule is hydrolyzed per translocation cycle (Rodnina et al., 2019). It also contains switch 1 (sw1) and 2 (sw2) regions that sense GTP, connect EF-G with SRL and the ribosome and mediate large structural rearrangements during translocation (Fig. 6) (Carbone et al., 2021; Petrychenko et al., 2021; Rodnina et al., 2019). Domain 4 contacts the codon-anticodon duplex in the A site in SSU via interactions with residues Q507 (loop I) and H583 (loop II, Fig. 6) (Brilot et al., 2013; Carbone et al., 2021; Gao et al., 2009; Petrychenko et al., 2021; Ramrath et al., 2013; Rundlet et al., 2021; Zhou et al., 2014). EF-G adopts two conformations (compact and elongated) that differ in the orientation of domains 4-5 relative to domains 1-2-3 (Lin et al., 2015; Salsi et al., 2014; Salsi et al., 2015).

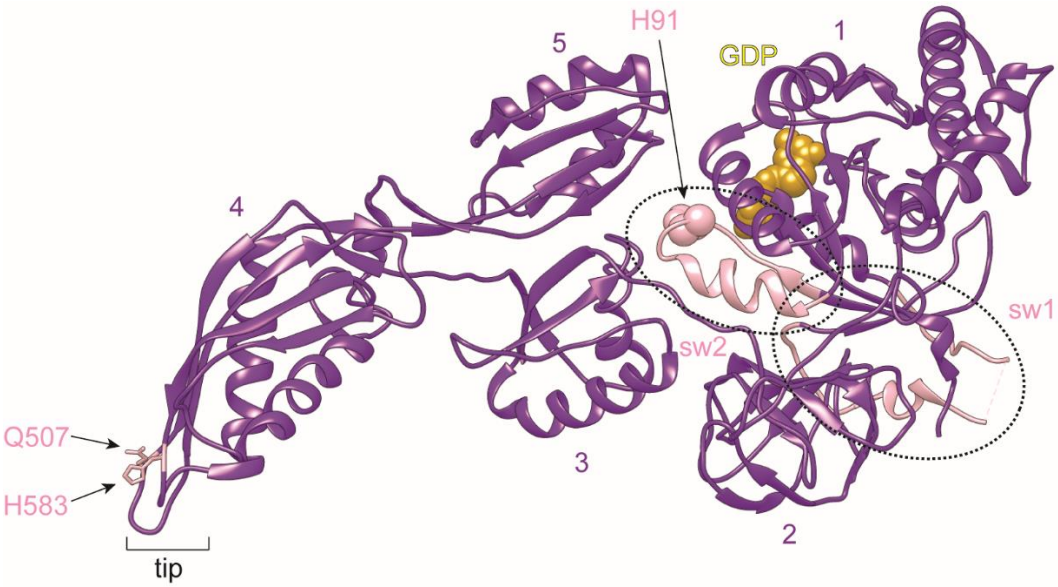

Figure 6. Anatomy of EF-G. Cryo-EM structure of EF-G (purple) bound to GDP (yellow). The domains are indicated. The catalytic H91 is shown in pink spheres. The sw1 and sw2 of domain 1 (dotted circles) and the key residues Q507 and H583 at the tip of domain 4 are shown in pink. The figure is adapted from PDB 7PJY (Petrychenko et al., 2021).

Initial binding of EF-G via the L7/L12 stalk in compact form is followed by a rotational rearrangement of domains 4-5 into the A site in SSU (elongated form, Fig. 7) (Brilot et al., 2013; Lin et al., 2015; Salsi et al., 2014; Salsi et al., 2015; Stark et al., 2000). EF-G in the GTP-bound state acts as a pawl that stabilizes the R state of the SSU body, the S state of SSU head domain, the H states of tRNAs and the closed state of L1 stalk (Fig. 7) (Adio et al., 2015; Carbone et al., 2021; Chen et al., 2011a; Fei et al., 2008; Holtkamp et al., 2014; Munro et al., 2010; Petrychenko et al., 2021; Sharma et al., 2016). The H91 of EF-G is positioned by SRL in a catalytically active orientation, leading to GTP hydrolysis (Maracci and Rodnina, 2016; Rodnina et al., 2019). After GTP hydrolysis but before Pi release, domain 4 of EF-G remains flexible, while sw1 develops interactions with GDP-Pi, SRL and the SSU body (Carbone et al., 2021; Petrychenko et al., 2021). Recent time-resolved cryo-EM studies reported that Pi release acts as a loaded spring to promote tRNA movement (Carbone et al., 2021; Petrychenko et al., 2021). Pi release unleashes sw1 from the SRL, leading to an upward rotational motion of the 1-3 domains of EF-G, which positions domain 4 deeper into the A site of SSU in contact with the tRNA-mRNA duplex (Carbone et al., 2021; Petrychenko et al., 2021). Subsequently, the interactions between EF-G and the SSU body are abolished leading to ribosome unlocking: the SSU body rotates back to the N state, while the SSU head domain remains swiveled ~18-21° (Fig. 7) (Belardinelli et al., 2016a; Carbone et al., 2021; Chen et al., 2016; Guo and Noller,

2012; Petrychenko et al., 2021; Ramrath et al., 2013; Sharma et al., 2016; Zhou et al., 2014). Before unlocking, the pathway from the P to the E site is obstructed by a structural constriction between the SSU body and head, called the P gate (Schuwirth et al., 2005). Unlocking widens the P gate and allows forward movement of the peptidyl- and deacylated tRNAs into EF-G-induced chimeric states (CHI), where the ASLs are located between the A and P and P and E sites in SSU respectively, following the movement of the SSU head (ap/P and pe/E, Fig. 7) (Adio et al., 2015; Belardinelli et al., 2016a; Bock et al., 2013; Carbone et al., 2021; Fischer et al., 2010; Petrychenko et al., 2021; Ramrath et al., 2013; Schuwirth et al., 2005; Zhou et al., 2014). When the tRNAs reach the P/P and E/E states respectively, EF-G-GDP dissociates from the ribosome (Carbone et al., 2021) and the SSU head swivels back to lock the peptidyl-tRNA in the P site (Fig. 7) (Belardinelli et al., 2016a; Gao et al., 2009; Wasserman et al., 2016). Simultaneously or shortly after, the deacylated tRNA is released from the ribosome with the help of L1 stalk (Fig. 7) (Adio et al., 2015; Belardinelli et al., 2016a; Bock et al., 2013; Chen et al., 2011b; Chen et al., 2013b; Choi and Puglisi, 2017; Fei et al., 2009; Fei et al., 2008; Lill et al., 1986; Munro et al., 2010; Petropoulos and Green, 2012; Semenkov et al., 1996; Uemura et al., 2010; Wasserman et al., 2016). The ribosome is then found in the posttranslocation state (POST), where the A site is available to accommodate the next aa-tRNA (Fig. 7). EF-G exchanges GDP for GTP spontaneously (Wilden et al., 2006).

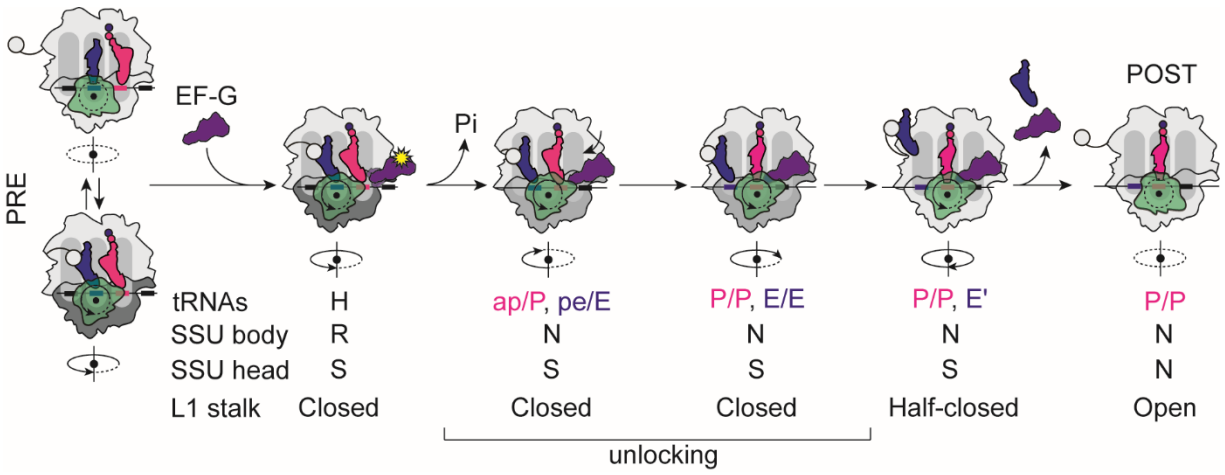

Figure 7. Molecular mechanics of translocation. Structural dynamics of the ribosome in the translocation reaction coordinate. EF-G stabilizes the H tRNA state, the R state of the SSU body, the S state of SSU head and the closed conformation of L1 stalk and, upon GTP hydrolysis (yellow), orchestrates the coordination of movements to catalyze translocation. The figure was created with input from (Belardinelli et al., 2016a; Belardinelli et al., 2016b; Carbone et al., 2021; Petrychenko et al., 2021; Wasserman et al., 2016).

2.4. Ribosome frameshifting

During translation elongation, the ribosome acts as a versatile molecular machine that interacts with a variety of tRNA substrates and exhibits high degree of structural plasticity. This structural plasticity ensures that translocation of ribosomes across the mRNA is performed with high fidelity, but also accounts for the existence of multiple (~500,000,000) alternative translocation pathways (Bock et al., 2013). Some of those alternative pathways may lead to recoding events that lead to the synthesis of different peptides from the same mRNA (Caliskan et al., 2015; Rodnina et al., 2020). One of such recoding events is ribosome frameshifting. The ribosome moves along the mRNA one codon at a time. However, it occasionally shifts several nucleotides towards the 5' end (– direction) or 3' end (+ direction) of the mRNA. The most frequent case is –1 frameshifting, which occurs on hotspot mRNA sequences, called slippery sequences (X XXY YYZ, 0-frame codons separated by gap, –1-frame codons underlined, Fig. 8a). On a slippery sequence, the same tRNA can base pair with two overlapping codons: the 0-frame (XXY and YYZ) and the –1-frame codons (XXX and YYY, Fig. 8a). Frameshifting is favored when the codon-anticodon interactions have lower free energy difference in the –1 than in 0 frame (Bock et al., 2019). After frameshifting, the codons downstream to the slippery sequence are decoded by different aa-tRNAs, compared to 0-frame codons (Fig. 8b). Additionally, termination occurs on alternative out-of-frame stop codons, thus leading to the synthesis of peptides of different length, compared to 0-frame peptides (Fig. 8b). In cells, frameshifting comes in three flavors: programmed, depletion-triggered (hungry) and spontaneous ribosome frameshifting.

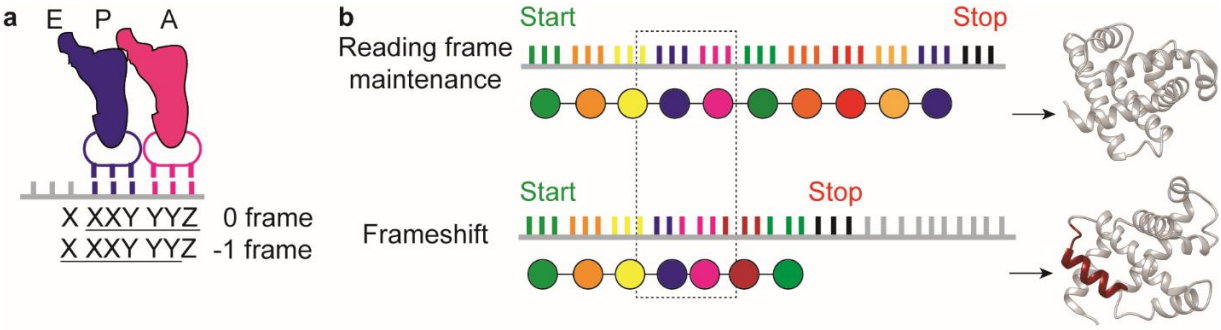

Figure 8. Slippery sequence and propagation of frameshifting across the peptide chain. (a) Schematic representation of tRNA slippage on heptameric –1 slippery sequence. The A-site (magenta) and P-site (blue) tRNAs can base pair with both 0-frame and –1-frame codons. (b) Schematic representation of peptide synthesis in 0 frame (upper) and after –1 frameshifting (lower). Dotted box indicates the position of the heptameric slippery sequence. Frameshifted peptide (lower) carries an alternative C-terminus (red) and is of different length compared to 0-frame peptide due to termination on out-of-frame stop codon.

Programmed ribosome frameshifting

Programmed ribosome frameshifting (PRF) involves, in addition to the slippery sequence, downstream mRNA secondary structure elements, such as stem loops (Fig. 9a) or pseudoknots (Fig. 9b) that hinder ribosome progression across the mRNA (Caliskan et al., 2014; Chung et al., 2010; Giedroc and Cornish, 2009; Namy et al., 2006). PRF is mainly prevalent in mobile genetic elements such as viruses, transposons and retroviral insertion remnants. In viruses, translation of the –1 frame of a viral ORF results in the synthesis of polyproteins that are essential for virus propagation and particle assembly (Atkins et al., 2021; Kelly et al., 2020; Kendra et al., 2018; Kendra et al., 2017; Moomau et al., 2016; Napthine et al., 2019; Napthine et al., 2021; Riegger and Caliskan, 2022; Wang et al., 2019; Zimmer et al., 2021). A well-studied example is the production of the Gag-Pol polyprotein of human immunodeficiency virus (HIV), the causative agent of the acquired immunodeficiency syndrome (AIDS, Fig. 9c) (Jacks et al., 1988). The synthesis of the Gag-Pol polypeptide chain depends on a –1PRF event at the 3' end of *gag* gene, where a stem loop is formed downstream to the slippery sequence (Fig. 9c). After frameshifting, the 0-frame stop codon that would terminate translation of the *gag* ORF is omitted and, instead, translation continues in –1 frame into the *pol* ORF (Jacks et al., 1988). Finally, the Gag-Pol polyprotein is produced, which is subsequently cleaved by viral proteases to generate the Gag and Pol viral proteins (Fig. 9c). Similar phenomena are observed in coronaviruses, such as SARS-CoV-2, the causative agent of the Covid-19 pandemic, where a pseudoknot structure downstream to slippery sequence stimulates frameshifting that produces the viral polyproteins (Fig. 9b) (Bhatt et al., 2021; Riegger and Caliskan, 2022).

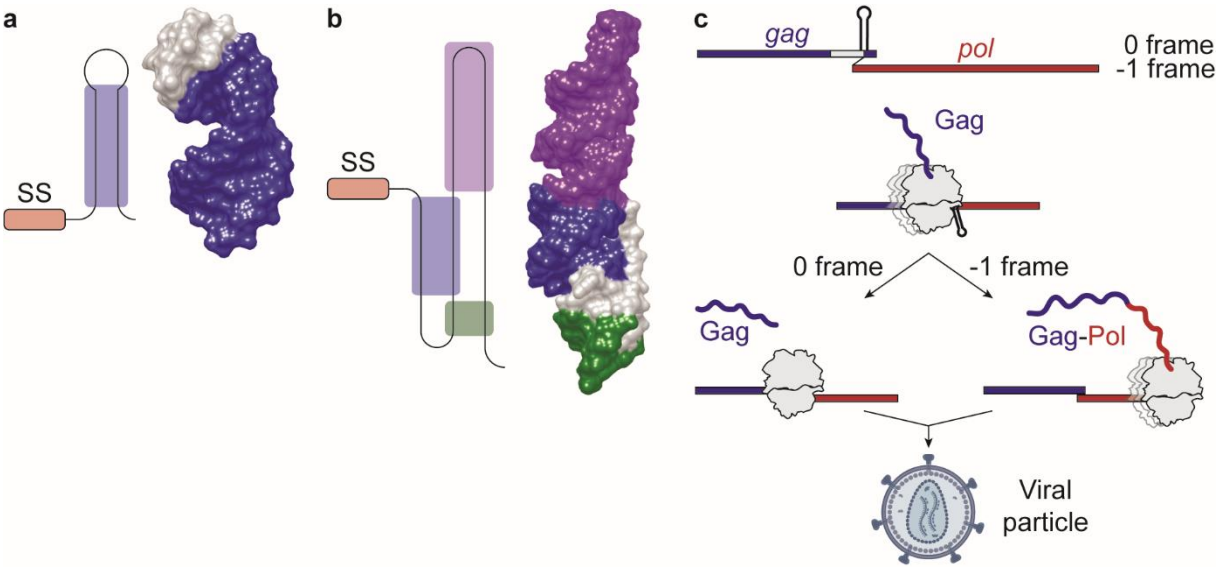

Figure 9. Stimulatory elements and programmed ribosome frameshifting in viruses. (a) Schematic and crystal structure of the stem loop of the HIV-1 frameshifting site. Slippery sequence (SS) is shown in red and the double stranded region in blue. The figure was adapted from PDB 1PJY (Staple and Butcher, 2005). (b) Schematic and crystal structure of the pseudoknot of the SARS-CoV-2 frameshifting site. The double-stranded regions are shown in purple, blue and green shades. The figure was adapted from PDB 7LYJ. (c) Schematic of the HIV frameshifting site and kinetic branch point of ribosome population that either continue synthesis in 0 frame (blue), synthesizing the Gag protein, or shift to –1 frame (red), synthesizing the Gag-Pol polyprotein (blue-red).

PRF plays a significant role in insertion elements, as well. In the example of the bacterial insertion sequence 1, a slippery sequence and a stimulatory downstream structure drive PRF at the 3' end of the upstream *insA* ORF, thus continuing towards the synthesis of the downstream –1-frame *insB* ORF and producing the fused insA-insB protein, which is an active transposase (Chandler and Fayet, 1993; Luthi et al., 1990; Rettberg et al., 1999; Sekine et al., 1992; Sekine and Ohtsubo, 1989). In mammals, analogous PRF events have been described in remnants of ancient retroviral insertion elements, where a fused protein is synthesized as a result of PRF (Clark et al., 2007; Manktelow et al., 2005; Shigemoto et al., 2001; Wills et al., 2006).

PRF has also been described in cellular genes with distinct functions in bacteria and eukaryotes. In bacteria, it is implicated in the fine tuning of protein stoichiometry (Blinkowa and Walker, 1990). The most prominent example is the *dnaX* mRNA of *E. coli*, which encodes for the γ and τ subunits of DNA polymerase holoenzyme (Blinkowa and Walker, 1990; Caliskan et al., 2017). Translation in 0 frame produces the τ subunit chain and terminates on a 0-frame stop codon. However, a frameshifting site at the 3' end of the τ subunit ORF leads to slippage

to –1 frame, so that translation continues towards the synthesis of the γ subunit. Another interesting example reports the role of PRF in copper tolerance in *E. coli* (Meydan et al., 2017). Translation of the *copA* mRNA in 0 frame produces a copper transporter, while shift to the –1 frame synthesizes a copper chaperone that facilitates the trafficking of copper ions to the transporter. In eukaryotic cells, PRF has been reported to regulate the stability and lifetime of cellular mRNAs. Illustrated in the example of genes involved in telomere maintenance in yeast, PRF creates premature out-of-frame stop codons leading to premature termination of translation, which in turn activates the nonsense mRNA decay mechanism that degrades the target mRNA (Advani et al., 2013; Belew et al., 2011; Jacobs et al., 2007). Although a similar phenomenon was described in human *CCR5* gene (Belew et al., 2014), re-evaluation by recent studies disputes this finding, indicating that there are currently no known cellular genes in humans that are regulated by PRF (Khan et al., 2022).

The mechanistic details of –1 programmed ribosome frameshifting (–1PRF) have been elucidated. During the impeded translocation in the presence of a stimulatory secondary structure, the order and timing of events are altered. While the early stages of translocation, such as EF-G binding and progression of tRNAs to the CHI state, are not affected, later stages such as the SSU head back swiveling and/or SSU body back rotation are severely delayed (Caliskan et al., 2014; Chen et al., 2014; Choi et al., 2020). Additionally, the dissociation of the deacylated tRNA from the E site is also delayed, indicating that –1PRF follows a two-tRNA slippage mechanism (Caliskan et al., 2014; Chen et al., 2013a). EF-G overall dwell time on the ribosome is increased, either due to commitment of EF-G to complete translocation (Caliskan et al., 2014) or via multiple EF-G binding attempts on the stalled ribosome (Chen et al., 2014; Choi et al., 2020). This change in the translocation kinetics opens a time window that allows the tRNAs to reach a thermodynamic equilibrium and basepair with the most thermodynamically favored codon, either in 0 or –1 frame (Bock et al., 2019). The completion of translocation occurs when the secondary structure unwinds, most likely by proteins S3, S4 and S5 that possess a passive helicase activity during translocation (Desai et al., 2019; Takyar et al., 2005).

Depletion-triggered ribosome frameshifting

The second type of frameshifting in the cell is depletion-triggered, also known as hungry frameshifting, triggered by limited availability of charged cognate 0-frame tRNAs or elongation factors. It is clearly distinct from PRF because it does not depend on mRNA secondary structures (Caliskan et al., 2017). Hungry frameshifting occurs in "idling" ribosome complexes residing on tetrameric slippery sequences and when the cognate tRNA reading the next A-site codon is omitted (Caliskan et al., 2017; Riegger and Caliskan, 2022). At the time window where the A site is unoccupied by tRNA for a long time, the P-site peptidyl-tRNA disrupts the interactions with the 0-frame codon and re-basepairs with the alternative-frame codon. Therefore, hungry frameshifting occurs in the POST complex, i.e. prior to PRE complex formation and translocation, and follows a single-tRNA slippage mechanism (Caliskan et al., 2017).

Hungry frameshifting has been reported on +1-frameshifting-prone mRNA sequences. Recent studies described POST complexes on the slippery sequence C<u>CC U</u>, in which the ASL of the P-site $tRNA^{Pro}$ moved in an intermediate position between the P and E sites in SSU (denoted as e*/E, clearly distinct from the canonical P/P conformation), accompanied by an mRNA constriction that confers +1 frameshifting (Hoffer et al., 2020). Additionally, low EF-P availability that causes a delay in peptide bond formation in post-decoding ribosome complexes assembled on slippery sequence increases +1 frameshifting (Gamper et al., 2015).

Hungry frameshifting has been described during HIV infection. A hallmark of HIV genome is the frameshifting site, where the second slippery codon (UUA) of the heptameric slippery sequence encodes for leucine (Leu). Additionally to the –1PRF event and under conditions where the 0-frame $tRNA^{Leu}$ is depleted, an alternative –1-frame product is formed as a result of hungry frameshifting (Korniy et al., 2019). Notably, the key $tRNA^{Leu}$ is significantly less abundant in human T lymphocytes and macrophages, the cell types mainly targeted by HIV. Therefore, HIV exploits two alternative pathways to maintain the frameshifting ratio: one following –1PRF mechanism and another relying on hungry frameshifting (Korniy et al., 2019).

Hungry frameshifting has recently been implied in neurodegeneration and cancer therapeutics. The pathological forms of *ATXN3* and *HTT* genes, the causative factors of spinocerebellar ataxia type 3 (SCA3) and Huntington's (HD) neurodegenerative diseases respectively, contain expanded CAG repeats at the genomic level that are translated into poly-glutamine (Gln) stretches in the respective proteins (Girstmair et al., 2013; McLoughlin et al.,

2020; Stochmanski et al., 2012; Tabrizi et al., 2020; Toulouse et al., 2005). However, poly-alanine (Ala) and poly-serine (Ser) variants have also been detected in SCA3 patients and postmortem brain samples of HD patients (Ayhan et al., 2018; Davies and Rubinsztein, 2006; Gaspar et al., 2000; Stochmanski et al., 2012; Toulouse et al., 2005; Wojciechowska et al., 2014). Previous studies suggested that the mRNAs that contain pathologically long CAG repeats exhaust the cellular pool of charged Gln-tRNA^{Gln} (Girstmair et al., 2013). This leads to ribosome stalling on CAG stretches and hungry frameshifting, thus allowing incorporation of alternative-frame tRNAs in the A site, such as tRNA^{Ala} in –1 frame or tRNA^{Ser} in +1 frame (Caliskan et al., 2017; Gallant and Lindsley, 1993; Temperley et al., 2010). Poly-Gln, poly-Ala and poly-Ser variants are highly prone to protein aggregation that results in neuron death and neurodegeneration (Ayhan et al., 2018; Davies and Rubinsztein, 2006; Girstmair et al., 2013). A recent study also reported that +1 frameshifting within the pathologically long CGG repeats in the *FMR1* mRNA, which cause the neurodegenerative fragile X-associated tremor/ataxia syndrome, leads to synthesis of aggregation-prone frameshifted peptides (Wright et al., 2022). In cancer therapeutics, it was recently shown that interferon-γ-based antitumor therapy causes upregulation of tryptophan (Trp) catabolism enzymes that leads to intracellular Trp depletion, thus decreasing the availability of charged tRNA^{Trp} and triggering cancer-specific hungry frameshifting (Bartok et al., 2021; Champagne et al., 2021). Aberrant frameshifted peptides are processed by the immunoproteasome, presented at the cancer cell surface and recognized by T cells, which then mediate cancer cell clearance (Bartok et al., 2021; Champagne et al., 2021).

Spontaneous ribosome frameshifting

The third type of frameshifting, spontaneous ribosome frameshifting (SRF), is clearly distinct from PRF and hungry frameshifting, because it occurs in the absence of stimulatory mRNA elements, does not rely on the abundance of cognate 0-frame aa-tRNAs and the frameshifted peptides usually do not have biological significance for the cell. SRF is practically a translation error that results in the loss of the reading frame and termination on out-of-frame stop codons, resulting in the production of dysfunctional peptides with aberrant amino acid sequence (Belew and Dinman, 2015; Drummond and Wilke, 2009; Fu and Parker, 1994). Due to the frameshifting error propagation across the peptide chain, but also the different length, the frameshifted peptides most probably fail to fold properly. For example, *est2* gene in yeast contains the slippery sequence A AAA AAA in the coding region (Belew et al., 2008), which supports frameshifting up to ~48% in equilibrium conditions (Bock et al., 2019). 0-frame translation of *est2* mRNA leads to a 884-aa-long protein, which adopts a native fold (Fig. 10a). However, –1 frameshifting leads to premature termination immediately after the slippery sequence, due to three consecutive stop codons in –1 frame, thus significantly reducing the length of the frameshifted peptide (445 aa, Fig. 10a). Protein structure prediction algorithms indicate that the folding of the frameshifted peptides significantly differs compared to the 0-frame peptide, especially in the region around the slippery sequence that becomes unstructured in the –1-frame peptide (Fig. 10a).

The fate and impact of erroneous peptides in the cell follow two main scenarios (Drummond and Wilke, 2009). In the first scenario, frameshifting causes loss of function, due to the fact that the frameshifted peptide fails to fold in a native state and is ultimately targeted for degradation. This may compromise the fitness of the cell, depending on the essentiality, turnover and production rate of the protein, but also due to sequestration of binding partners and clean-up burden of persistent erroneous peptides (Stoebel et al., 2008). Alternatively, accumulation of misfolded peptides may follow a toxic gain-of-function scenario, because they often cause protein aggregation, membrane destabilization and depolarization (Stefani and Dobson, 2003), sequestration of quality control factors and ultimately proteotoxic stress and cell death (Choe et al., 2016; Drummond and Wilke, 2009; Kohanski et al., 2008).

Yet, despite the detrimental risks implied in the translation of slippery mRNAs, the abundance of slippery sequences in the coding genome is relatively high. In *E. coli*, slippery sequences exist in many copies (up to ~3000 for the slippery sequence A AAA AAA, Fig. 10b),

supporting spontaneous frameshifting levels ranging from ~0.1% to ~10% (Sharma et al., 2014). Another study reports that the slippery sequence A AAA AAG is found 70 times in 68 genes (even twice in one gene) in *E. coli* and, estimated by the codon usage, is only mildly underrepresented in the coding genome (Gurvich et al., 2003). Respectively, ~10% of all cellular mRNAs are predicted to contain a slippery sequence in human coding genome (Fig. 10b) (Belew et al., 2008). Slippery sequences are evenly distributed across ORFs (Fig. 10c) and, for the vast majority (99.93%), frameshifting exposes out-of-frame stop codons within ~30 codons after the slippery sequence, resulting in premature termination and production of truncated frameshifted products (Fig. 10d) (Belew and Dinman, 2015; Belew et al., 2008). Notably, out-of-frame stop codons are frequent in the coding genome indicating an evolutionary ambush hypothesis, where stop codons in alternative frames are under positive selection in order to minimize the energy cost for the synthesis of frameshifted peptides and their impact in the cell (Seligmann and Pollock, 2004).

SRF is a major error source in the cell, as estimated by the ratio of –1-frame products to the total amount of 0- and –1-frame products during translation of slippery mRNA sequences. Initially, the SRF rate was monitored within the context of ribosome processivity errors, a term that collectively describes translation errors that cause synthesis of truncated peptides (Kurland, 1992). Previous *in vivo* studies estimated that ~25-30% of newly synthesized β-galactosidase chains end up as truncated products (Jorgensen and Kurland, 1990; Manley, 1978; Tsung et al., 1989). In recent *in vitro* studies using biochemical assays designed to measure specifically SRF, synthesis of –1-frame products is high ranging between ~15% and ~30%, depending on the slippery sequence (Caliskan et al., 2014; Chen et al., 2014; Niblett et al., 2021; Peng et al., 2019), in agreement with *in vivo* SRF levels (~25%) (Caliskan et al., 2014; Gurvich et al., 2003). In summary, SRF on slippery mRNA sequences is not negligible but rather is a major, yet previously underestimated, source of translation errors in the cell.

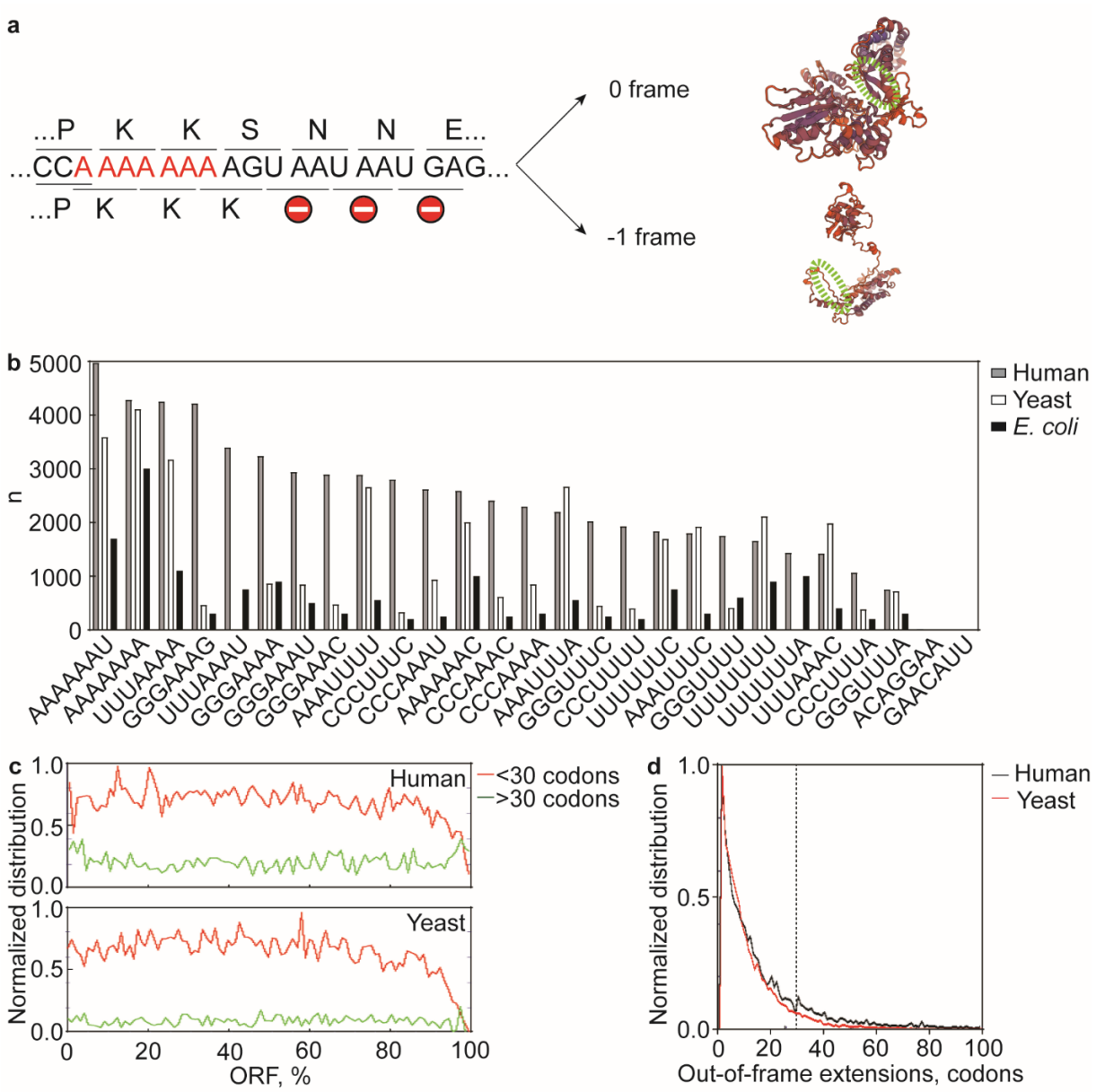

Figure 10. Frameshifting errors and the abundance of slippery sequences in the coding genome. (a) 0- and –1-frame translation of the *est2* mRNA and protein structure prediction of the 0- and –1-frame peptides. The area around the slippery sequence is shown in dotted green circle. (b) Abundance of common slippery sequences in the human (grey), yeast (white) and *E. coli* (black) coding genomes. Data are taken from (Belew et al., 2008) for human and yeast and from (Sharma et al., 2014) for *E. coli*. (c) Distribution of slippery sequences across the ORFs in human (upper) and yeast (lower) coding genomes. Slippery sequences are distinguished based on whether they lead to –1-frame extensions of less (red) or more (green) than 30 codons after the slippery sequence. (d) Frequency of slippery sequences regarding the number of –1-frame codons after the slippery sequence until an out-of-frame stop codon is reached. The dotted line indicate the number of codons where more than 99% of –1 frameshifting events terminate translation. Data in (a), (c) and (d) are from PRFdb (Belew and Dinman, 2015; Belew et al., 2008). No reuse/reprint permission required.

2.5. Maintenance of the translational reading frame

Due to the fact that SRF is a major error source for the cell, it is important to understand the mechanism that prevents ribosome frameshifting, but also describe the error-prone pathway that leads to SRF. In order to approach this, we discuss key properties of tRNAs, the interactions between ribosome and tRNAs and the role of EF-G in reading frame maintenance.

ASL modifications affect the coding capacity of tRNAs

tRNAs are key players in the maintenance of the reading frame, because they can base pair with the codons in the two overlapping reading frames on the slippery sequence. A characteristic feature of tRNAs is the degree of post-transcriptional modifications on nucleotides at the ASL, especially modifications at residues 34 (5' nucleotide of the anticodon, Fig. 11a) and 37 (adjacent to the anticodon 3' end, Fig. 11a) that modify the coding capacity of the tRNA (Boccaletto et al., 2018). For example, in bacterial decoding systems, a modified U34 is restricted to recognize only A- and G-ending codons (Suzuki, 2021).

E. coli $tRNA^{Lys}_{UUU}$ mediates frameshifting in the A AAA AAA and A AAA AAG slippery mRNA sequences and is heavily modified in the ASL (Fig. 11a).The same $tRNA^{Lys}_{UUU}$ recognizes both AAA and AAG codons due to a 5-methylaminomethyl-2-thio (mnm^5s^2) modification at uridine 34 (Fig. 11a) (Murphy et al., 2004; Rozov et al., 2016; Weixlbaumer et al., 2007). The mnm^5 group allows efficient decoding of AAG codons, while the s^2 modification and the modified residue 37 (N6-threonylcarbamoyladenosine, t^6A37) stabilize the codon-anticodon duplex via stacking interactions with the 5' codon nucleotide, thus facilitating decoding of both AAA and AAG codons (Fig. 11b, c) (Bock et al., 2019; Murphy et al., 2004; Ranjan and Rodnina, 2017; Rezgui et al., 2013; Rozov et al., 2016; Weixlbaumer et al., 2007). Although previous studies highlighted the contribution of ASL modifications in reading frame maintenance (Urbonavicius et al., 2001), the modifications at residue 34 prevent +1 frameshifting but have no effect in the prevention of –1 frameshifting (Urbonavicius et al., 2003).

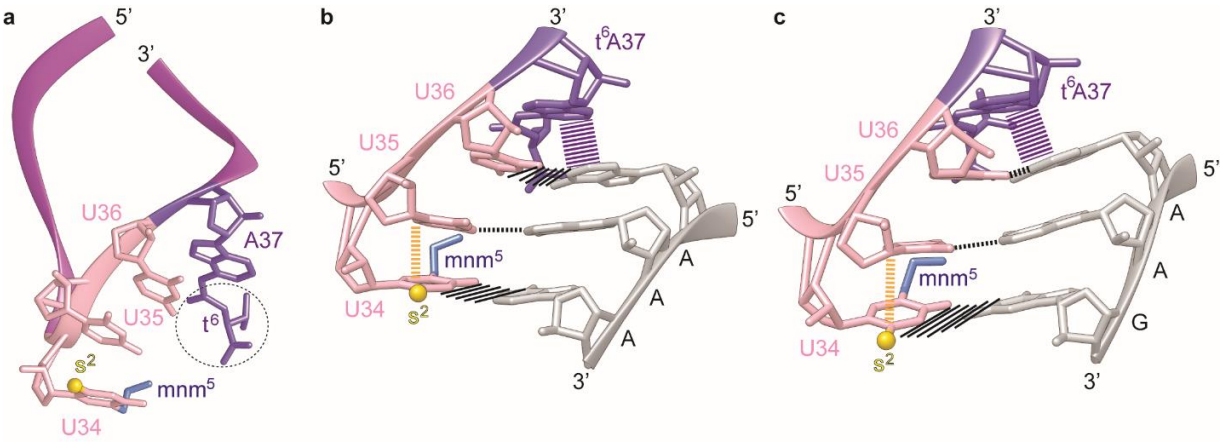

Figure 11. tRNA$^{Lys}_{UUU}$ ASL modifications and codon-anticodon interactions. (a) Crystal structure of the anticodon stem loop of tRNA$^{Lys}_{UUU}$. Anticodon nucleotides U34, U35 and U36 are shown in pink, residue t^{6}A37 in purple, mnm^5 group in blue and s^2 group in yellow. (b-c) Codon-anticodon interactions between tRNA$^{Lys}_{UUU}$ and mRNA codons AAA (b) and AAG (c). Codon-anticodon interactions are shown as black dashed lines. Stacking interactions between s^2 and U35 is shown in yellow dashed line and stacking interactions between t^{6}A37 and the 5' nucleotide of the codon (A1) in purple dashed line. mRNA is shown in grey. The figure is adapted from PDB 5E7K (a, b) and 5E81 (c) (Rozov et al., 2016).

The ribosomal grip of tRNAs

The stability of the ribosome complex is to a large extent determined by interactions between the tRNAs and the ribosome (Bock et al., 2015). The ribosomal subunits maintain interactions with the tRNAs throughout the elongation cycle, supporting the codon-anticodon duplex in the SSU (Bock et al., 2015; Noller et al., 2005; Ogle et al., 2001) and the tRNA body in the LSU (Jenner et al., 2010). Therefore, the tRNA-ribosome interactions in the A, P and E sites are plausible key players for the maintenance of the reading frame.

In the A site, the ribosome anchors the tRNA via a network of protein-RNA and RNA-RNA interactions (Fig. 12). On SSU, 16S rRNA helices h44 and h34 in the decoding center contact the codon-anticodon duplex and, in combination with elements outside the decoding center such as 23S rRNA helices H38, H69 and H89 and protein S19, anchor the tRNA ASL (Fig. 12 in magenta) (Ogle et al., 2001). Mutations at several residues of h34 increase +1 or –1 frameshifting (Kubarenko et al., 2006; Moine and Dahlberg, 1994). In the P site, 23S rRNA helix H69 and proteins S13 and S9 anchor the P-site tRNA (Fig. 12a in blue) (Jenner et al., 2005; Moazed and Noller, 1989a, 1991; Noller et al., 2005). Mutations and deletions of the C-terminal tail of S9 that interacts with the tRNA ASL increase frameshifting (Arora et al., 2013; Nasvall et al., 2009). In the E site, proteins S7 and S11 and 16S rRNA helices h23, h24 and

h28 contact the E-site tRNA on the SSU (Fig. 12a in grey) (Jenner et al., 2005; Jenner et al., 2010; Moazed and Noller, 1989a). On LSU, the acceptor stem interacts with 23S rRNA helices H68, H78 and H88 and proteins L31 and L33, while tRNA elbow region develops interactions with protein L1 of the L1 stalk (Fig. 12a, b in grey) (Bocchetta et al., 2001; Jenner et al., 2005; Mohan and Noller, 2017). Deletion of the tRNA-interacting β-hairpin of S7 (Devaraj et al., 2009), as well as mutations in residue C2394 of H88 of the E-site 23S rRNA and in tRNA ASL residues that are contacted by the ribosome in the E site, increase frameshifting (Sanders et al., 2008; Sergiev et al., 2005). These E-site elements may contribute to maintenance of the reading frame by preventing premature release of E-site tRNA that would expose the E-site codon to the peptidyl-tRNA.

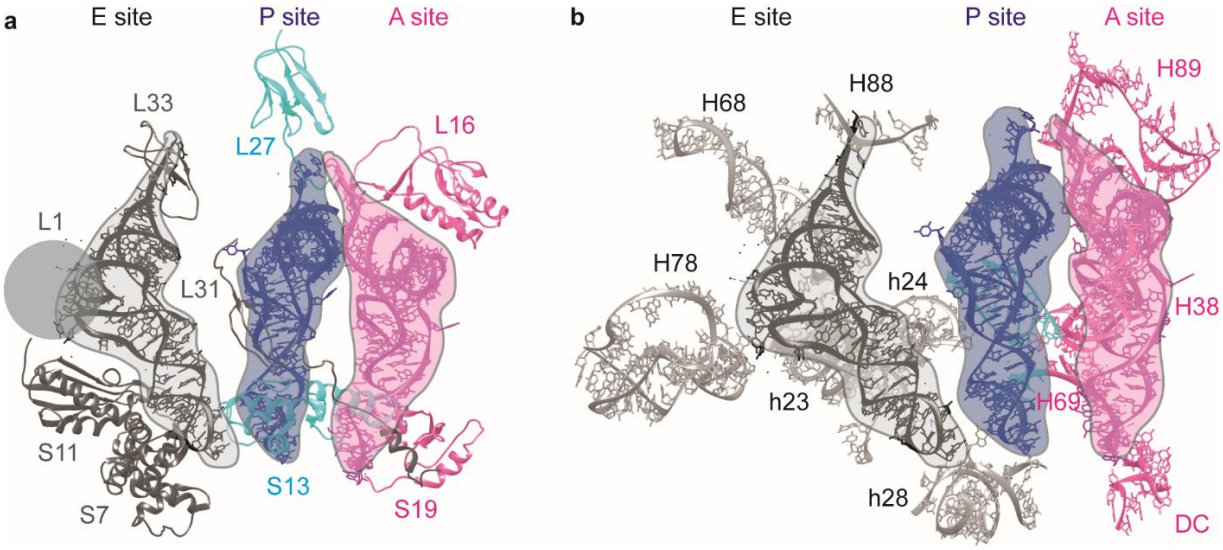

Figure 12. tRNA-ribosome interactions in the A, P and E sites. (a) Interaction network between ribosomal proteins (ribbons) and tRNAs in the ribosomal A, P and E sites. A-site (magenta), P-site (cyan) and E-site (grey) ribosomal proteins are shown (Jenner et al., 2005). The C-terminal tail of protein S9 is not shown because it is not resolved in the structure. tRNAs are partially masked for clarity. (b) Interaction network between rRNA (ribbon-stick) and tRNAs in the ribosomal A, P and E sites. Regions of A-site (magenta), P-site (cyan) and E-site (grey) rRNA is shown. The figure is adapted from PDB 4V6F (Jenner et al., 2010).

EF-G in reading frame maintenance during translocation

Recent studies revealed that EF-G contributes to the maintenance of the reading frame during translocation (Niblett et al., 2021; Peng et al., 2019; Zhou et al., 2019). X-ray crystallography studies reported PRE complexes containing two tRNAs in the A and P sites that moved spontaneously (in the absence of EF-G) into CHI state (Fig. 13a) (Zhou et al., 2019). Although it is for long known that translocation is an intrinsic property of the ribosome that can occur in the absence of EF-G (Fischer et al., 2010; Konevega et al., 2007), noteworthy in this study is that base pairing between the anticodon of the deacylated tRNA and the P-site codon is partially disrupted at the third position (Fig. 13a). The 3' nucleotide of the P-site codon is additionally flipped towards the A-site peptidyl-tRNA anticodon, resulting in a shift by –1 nucleotide (Fig. 13a). Notably, the SSU head domain is spontaneously swiveled to a higher degree (~21°) than observed in absence of EF-G (~3°) (Carbone et al., 2021; Fischer et al., 2010; Petrychenko et al., 2021; Rundlet et al., 2021; Zhang et al., 2009). In fact, similar swiveling angles (~18-21°) were previously observed only in EF-G–bound intermediate states of translocation (Carbone et al., 2021; Petrychenko et al., 2021; Ramrath et al., 2013; Rundlet et al., 2021; Zhou et al., 2014).

The study by Zhou et al., 2019 laid the foundations that EF-G plays a role in the maintenance of the mRNA reading frame during translocation. Further research corroborated and expanded it via mutational and kinetics studies of frameshifting-prone translocation (Niblett et al., 2021; Peng et al., 2019). Mutations on the highly conserved EF-G residues Q507 and H583 at the tip of domain 4 (Fig. 13b-c) increase –1 spontaneous frameshifting on slippery sequences *in vitro* by changing the timing and order of events during translocation (Peng et al., 2019). In this error-prone pathway, the tRNAs follow uncoupled movement, while the SSU head domain remains swiveled for a longer time, thus opening a time window that allows frameshifting to occur (Niblett et al., 2021; Peng et al., 2019). EF-G suppresses this error-prone pathway by driving fast and synchronized translocation (Peng et al., 2019). Together, these studies establish the intrinsic error-prone nature of the ribosome and the role of EF-G in reading frame maintenance during translocation.

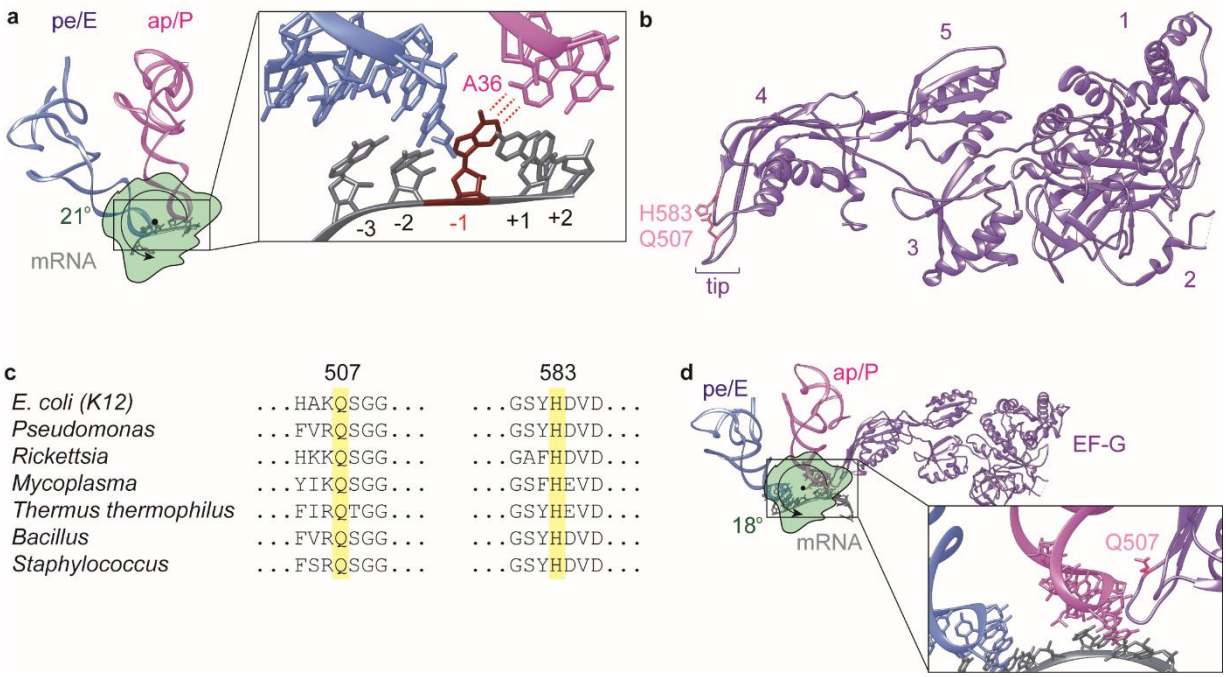

Figure 13. The role of EF-G in reading frame maintenance. (a) Crystal structure of PRE complex showing spontaneous transition to CHI state. Zoom-in shows interactions of the –1 mRNA nucleotide (red) disrupting interactions with the deacylated tRNA (blue) and developing interactions with the peptidyl-tRNA (magenta), resulting in –1 frameshifting. The SSU head shows a profound swiveling of 21° (green). The figure is adapted from PDB 6N1D (Zhou et al., 2019). (b) Cryo-EM structure of EF-G with the key residues Q507 and H583 highlighted in pink. The figure is adapted from PDB 4PJY (Petrychenko et al., 2021). (c) Multiple sequence alignment of loop I and II of domain 4 of EF-G from various bacterial species. Highlighted in yellow shade are the conserved residues Q507 and H583. Sequences are taken from UniProt entries P0A6M8 (*E. coli*), A4VHM7 (*Pseudomonas*), Q8KTB8 (*Rickettsia*), Q6MU82 (*Mycoplasma*), P13551 (*Thermus thermophilus*), P80868 (*Bacillus*) and P68790 (*Staphylococcus*). (d) Cryo-EM structural snapshot showing CHI tRNA conformations during EF-G—induced translocation. Zoom-in shows the interactions of key residue Q507 of EF-G (pink) with the tRNA-mRNA duplex. The figure is adapted from PDB 7PJY (Petrychenko et al., 2021).

2.6. Single molecule FRET to study frameshifting

Frameshifting has been approached by a wide range of techniques. Structural studies and *in vivo* and *in vitro* biochemical studies are able to demonstrate crucial interactions and conformations, as well as quantify the efficiency of spontaneous frameshifting. However, it would be desirable to monitor the real-time motions of the mobile elements of the ribosome during translocation in order to decipher the molecular mechanism of spontaneous ribosome frameshifting. Here, we present single molecule Förster resonance energy transfer (FRET) as a suitable technique to monitor molecular dynamics of the mobile elements of the ribosome during translocation.

Physical features of FRET

FRET is a mechanism of non-radiative transfer of energy from one light-interacting molecule (donor) to another (acceptor) (Roy et al., 2008). Electromagnetic radiation close to the absorption maximum of the donor leads to donor excitation. Subsequently, the energy can either be released in a non-radiative process (in the form of heat), in a radiative process (in the form of emitted photon) or transferred non-radiatively to a nearby acceptor (via FRET). If the energy is transferred to the acceptor via FRET, the acceptor is in turn excited. At the end, the energy is radiatively released via a photon from the acceptor. Due to dipole-dipole coupling mechanism, FRET depends on the intramolecular distance between donor and acceptor in the sixth power, thus being a highly distance-dependent process (Fig. 13a). The relationship between FRET efficiency (E_{FRET}) and intramolecular donor-acceptor distance (r) is described in the equation:

$$E_{FRET} = 1/[1+(r/R_0)^6]$$

where R_0 is the Förster radius, i.e. the intramolecular distance with E_{FRET}=0.5 (Fig. 14a). R_0 depends on the properties of donor and acceptor and it is calculated from the equation:

$$R_0 = 0.0211 \bullet n^{-4} \bullet Q_D \bullet \kappa^2 \bullet J$$

where n is the refractive index of the medium, Q_D the quantum yield of the donor in the absence of acceptor (i.e. the ratio of the emitted to absorbed photons, related to the brightness of the fluorophore), κ^2 the orientation factor and J the spectral overlap integral. The orientation factor κ^2 describes the relative orientation of the donor and acceptor during the excitation event. It depends on the angle between them and is assumed as 2/3, for freely rotating molecules which

have an isotropic orientation during the excitation event. The spectral overlap integral *J* represents the overlapping area between the donor emission and the acceptor absorption spectra, which is a prerequisite of FRET (Fig. 14b).

Due to donor and acceptor sensitization, i.e. the change in fluorescence intensity when they are found at a particular distance, the FRET efficiency can be calculated as the ratio of acceptor fluorescence to the total fluorescence of donor and acceptor. The fluorescence time courses of donor-acceptor couples shows negative correlation (anticorrelation), i.e. when acceptor fluorescence increases, donor fluorescence decreases and vice versa.

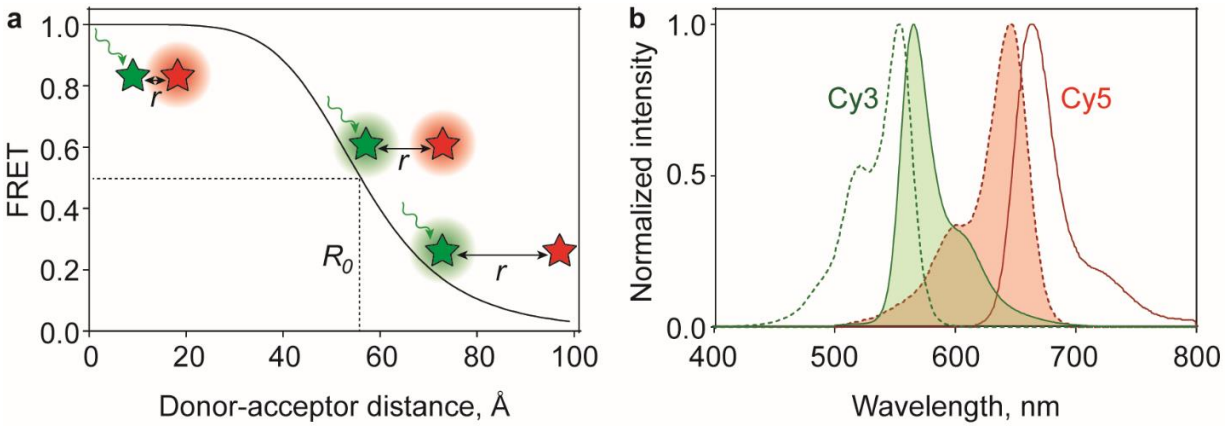

Figure 14. Key features of FRET. (a) Dependence of FRET on the distance (*r*) between donor (green star) and acceptor (red star). In small distances and upon excitation of the donor (green arrow), the rate of FRET is high leading to increased acceptor fluorescence (red halo), while in large distances, the rate of FRET is low leading to increased donor fluorescence (green halo). The graph is simulation of the Förster equation for the Cy3-Cy5 FRET pair (R_0=56Å). (b) Absorption (dotted lines) and emission (solid lines) spectra of donor Cy3 (green) and acceptor Cy5 (red). The overlap (yellow shade) of the emission spectrum of the donor (green shade) with the excitation spectrum of the acceptor (red shade) is a prerequisite for FRET. The absorption and emission spectra of Cy3 and Cy5 were generated using Fluorescence Spectra Viewer (ThermoFisher Scientific).

One ribosome at a time: smFRET using TIRF microscopy

Ribosome populations are frequently heterogeneous and subpopulations can follow distinct reaction pathways, as seen during frameshifting, where a fraction of ribosomes maintains the reading frame while another fraction shifts to the alternative frame (Caliskan et al., 2014; Chen et al., 2014; Peng et al., 2019). Monitoring these events using ensemble methods leads to averaging-out of the signals of individual ribosomes, thereby obscuring the potential alternative pathways and reversible intermediates. Therefore, the analysis of heterogeneous ribosome population requires detection of FRET signals at single molecule level.

Single molecule fluorescence techniques can monitor individual molecules either free in a tiny illuminated volume or immobilized on a surface. Surface immobilization is suitable for revealing distinct subpopulations of complexes, because it allows simultaneous detection of many individual molecules, and describing pre-steady state structural dynamics of macromolecular complexes, because different ligands can be exchanged inside the reaction chamber. Immobilization on microscope glass cover slips can be done via biotin-neutravidin interaction, nucleic acid hybridization, attraction between opposite charges or affinity binding, e.g. via antibodies or Ni^{2+}-covered surfaces (Roy et al., 2008). The detection of single fluorophores requires high resolution microscopy such as total internal reflection fluorescence (TIRF) microscopy combined with a very sensitive detector (Fig 15a) (Roy et al., 2008). In TIRF microscopy, the incident laser beam arrives at the coverslip at an angle greater than a critical value (θ_c) and is entirely reflected back (Fig. 15b) (Poulter et al., 2015). However, an electric component of the incident beam is transmitted into the glass coverslip in perpendicular direction to the interface (Fig. 15b). This component forms the evanescent wave which has the same wavelength as the incident beam but its intensity decays exponentially to the direction perpendicular to the interface and into the coverslip. Thus, a thin layer ~100-150 nm from the glass surface is illuminated, which selectively excites the immobilized molecules, while free molecules are outside the evanescent field and, thus, not excited (Fig. 15b). Therefore, TIRF illumination has a superior signal-to-noise ratio compared to conventional epi-fluorescence microscopy (i.e. where the incident beam arrives at 0° angle and traverses completely towards the second medium illuminating the whole sample) and allows the detection of individual molecules.

The emitted photons from donor and acceptor fluorescence are separated via dichroic mirrors and are subsequently directed towards an electron-multiplying charge-coupled device

(EM-CCD, Fig. 15a). The CCD image sensors consist of photosensitive semiconductors that receive the energy from the incident beam (Fig. 15a). The electrons of the semiconductor are then collected to a capacitor in the form of charge that is proportional to the amount of photons. The charges from individual capacitor cells are transferred eventually to the amplifier that creates an electrical voltage as output. In the present study, double-labeled ribosome complexes were immobilized via biotin-neutravidin interactions with the 5'-biotinylated end of the mRNA on PEG-biotin functionalized coverslips (Fig. 15b) (Adio et al., 2015). The donor fluorophore is excited using a laser beam with a wavelength of 561 nm, close to the donor absorption maximum, and the fluorescence intensities of donor and acceptor are monitored simultaneously in a time course (Fig. 15c). For each time point, FRET is calculated as the ratio of acceptor fluorescence intensity (FI) in total fluorescence intensity of donor and acceptor, $FI_{acceptor}/(FI_{acceptor}+FI_{donor})$ (Fig. 15c).

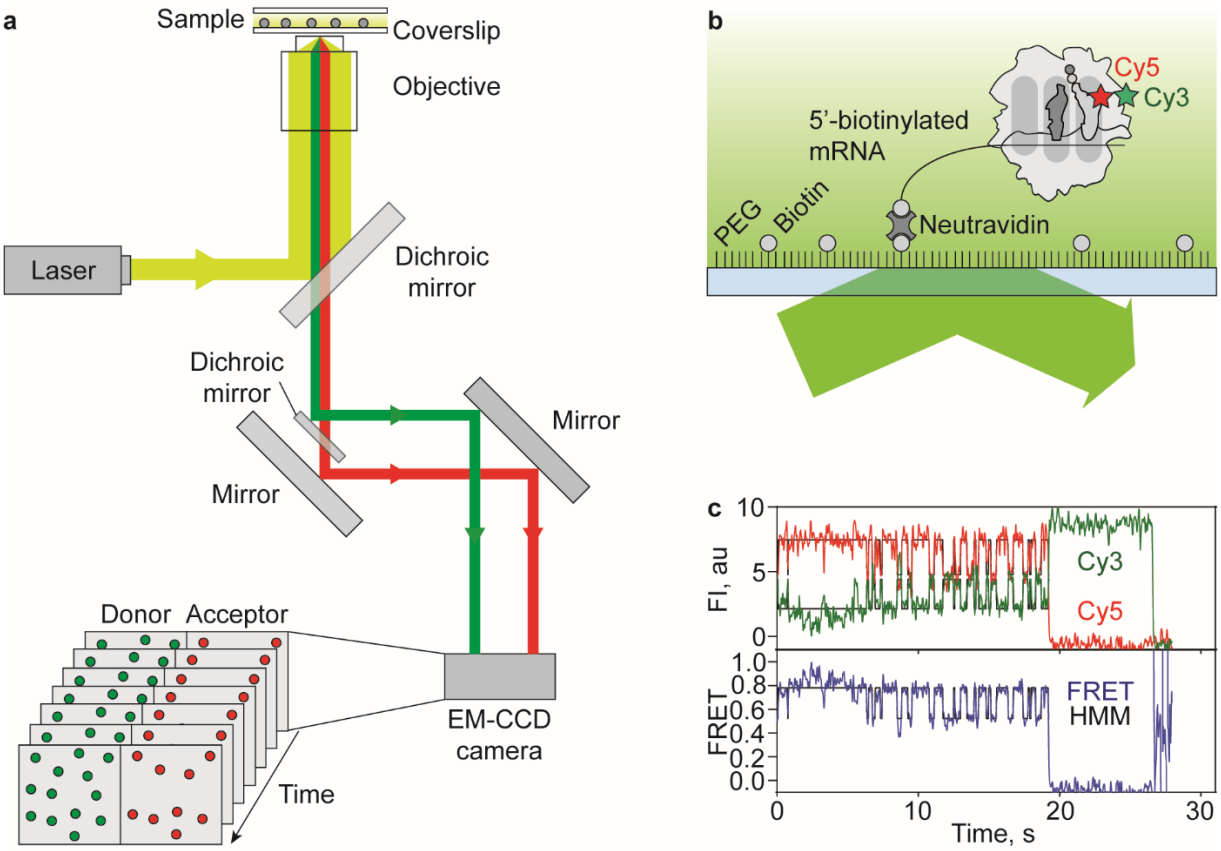

Figure 15. Objective-based TIRF microscopy for single molecule detection. (a) Schematic representation of objective-based TIRF microscopy setup. The excitation beam (yellow) is guided towards the sample where it reaches the coverslip at a super-critical angle. The emission fluorescence of donor (green) and acceptor (red) are separated by dichroic mirrors and guided towards an EM-CCD camera chip, where they are displayed in separate channels. The figure is created with input from (Roy et al., 2008). (b) smFRET setup of the present study. The ribosome (grey) is labelled with donor Cy3 (green star) and acceptor Cy5 (red star) in strategic positions and immobilized via biotin-neutravidin interactions of the functionalized coverslip (sky blue) and the 5'-biotinylated mRNA. (c) Representative smFRET time trace showing donor Cy3 (green) and acceptor Cy5 (red) fluorescence intensities (FI, arbitrary units, au), calculated FRET (blue) and Hidden Markov fitting (HMM) of the data (black). The colors for donor and acceptor FI, FRET and HMM fit are the same throughout the thesis.

3. Scope of the thesis

Translocation is a crucial phase for reading frame maintenance and EF-G plays an important role by guiding the tRNA-mRNA duplex intact through the ribosome. Recent studies suggested that slow translocation is a hallmark of frameshifting. However, it remains unclear how the peptidyl- and deacylated tRNAs move during translocation on slippery sequences, how non-canonical tRNA motions lead to frameshifting, when frameshifting occurs in the translocation reaction coordinate and how the ribosome dynamics affects tRNA movement leading to frameshifting. Here, we use smFRET to follow the tRNA trajectories during translocation on slippery mRNA. we correlate our findings with frameshifting by using error-prone EF-G mutants carrying point mutations at the key residue Q507. Specifically, we address the following:

- We describe the trajectory of the peptidyl-tRNA from the A to the P site during slow translocation on slippery mRNA and correlate the slow translocation of the peptidyl-tRNA with the incorporation of the –1-frame tRNA on the slippery mRNA.
- We show that the trajectory of the deacylated tRNA from the P to the E site during translocation is not affected during spontaneous frameshifting.
- We narrow down the time window of spontaneous frameshifting by showing that delay in translocation prior to the frameshifting-prone stage due to the presence of the non-hydrolysable GTP analog GTPγS or the antibiotic spectinomycin (Spc) do not lead to spontaneous frameshifting.
- Finally, we demonstrate that the SSU head domain is a determinant of spontaneous frameshifting, because it allows the peptidyl-tRNA to sample the 0- and –1-frame codons.

Together, our data show that spontaneous ribosome frameshifting is a result of altered choreography of ribosome and tRNA movements during translocation on slippery mRNA. We are able to describe a complete mechanistic model of spontaneous ribosome frameshifting, including intermediate states and reaction rates during translocation.

4. Materials and Methods

4.1. Materials, chemicals & enzymes

Table 1. Materials, chemicals and enzymes used in this study.

Glass coverslips and objective slides	Menzel-Gläser
GTP, GTPγS	Jena Bioscience
Phosphoenol pyruvate (PEP)	Sigma-Aldrich
N1-[3-(trimethoxysilyl)propyl]diethylenetriamine (DETA)	Sigma-Aldrich
Biotin-PEG-NHS, MeO-PEG-NHS	Iris Biotech GmbH
[^{3}H]fMet, [^{14}C]Gly, [^{14}C]Ala, [^{14}C]Lys	Hartmann Analytic, PerkinElmar
Scintillation cocktail Ultima Gold™ XR	PerkinElmar
6-hydroxy-2,5,7,8-tetramethylchroman-2-carboxylic acid (Trolox)	Sigma-Aldrich
Methylviologen (MV)	Sigma-Aldrich
Neutravidin (NA)	Thermo Scientific
Protocatechuic acid (PCA)	Sigma-Aldrich
Spermidine	Sigma-Aldrich
Putrescine	Carl Roth
Fusidic acid (FA)	Sigma-Aldrich
Spectinomycin (Spc)	Sigma-Aldrich
Trifluoroacetic acid (TFA)	Sigma-Aldrich
Acetonitrile (ACN)	Merck
Potassium hydroxide (KOH)	Merck
Methanol	Carl Roth
Activated charcoal	Merck
Cy™5 mono NHS ester	Cytiva
Cy™5 maleimide mono-reactive dye	GE Healthcare
Cy™3 maleimide mono-reactive dye	GE Healthcare
BlackHole quencher 2 NHS ester	Biosearch Technologies
Pyruvate kinase (PK)	Roche
Pseudomonas protocatechuic acid dehydrogenase (PCD)	Sigma-Aldrich
Puromycin (Pmn)	Sigma-Aldrich

4.2. Buffers

Table 2. Composition of buffers used in this study.

Translation and frameshifting assay	
$TAKM_7$	50 mM Tris-HCl, pH 7.5 at 37°C or room temperature 70 mM NH_4Cl 30 mM KCl 7 mM $MgCl_2$
Ribosome complex purification for smFRET	
$TAKM_{20}$	50 mM Tris-HCl, pH 7.5 at 37°C 70 mM NH_4Cl 30 mM KCl 20 mM $MgCl_2$
$TAKM_{21}$	50 mM Tris-HCl, pH 7.5 at 37°C 70 mM NH_4Cl 30 mM KCl 21 mM $MgCl_2$
smFRET experiments	
$TAKM_{15}$	50 mM Tris-HCl, pH 7.5 at room temperature 70 mM NH_4Cl 30 mM KCl 15 mM $MgCl_2$
$TAKM_7$	50 mM Tris-HCl, pH 7.5 at room temperature 70 mM NH_4Cl 30 mM KCl 7 mM $MgCl_2$
HPLC peptide separation	
Buffer A	0.1% TFA
Buffer B	0.1% TFA 65% ACN

4.3. Columns

Table 3. Commercially available columns used in this study.

Column	Source	Function
Protino Ni-IDA 2000 Packed Columns	Macherey-Nagel	Gly-tRNA^{Gly} preparation
LiChrospher 100 RP-8 (5µm) LiChroCART 250-4	Merck	HPLC peptide separation
HiTrap SP HP	GE Healthcare	Protein purification
Resource S	Cytiva	Protein purification

4.4. mRNAs

The following 5'-biotinylated mRNAs were used for biochemical and single molecule experiments. Sequence is written in 5'→3' direction, coding sequence is shown in bold, slippery sequence in red, Shine-Dalgarno sequence is underlined.

Table 4. mRNA sequences used in this study.

mRNA	5'→3' sequence	Source
+SS fMGKF	Biotin,CAACCUAAAACUUACACACCCGGCAAGGAGG UAAAUA**AUGGGAAAGUUC**AUUACCUAA	IBA Lifesciences
-SS fMFKF	Biotin,CAACCUAAAACUUACACACCCGGCAAGGAGG UAAAUA**AUGUUUAAGUUC**AUUACCUAA	Eurofins
+SS fMAKKF	Biotin,CAACCUAAAACUUACACACCCGGCAAGGAGG UAAAUA**AUGGCAAAAAAGUUC**AUUACCUAA	IBA Lifesciences
-SS fMAKKF	Biotin,CAACCUAAAACUUACACACCCGGCAAGGAGG UAAAUA**AUGGCUAAGAAGUUC**AUUACCUAA	IBA Lifesciences

4.5. Instruments, software & databases

Table 5. Instruments, software and databases used in this study.

Instruments	
MilliQ Advantage A10 water purification system	Merck
Lab pH meter inoLab® pH720	WTW
Water bath E100	Lauda-Brinkmann
Centrifuge 5424 and 5415R	Eppendorf AG
ÄKTA FPLC Äkta Purifier Plus	GE Healthcare
Liquid scintillation counter	PerkinElmer
High Performance Liquid Chromatography	Waters
Optima Tm MAX-XP ultracentrifuge	Beckman Coulter
Rotor TLS 55	Beckman Coulter
Spectrophotometer Lambda Bio +	PerkinElmer
FEMTO plasma cleaner	Diener Electronic GmbH
IX 81 inverted microscope and PLAPON 60 1.45 numerical aperture objective	Olympus
561 nm solid-state laser, 25 mW	Olympus Soft Imaging Solutions GmbH
CCD-C9100-13 camera	Hamamatsu
dual view micro imager DV2 image splitter	Photometrics
HQ 605/40, HQ 680/30 filters	Chroma Technology
Software	
GraphPad Prism 8	GraphPad software
UCSF Chimera	RBVI University of California
Matlab R2011b	MathWorks
vbFRET software	http://vbfret.sourceforge.net/ (Bronson et al., 2009)
xCellence rt image acquisition software	Olympus

Public databases	
Protein Data Bank (PDB)	Research Collaboratory for Structural Bioinformatics, USA
PRFdb	University of Maryland, USA (Belew et al., 2008)
Universal Protein Resource (UniProt)	EMBL-EBI, SIB, PIR

4.6. Ribosomes, translation factors and tRNAs

E. coli ribosomes, f[^{3}H]Met-tRNA^{fMet}, [^{14}C]Ala-tRNA^{Ala}, Lys-tRNA^{Lys}, Phe-tRNA^{Phe}, Val-tRNA^{Val}, IFs, EF-Tu and EF-G were prepared as previously described (Holtkamp et al., 2014; Milon et al., 2007; Rodnina and Wintermeyer, 1995). [^{14}C]Gly-tRNA^{Gly} was prepared from total tRNA from *E. coli* by *in vitro* aminoacylation with [^{14}C]Gly. TC was formed by mixing EF-Tu (3-fold excess over total tRNA) with GTP (1 mM), phosphoenolpyruvate (3 mM) and pyruvate kinase (0.5%) in TAKM$_7$, incubation for 15 min at 37°C, addition of [^{14}C]Gly-tRNA^{Gly} (3 µM) and loading onto Protino Ni-IDA 2000 Packed Columns. [^{14}C]Gly-tRNA^{Gly} was purified by phenolization followed by ethanol precipitation as described (Korniy et al., 2019).

4.7. Site-specific labeling of ribosomes & tRNAs

Reconstitution of L11-Cy3 70S ribosomes

Protein L11 was expressed in *E. coli* BL21(DE3) induced with isopropyl-β-D-thiogalactoside (IPTG, 1 mM) and lysed by sonication in buffer (50 mM HEPES, 10 mM $MgCl_2$, 10 mM NH_4Cl, 1 mM dithiothreitol, 0.5 mM EDTA, pH 7.2). L11-containing inclusion bodies were solubilized in the same buffer containing 6 M urea, dialysis against 100 volumes of the same buffer and L11 was purified by fast protein liquid chromatography (FPLC) using a HiTrap SP HP column using a linear gradient of 10–500 mM NH_4Cl in the same buffer with 6 M urea. Cy3-labeling of L11 at position C38 was performed by adding 3-fold excess of Cy3-maleimide dissolved in dimethylsulfoxide (DMSO) and incubating for 12 h at 4°C in the same buffer containing 0.5 M NH_4Cl. Excess dye was removed on an FLPC HiTrap SP HP column using a linear gradient of 10–500 mM NH_4Cl. For L11 refolding, Vivaspin 5,000 concentrator was used to gradually replace the buffer with 50 mM HEPES, 10 mM $MgCl_2$, 300 mM NH_4Cl, 1 mM dithiothreitol, 0.5 mM EDTA, pH 7.2, 25% glycerol (Adio et al., 2015). Ribosomes lacking protein L11 (70S ΔL11) were purified from *E. coli* AM68 as previously described (Rodnina and Wintermeyer, 1995).

L11-Cy3 70S reconstitution was carried out by mixing ΔL11 70S with 10-fold excess of L11-Cy3 and incubation for 45 min at 45°C in $TAKM_{21}$. L11-Cy3 70S were purified by sucrose cushion centrifugation (1.1 M sucrose in $TAKM_{21}$) and dissolved in $TAKM_7$. Concentration was determined by absorption at 260 nm.

Reconstitution of S13-Cy3 SSU

A single-cysteine variant of protein S13 (C85S P112C) was expressed in *E. coli* BL21(DE3) induced with IPTG (1 mM) and lysed by sonication in buffer (50 mM HEPES pH 7.5, 150 mM KCl, 5% glycerol, 6 mM β-mercaptoethanol). S13-containing inclusion bodies were dissolved in buffer (50 mM HEPES pH 7.5, 300 mM KCl, 5% glycerol, 6 mM β-mercaptoethanol, 8 M urea). S13 was diluted in the same buffer without KCl and purified by FPLC using a HiTrap SP HP column with a linear gradient of 50–1000 mM KCl in the same buffer with 6 M urea, followed by a Resource S column with the same KCl gradient. Cy3-labeling of S13 at C112 was performed by adding 3-fold excess of Cy3-maleimide dissolved in DMSO and incubating for 2 h at room temperature in the same buffer supplemented with 0.5 M NH_4Cl. Excess dye was removed on a HiTrap SP HP column using the same salt gradient as above. S13(C112-Cy3) was dialyzed into 50 mM HEPES, 20 mM $MgCl_2$, 400 mM KCl, pH 7.5, 5% glycerol, 6 mM mercaptoethanol, concentrated and stored at -80°C. 30S subunits lacking protein S13 (30S ΔS13) were purified from *E. coli* AM68 as previously described (Belardinelli et al., 2016a; Cunha et al., 2013). 30S S13-Cy3 reconstitution was performed by mixing ΔS13 30S with 1.5-fold excess of S13-P112C-Cy3 and incubation at 42°C for 30 min in $TAKM_{20}$ buffer. Purification of S13-Cy3 30S was performed by sucrose cushion centrifugation (0.9 M sucrose in $TAKM_{21}$) and pellets were dissolved in $TAKM_7$. Concentration was determined by absorption at 260 nm.

Reconstitution of L33-Cy5 LSU

50S subunits lacking protein L33 (50S ΔL33) and a single cysteine variant of protein L33 (P31C) were purified and labeled as previously described (Belardinelli et al., 2016a). 50S L33-Cy5 reconstitution was performed by mixing ΔL33 50S with 1.1-fold excess of L33-P31C-Cy5 and incubation for 90 min at 37°C in buffer (50 mM HEPES, pH 7.5, 400 mM KCl, 20 mM $MgCl_2$ and 6 mM mercaptoethanol). Purification of 50S-L33-Cy3 was performed by sucrose cushion centrifugation (0.9 M sucrose in $TAKM_{21}$) and pellets were dissolved in $TAKM_7$. Concentration was determined by absorption at 260 nm.

Labeling of $tRNA^{Lys}$, $tRNA^{Phe}$ and $tRNA^{Val}$

Cy5-labeling of $tRNA^{Phe}$ and $tRNA^{Val}$ and Cy5- or Black Hole Quencher® 2 (BHQ2) (Chen et al., 2012) labeling of $tRNA^{Lys}$ was carried out at the 3-amino-3-carboxypropyl group (acp) at U47 by mixing *E. coli* tRNA with 100-fold excess of Cy5 or BHQ2 NHS ester in 50 mM HEPES, pH 8.5, for 4 h at 37°C. tRNA(acp47-Cy5) was extracted by phenolization and ethanol precipitation, aminoacylated and purified by HPLC (Adio et al., 2015; Milon et al., 2007).

4.8. Single molecule FRET and data analysis

Ribosome complex purification for smFRET

To prepare PRE complex carrying L11-Cy3 and pept-$tRNA^{Lys}$-Cy5, ICs were prepared by mixing L11-Cy3 70S ribosomes (2 µM) with 3-fold excess of IF1, IF2, IF3, mRNA and [^{3}H]fMet-$tRNA^{fMet}$ and GTP (1mM) in $TAKM_7$ and incubation for 30 min at 37°C. TCs were prepared by incubating EF-Tu (3-fold excess over tRNA) with GTP (1 mM), phosphoenolpyruvate (3 mM) and pyruvate kinase (0.5%) in $TAKM_7$ for 15 min at 37°C and subsequent addition of [^{14}C]Gly-$tRNA^{Gly}$ (10 µM) or [^{14}C]Phe-$tRNA^{Phe}$ (10 µM) according to the mRNA sequence. IC (1 µM) was mixed with TC (5 µM) and EF-G–GTP (1 µM) and incubated for 5 min at 37°C. The POST complexes were purified by sucrose cushion centrifugation (1.1 M sucrose in $TAKM_{21}$), pellets were dissolved in $TAKM_7$ and the concentration was determined by [^{14}C]Gly or [^{14}C]Phe scintillation counting. Purified POST complex (0.1 µM) was incubated with 3-fold excess of TC (EF-Tu–GTP–Lys-$tRNA^{Lys}$-Cy5) in $TAKM_7$ for 5 min at 37°C. The PRE complex carrying fMGK-$tRNA^{Lys}$-Cy5 or fMFK-$tRNA^{Lys}$-Cy5 in the A site and $tRNA^{Gly}$ or $tRNA^{Phe}$ in the P site was immobilized in the coverslip as described below.

To prepare PRE complexes carrying S13-Cy3 and pept-$tRNA^{Lys}$-Cy5, 30S S13-Cy3 (2 µM) were incubated in $TAKM_{20}$ at 37°C for 30 min and used to prepare ICs as described above (50S in 1.5-fold excess over 30S, IFs, mRNA and [^{3}H]fMet-$tRNA^{fMet}$ in 3-fold excess over 30S). TCs were prepared as described above using [^{14}C]Ala-$tRNA^{Ala}$ (10 µM). IC (1 µM) was mixed with TC (5 µM) and EF-G–GTP (1 µM) and incubated for 5 min at 37°C. The POST complexes were purified by sucrose cushion centrifugation (1.1 M sucrose in $TAKM_{21}$), pellets were dissolved in $TAKM_7$ and the concentration was determined by [^{14}C]Ala scintillation counting. Purified POST complex (0.1 µM) was incubated with 3-fold excess of TC (EF-Tu—Lys-$tRNA^{Lys}$-Cy5—GTP) and EF-G—GTP (0.5 µM) and incubated at 37°C for 5 min. The POST complex

was immobilized in the cover slip as described below and excess of TC and EF-G was washed away. EF-Tu–GTP–Lys-tRNA^{Lys} was then added to the flow chamber.

To prepare PRE complexes carrying S13-Cy3/L33-Cy5 and pept-tRNA^{Lys}, 30S S13-Cy3 were incubated in TAKM$_{20}$ at 37°C for 30 min and used to form ICs as described above. TCs were prepared as described above using [^{14}C]Gly-tRNA^{Gly} or [^{14}C]Phe-tRNA^{Phe}, according to the mRNA sequence. IC (1 µM) was mixed with TC (5 µM) and EF-G–GTP (1 µM) and incubated for 5 min at 37°C. The POST complexes were purified by sucrose cushion centrifugation (1.1 M sucrose in TAKM$_{21}$), pellets were dissolved in TAKM$_7$ and the concentration was determined by [^{14}C]Gly or [^{14}C]Phe scintillation counting, respectively. Purified POST complex (0.1 µM) was then mixed with TC (EF-Tu—Lys-tRNA^{Lys}—GTP) and incubated at 37°C for 5 min. The PRE carrying fMGK-tRNA^{Lys} or fMFK-tRNA^{Lys} in the A site and tRNA^{Gly} or or tRNA^{Phe} in the P site complex was immobilized in the coverslip as described below.

Objective slide and cover slip preparation

Cover slips and objective slides were treated via sonication in 1 M KOH for 10 min, plasma cleaner, incubation with 3.9 mM DETA and 1.7 mM acetic acid for 5 min, followed by 20 min at 110°C. Subsequently, they were treated with 20 mM PEG-NHS and 0.2 mM Biotin-PEG-NHS in 100 mM KBO_3 for 1 h at room temperature, followed by drying at 50°C and storage under vacuum. Flow chambers were assembled by attaching cover slips on objective slides with double-sided tape.

Sample preparation and TIRF microscopy

All single molecule experiments were carried out in TAKM$_7$ containing 8 mM putrescine and 1 mM spermidine at 22°C. Flow chambers were incubated for 5 min at room temperature with the same buffer complemented with 10 mg/ml BSA and 1 µM neutravidin, followed by washing with 5-fold volume excess of the same buffer containing 1 mg/ml BSA. Ribosome complexes were diluted to 1nM, added to the flow chamber and incubated for 5 min at room temperature. Images were recorded after manual addition of imaging buffer (same buffer complemented with 2.5 mM PCA, 50 nM PCD, 2 mM Trolox and 1 mM MV) to the flow chamber. For translocation experiments, 0.1 µM EF-G and 1 mM GTP or GTPγS to the imaging buffer. In the experiments with FA, Pmn or Spc, 200 µM FA, 1 mM Pmn or 1 mM Spc were added respectively to the sample and imaging buffer. Labelled tRNAs were added to the imaging buffer at final

concentration of 10 nM. Imaging was performed on an inverted microscope (Table 5). Cy3 fluorescence was excited by a 561 nm laser and images were recorded with an electron multiplying charge-coupled device (em-CCD) camera (Table 5). Color channels were separated using an image splitter. Movies were recorded at 30.3 frames per s (33 ms per frame). For the S13-L33 FRET using EF-G(Q507D), movies were recorded at a rate of 10 frames per s (100 ms per frame).

Data analysis

Fluorescence time courses for donor (Cy3) and acceptor (Cy5) were extracted from recorded frames using a custom-made Matlab software (Adio et al., 2015). A semi-automated algorithm was used to select anti-correlated fluorescence traces exhibiting characteristic single fluorophore intensities (Adio et al., 2015). Bleed-through of Cy3 signal into the Cy5 channel was corrected using an experimentally determined coefficient of 0.13. FRET efficiency was calculated as the ratio of measured emission fluorescence intensities, $F.I._{Cy5}/(F.I._{Cy3}+F.I._{Cy5})$. Trajectories were truncated to remove photobleaching and photoblinking events and fitted by Hidden Markov model using the vbFRET software package. Two-dimensional contour plots were generated from raw time-resolved FRET trajectories using a custom-made Matlab software based on in-built toolbox. All FRET values were compiled into a histogram, which fitted to a sum of Gaussian function. Mean values (μ) and s.d. for individual Gaussian distributions were derived using an unconstrained nonlinear minimization procedure (fminsearch, Matlab, R2011b). Post-synchronization was performed relative to the first transition to FRET≤ 0.1 than the lowest value of the PRE state, if not stated otherwise. FRET changes in idealized trajectories that were smaller than the s.d. of the Gaussian distribution of the FRET states were not considered as transitions because they were not distinguished from the noise. Dwell times of different FRET states of fluctuating traces were extracted from idealized trajectories, compiled into dwell time histogram and fitted to an exponential function, $y=y_0+Ae^{-t/\tau}$. Rates (k) were calculated as taking the inverse of dwell times (τ). The observed rates were corrected, when necessary, according to $k_{corrected}=k_{observed}-k_{photobleach}-1/T$, where $k_{observed}$ the rate of the exponential function, T observation time, $k_{photobleach}=0.03\pm0.01\ s^{-1}$ (derived from independent experiments, Fig. 35).

4.9. Frameshifting assay

ICs were formed as described above using unlabeled components and purified by sucrose cushion centrifugation (1.1 M sucrose in $TAKM_{21}$). Pellets were dissolved in $TAKM_7$ buffer and the concentration was determined by f[^{3}H]Met scintillation counting. TCs were prepared as described above with subsequent addition of aminoacyl-tRNAs (5-fold excess to 70S) cognate to the mRNA coding sequence in 0 and –1 frame. Translation was carried out by mixing IC (0.1 µM) with TCs (5-fold excess over IC) and EF-G (1 µM) with GTP or GTPγS (1 mM) at 22°C or 37°C for 2 min. In the experiments with Spc, Spc was added to final concentration of 1mM. Reaction was quenched with 0.5 M KOH and the peptides were released by hydrolysis at 37°C for 30 min, neutralized by adding 1/10 volume of glacial 100% acetic acid and analyzed by reversed-phase high performance liquid chromatography using a 0 to 65% acetonitrile gradient in 0.1% trifluoroacetic acid (Peng et al., 2019). The 0- and −1-frame products were quantified by [^{14}C]Gly or [^{14}C]Ala scintillation counting.

5. Results

Results of the study have been published (Poulis et al., 2022). No reuse/reprint permission required by authors.

5.1. Translocation of pept-tRNA on slippery mRNA

First, we followed the trajectory of the pept-tRNA from the A to the P site during translocation. To that end, we monitored FRET between ribosomal protein L11 of the LSU labeled with Cy3 (L11-Cy3) and fMet-Gly-Lys-tRNA^{Lys} labeled with Cy5 (pept-tRNA^{Lys}-Cy5, Fig. 16a) (Adio et al., 2015; Chen et al., 2011a). This FRET pair has been previously used in smFRET experiments to characterize the kinetics and intermediate states during translocation from the A to the P site (Adio et al., 2015; Chen et al., 2011a; Wang et al., 2007). In PRE complexes, the distance between L11 and pept-tRNA is ~50Å when the pept-tRNA is found in the A/A or A/P conformation and increases to ~66Å when it transits to the A/P* conformation (Fig. 16a-b) (Dunkle et al., 2011; Fischer et al., 2010; Jenner et al., 2010; Petrychenko et al., 2021; Rundlet et al., 2021; Zhang et al., 2009). These distances give estimated FRET efficiencies of ~0.8 (A/A and A/P) and ~0.6 (A/P*, Fig. 16c) (Adio et al., 2015; Chen et al., 2011a). Respectively, in the POST complex, where the peptidyl-tRNA is accommodated in the P site (P/P), the distance with L11 increases to ~80Å, giving an estimated FRET efficiency of ~0.1-0.2 (Fig. 16a-c) (Adio et al., 2015; Carbone et al., 2021; Chen et al., 2011a; Fischer et al., 2010; Gao et al., 2009; Rundlet et al., 2021). Therefore, the distance change during translocation is within the dynamic range of Cy3-Cy5 FRET pair and allows the identification of discernible translocation intermediates, such as the CHI state that has an intermediate L11-tRNA distance between PRE and POST (Fig. 16b, c) (Adio et al., 2015; Chen et al., 2011a; Fischer et al., 2010; Petrychenko et al., 2021; Ramrath et al., 2013; Zhou et al., 2014).

We reconstituted PRE complexes assembled on two mRNAs: one carrying the heptameric slippery sequence G GGA AAG and a non-slippery control mRNA where the GGA codon is replaced by UUU (Fig. 16d). On the slippery mRNA, the pept-tRNA^{Lys} can base pair with the AAG in the 0 frame and AAA in the –1 frame (Fig. 16d). In contrast, on the non-slippery mRNA, frameshifting is prevented because base pairing of the pept-tRNA^{Lys} with the –1-frame UAA codon is unfavorable due to first-position U•U mismatch (Fig. 16d) (Bock et al., 2019). L11-Cy3 PRE complexes carrying a deacylated tRNA^{Gly} in the P site and pept-tRNA^{Lys}-Cy5 in the A site were immobilized on a coverslip and were the start point of the experiments.

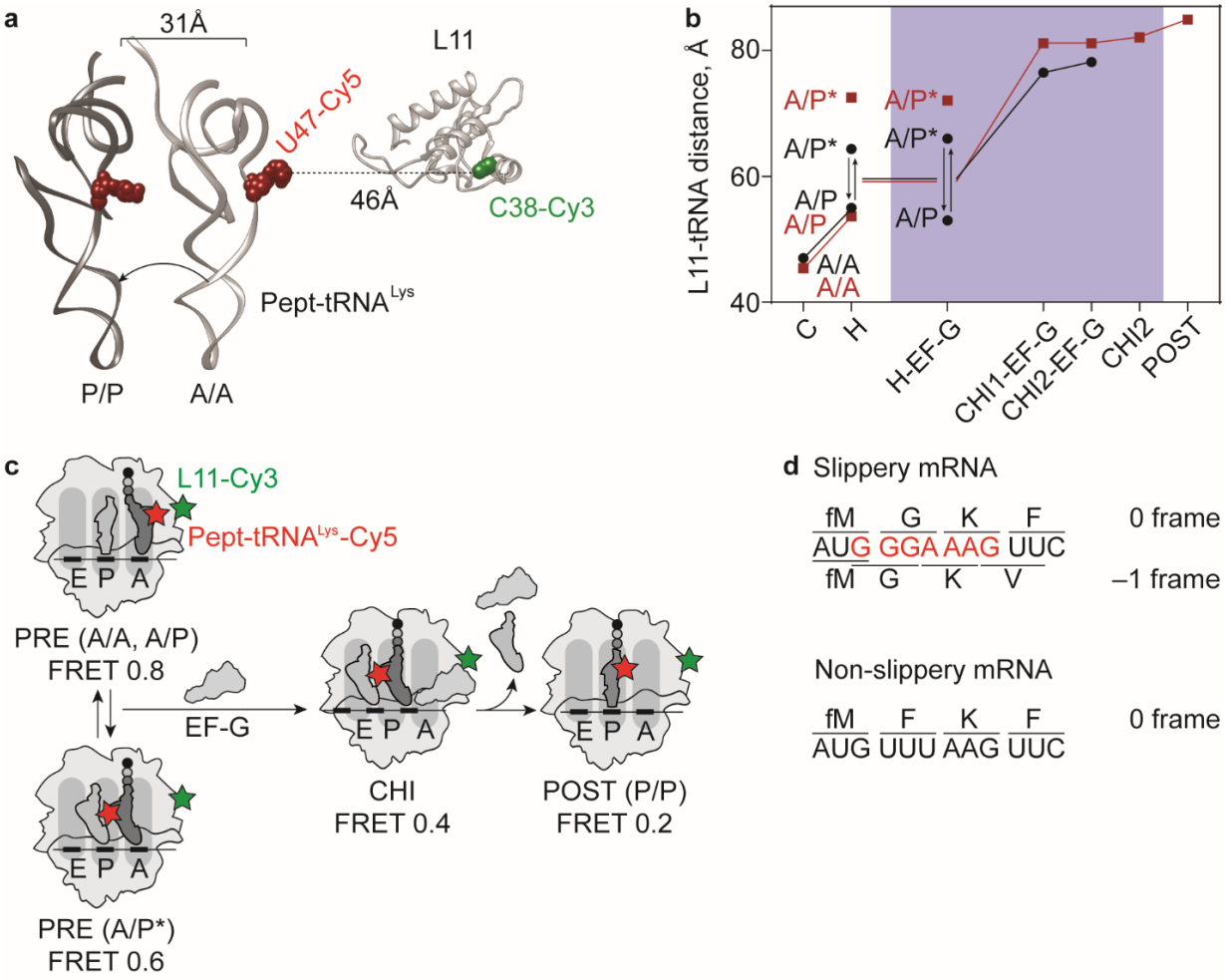

Figure 16. smFRET between L11 and pept-tRNA^{Lys} during translocation. (a) Comparison of L11-tRNA distance in the A/A (start point of translocation) and P/P (end point of translocation) tRNA conformation. The positions at L11 and pept-tRNA where the fluorophores are attached are indicated in green (for Cy3) and red (for Cy5). The figure was adapted from PDB 7N1P (A/A) and 7N31 (P/P) (Rundlet et al., 2021). (b) L11-tRNA distance change in consecutive structural snapshots of tRNA translocation, based on time-resolved cryo-EM studies. Black circles and connecting line are from (Petrychenko et al., 2021) and maroon squares and connecting line are from (Carbone et al., 2021). The translocation phase is shown in blue shade. (c) Schematic of pept-tRNA translocation from the A to the P site, catalyzed by EF-G. (d) mRNA sequences used in this study. The slippery mRNA carries a slippery sequence (red) that encodes for fMGKF peptide in 0 frame and fMGKV peptide in –1 frame. Non-slippery mRNA does not allow shift into the –1 frame due to replacement of GGA with UUU.

Pept-tRNA conformations in PRE and POST complex

First, we determined the smFRET of the pept-tRNA^{Lys}-Cy5 in PRE complexes in the absence of EF-G. Three types of smFRET traces were observed. The first type shows high FRET values without transitions to higher or lower FRET (Fig. 17a). The second type shows lower FRET values without transitions to higher or lower FRET (Fig. 17b). The third type shows reversible transitions (fluctuations) between high and lower FRET values (Fig. 17c). 2D FRET population distribution histogram of smFRET traces revealed two Gaussian distributions with FRET values of 0.77±0.09 and 0.59±0.08 (Fig. 17d, FRET states are expressed as μ±s.d. of the Gaussian distribution of the FRET values, where μ is the arithmetic mean and s.d. the standard deviation of the distribution). The high FRET values are in agreement with the small distance between L11 and pept-tRNA^{Lys} in the PRE complex (Carbone et al., 2021; Petrychenko et al., 2021; Rundlet et al., 2021). According to structural and smFRET studies, the FRET 0.8 state represents the A/A and A/P conformations, while the FRET 0.6 state represents the A/P* conformation (Fig. 17d). The pept-tRNA^{Lys}-Cy5 spontaneously interconverts between the A/A, A/P and A/P* conformations. In order to calculate the transition rates between FRET 0.8 and 0.6 states, we extracted from the fluctuating traces the dwell time of the FRET 0.8 before transiting to the FRET 0.6 state and the dwell time of the FRET 0.6 before transiting to the FRET 0.8 state. Dwell-time distribution and fitting with single exponential function (Methods) reveal the transition rate from the FRET 0.8 to 0.6 state ($k_{0.8\rightarrow0.6}$) and the reverse rate from the FRET 0.6 to 0.8 state ($k_{0.6\rightarrow0.8}$) (Fig. 17e). The two rates are at the same range indicating the equilibrium-like metastable behavior of the pept-tRNA in the PRE complex (Fig. 17e), in agreement with previous smFRET studies (Adio et al., 2015; Chen et al., 2011a; Geggier et al., 2010; Munro et al., 2009).

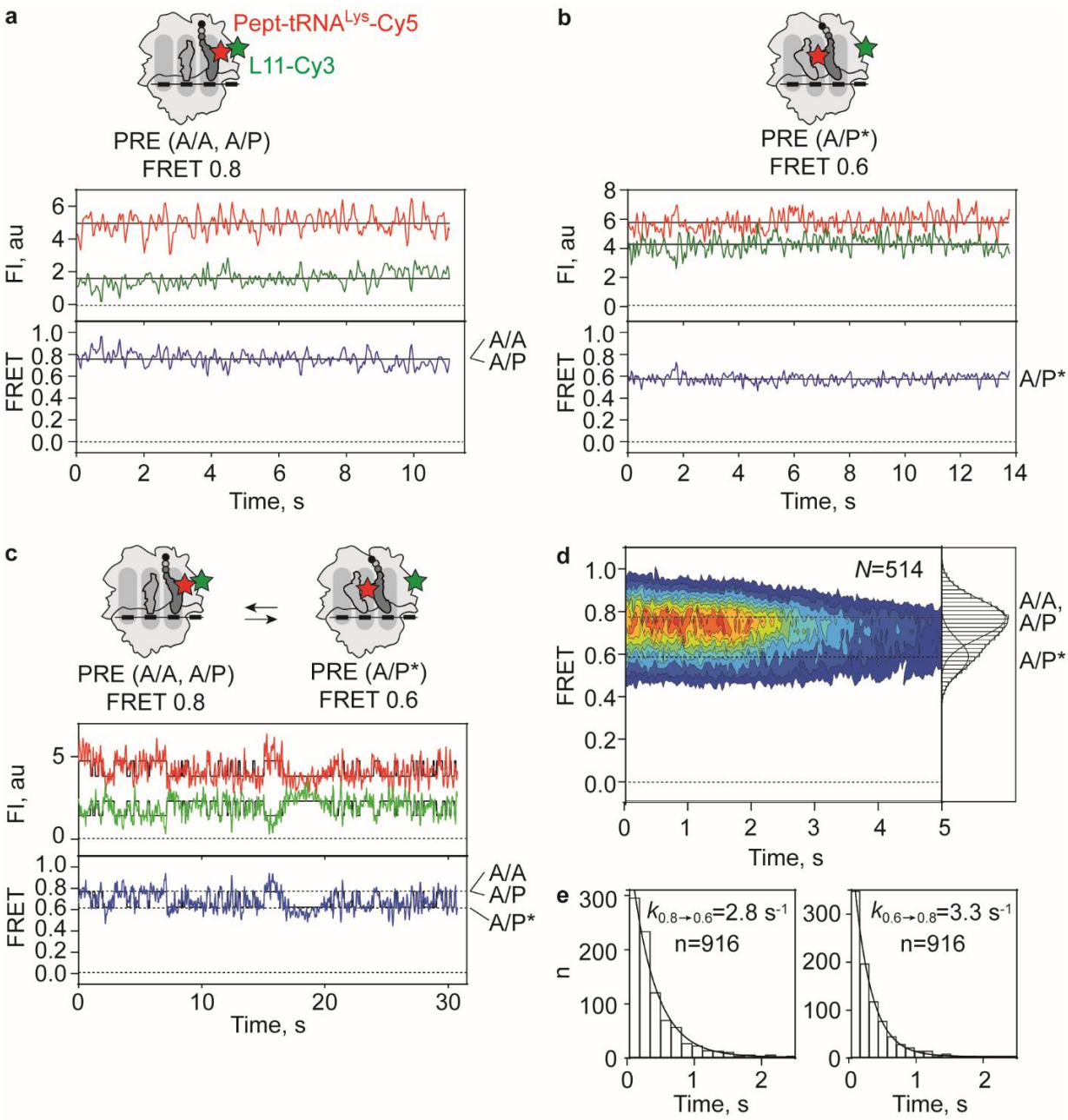

Figure 17. L11-tRNA smFRET in PRE complex. (a) Schematic of pept-tRNA^{Lys}-Cy5 in A/A and A/P conformations and representative smFRET trace showing donor and acceptor FI, calculated FRET and HMM fit. (b) Schematic of pept-tRNA^{Lys}-Cy5 in A/P* conformation and representative smFRET trace. (c) Schematic of pept-tRNA^{Lys}-Cy5 showing fluctuations between A/A, A/P and A/P* conformations and representative smFRET trace. (d) Contour plot showing FRET distribution in the PRE complex. Histogram at the right reveals two states with FRET 0.77±0.09 and 0.59±0.08. Data was obtained in at least three independent experiments. *N*, number of smFRET traces throughout the thesis. (e) Dwell-time distributions of the FRET 0.8 state before transition to the FRET 0.6 state (left, 2.8±0.1 s^{-1}) and of the FRET 0.6 state before transition to the FRET 0.8 state (right, 3.3±0.3 s^{-1}). Black line is single exponential fit. n, number of transitions throughout the thesis.

Next, we determined the FRET values in the POST complex by mixing the purified POST complexes with EF-Tu—GTP—Lys-tRNA^{Lys}-Cy5 and EF-G(wt)—GTP and incubating at 37°C for 5 min. This leads to the incorporation of Lys-tRNA^{Lys}-Cy5 in the ribosome, peptide bond formation and translocation of pept-tRNA^{Lys}-Cy5 to the P site by EF-G (POST complex, Fig. 18a). All smFRET traces showed low FRET values without transitions to lower or higher values (Fig. 18b). 2D FRET population distribution of smFRET traces revealed one Gaussian distribution (0.26±0.09, Fig. 18c), indicating that the pept-tRNA adopts a single P/P conformation in the P site (Adio et al., 2015; Carbone et al., 2021; Chen et al., 2011a; Moazed and Noller, 1989b; Rundlet et al., 2021).

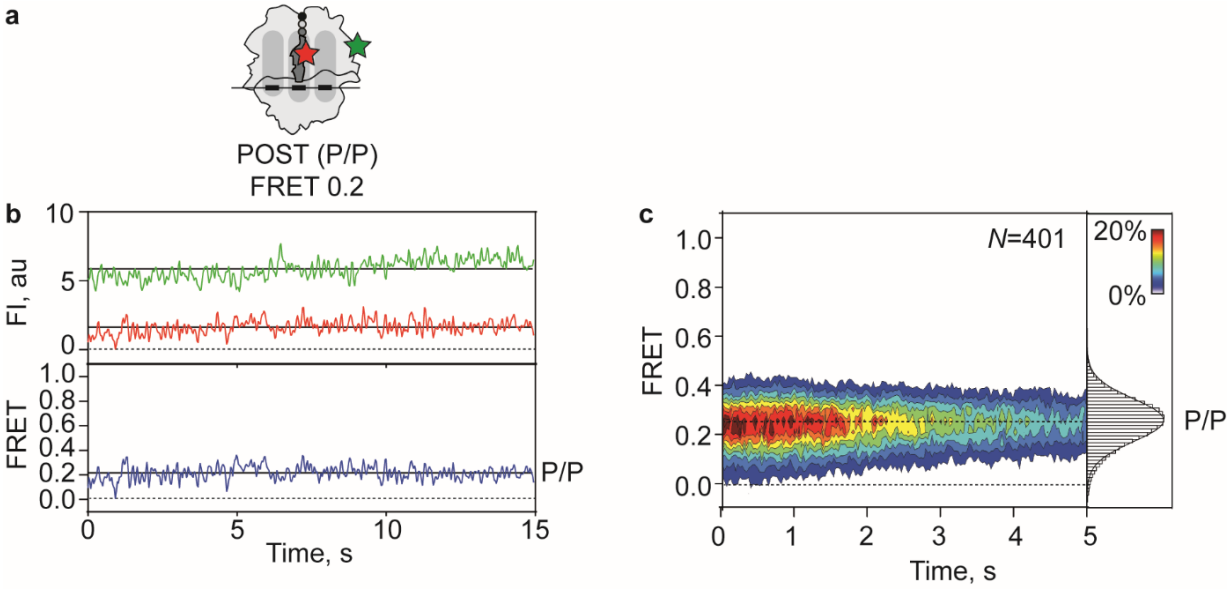

Figure 18. L11-tRNA smFRET in POST complex. (a) Schematic of pept-tRNA^{Lys}-Cy5 in P/P conformation in POST complex. (b) Representative smFRET trace showing donor and acceptor FI, calculated FRET and HMM fit. (d) Contour plot showing FRET distribution in the POST complex. Histogram at the right reveals one state with FRET 0.26±0.09. Data was obtained in at least three independent experiments.

Translocation of pept-tRNA on slippery mRNA

Having determined the FRET values of the start (PRE) and end point (POST) of translocation, we followed the trajectory of the pept-tRNA^{Lys}-Cy5 from the A to the P site in real time. To do this, we immobilized PRE complexes carrying pept-tRNA^{Lys}-Cy5 in the A site and deacylated tRNA^{Gly} in the P site and injected EF-G(wt) and GTP into the flow chamber. Translocation was monitored as a decrease from FRET 0.8 or 0.6 to FRET 0.2 (Fig. 19a). On the non-slippery mRNA, the transition was direct and occurred in one camera frame, i.e. within 33 ms, giving a lower limit estimation of the translocation rate as ≥ 30 s^{-1}. Synchronization of the traces at the time point where transition to FRET≤ 0.5 is observed and population distribution of the FRET values after the synchronization point revealed one Gaussian distribution with FRET 0.19±0.08 (P/P) and no additional discernible intermediate FRET states (Fig. 19b). This result indicates that translocation from A to P site by EF-G(wt) on non-slippery mRNA is rapid, in agreement with previous ensemble and smFRET kinetic studies that report translocation rates ranging from 7 to 30 s^{-1} (Adio et al., 2015; Belardinelli et al., 2016a; Chen et al., 2011a; Cunha et al., 2013; Holtkamp et al., 2014; Katunin et al., 2002; Pan et al., 2007; Peng et al., 2019; Rodnina et al., 1997; Savelsbergh et al., 2003; Savelsbergh et al., 2000).

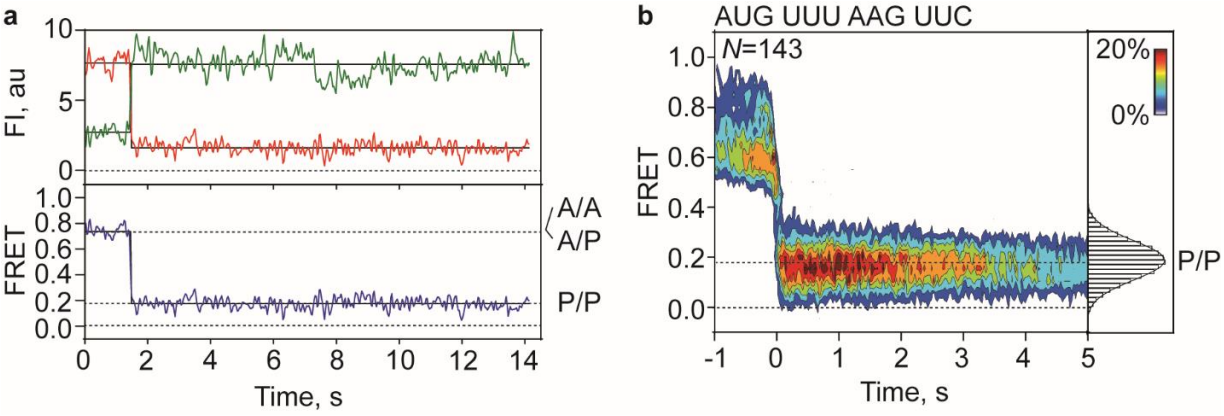

Figure 19. Translocation of pept-tRNA^{Lys} on non-slippery mRNA, catalyzed by EF-G(wt). (a) Representative smFRET trace showing donor and acceptor FI, calculated FRET and HMM fit, corresponding to translocation of pept-tRNA^{Lys}-Cy5 from the A to the P site by EF-G(wt) on non-slippery mRNA. (b) Contour plot showing FRET distribution during translocation of pept-tRNA^{Lys}-Cy5 on non-slippery mRNA. Traces are synchronized to the first transition with FRET≤ 0.5, unless stated otherwise. Histogram at the right shows FRET distribution after synchronization. Data was obtained in at least three independent experiments.

To address the effect of the slippery sequence on the trajectory of pept-tRNA^{Lys}-Cy5, we monitored smFRET during translocation by EF-G(wt) on the slippery mRNA. The majority of traces (81%) showed a direct transition from FRET 0.8 or 0.6 to FRET 0.2 (Fig. 20a), identical to the pattern observed on the non-slippery mRNA (Fig. 19b). However, a fraction of the population (19%) showed transition to an intermediate FRET state before transition to the low FRET state (Fig. 20b). Synchronization of the traces at the time point where transition to FRET≤ 0.5 is observed and population distribution of the FRET values after the synchronization point revealed one major Gaussian distribution with FRET 0.2 (P/P), a second distribution with FRET 0.6 (A/P*) and an additional distribution with FRET 0.4 (Fig. 20a). Previous structural and smFRET studies described the FRET 0.4 state as the canonical EF-G—induced CHI state (Adio et al., 2015; Carbone et al., 2021; Chen et al., 2011a; Petrychenko et al., 2021; Ramrath et al., 2013; Zhou et al., 2014). On non-slippery mRNA and in the major population on the slippery mRNA, CHI is an authentic translocation intermediate that occurs en route of translocation but it is transiently sampled and resolves very fast towards P/P (Adio et al., 2015; Chen et al., 2011a). However, for the fraction of ribosomes where CHI state is observed, translocation of the pept-tRNA from the A to the P site on slippery mRNA is delayed (Fig. 20c).

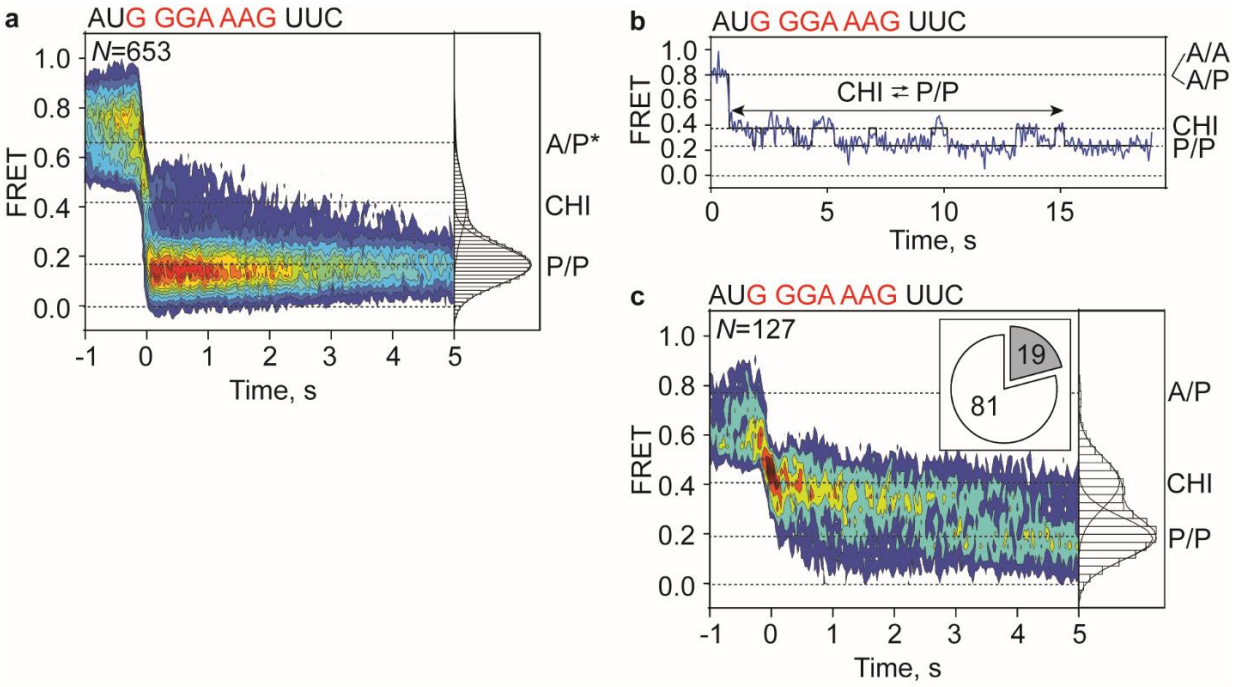

Figure 20. Translocation of pept-tRNA^{Lys} on slippery mRNA, catalyzed by EF-G(wt). (a) Contour plot showing FRET distribution after synchronization during pept-tRNA^{Lys}-Cy5 translocation on slippery mRNA. Data was obtained in at least three independent experiments. (b) Representative smFRET trace corresponding to pept-tRNA^{Lys}-Cy5 translocation via CHI state on slippery mRNA. (c) Contour plot showing FRET distribution after synchronization of the fraction of ribosomes that show slow translocation of pept-tRNA^{Lys}-Cy5 on slippery mRNA. Pie chart indicates the fraction of smFRET traces that show slow translocation (grey).

Next, we asked whether delay of translocation in CHI state correlates with spontaneous frameshifting. To that end, we used EF-G mutants carrying single amino acid substitutions at the key residue Q507 at the tip of domain 4 (Fig. 21). These mutants have been shown to increase spontaneous frameshifting depending on the amino acid substitution (Niblett et al., 2021; Peng et al., 2019). We followed the trajectory of the pept-tRNA^{Lys}-Cy5 from the A to the P site during translocation on slippery mRNA by EF-G(Q507A), EF-G(Q507N) and EF-G(Q507D), mutants that show distinct frameshifting levels *in vitro* (Fig. 21) (Niblett et al., 2021; Peng et al., 2019). In all cases, there was a mixture of ribosome populations in different percentages. One subpopulation shows direct transition from PRE to POST state (Fig. 21a, c, e) while the second subpopulation shows translocation via CHI state (Fig. 21b, d, f). Synchronization of the traces at the time point where transition to FRET≤ 0.5 is observed and population distribution of the FRET values after the synchronization point revealed Gaussian distributions with FRET 0.6 (A/P*), 0.4 (CHI) and 0.2 (P/P) in all cases (Fig. 21b, d, f and Table 6).

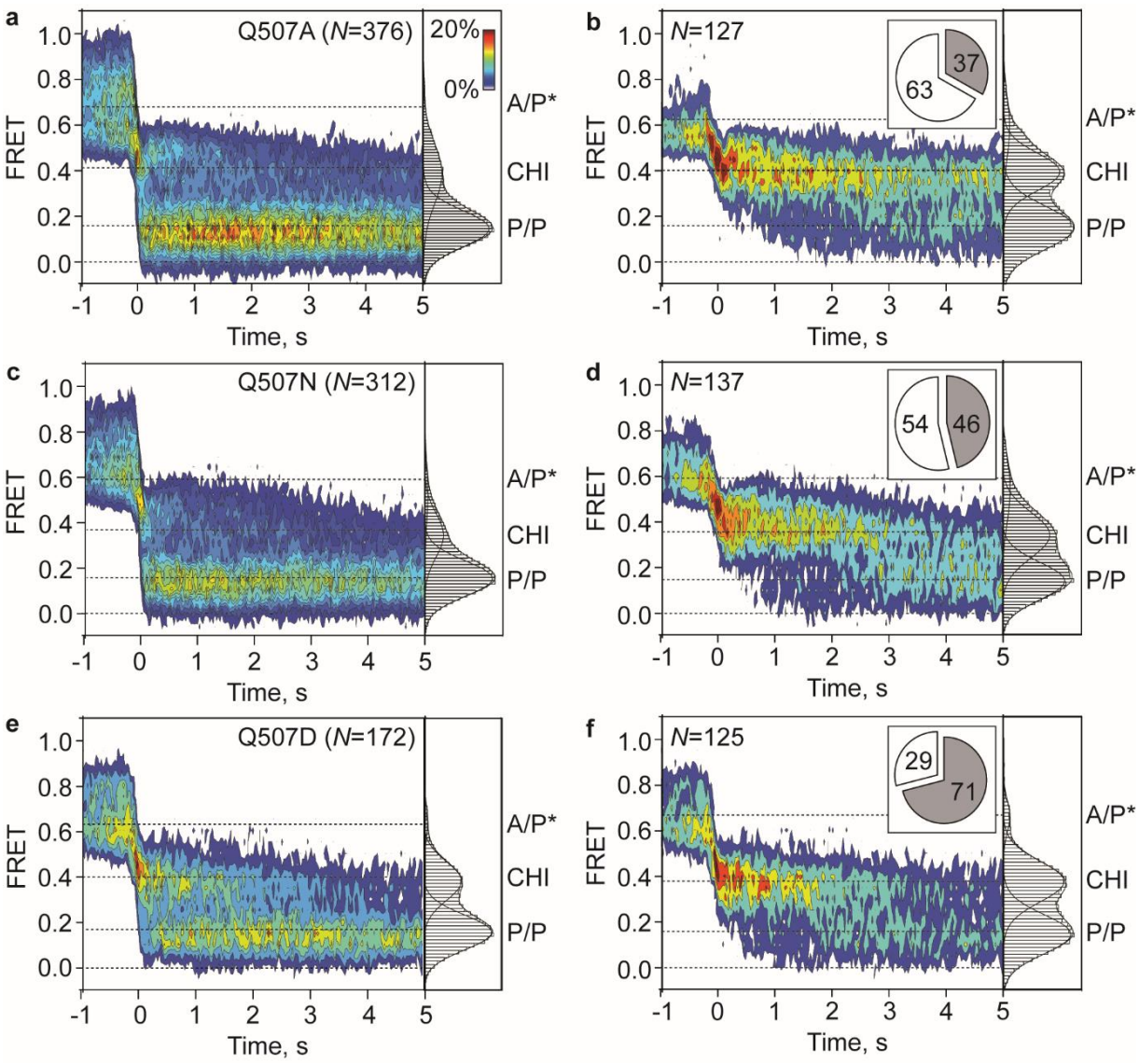

Figure 21. Translocation of pept-tRNA^{Lys} on slippery mRNA, catalyzed by frameshifting-promoting EF-G(Q507) mutants. (a, c, e) Contour plots showing FRET distribution after synchronization during pept-tRNA^{Lys}-Cy5 translocation on slippery mRNA by EF-G(Q507A) (a), EF-G(Q507N) (c) and EF-G(Q507D) (e). (b, d, f) Contour plots showing FRET distribution after synchronization for the fraction of ribosomes that show slow translocation on slippery mRNA by EF-G(Q507A) (b), EF-G(Q507N) (d) and EF-G(Q507D) (f). Pie charts indicate fraction of ribosomes that show slow translocation (grey). Data was obtained in at least three independent experiments.

Pept-tRNA dynamics during translocation

We then systematically analyzed the translocation pattern of pept-tRNA^{Lys} on slippery mRNA of the ribosomes that show slow translocation. The first step of translocation that occurs before or after GTP hydrolysis but before Pi release is the stabilization of the hybrid tRNA conformation by EF-G (Adio et al., 2015; Carbone et al., 2021; Holtkamp et al., 2014; Petrychenko et al., 2021). In order to investigate whether the mutations at Q507 residue affect this step, we extracted the FRET values of the last 33 ms (one frame) of each smFRET trace before the synchronization point. The pre-synchronization FRET values were distributed, fitted to Gaussian functions and their amplitudes were compared to the FRET values of the PRE complex (Fig. 22a) (Adio et al., 2015). We observe an increase in the amplitude of the FRET 0.6 (A/P*) state in all cases, indicating a stabilization of the hybrid states by EF-G(wt) but also by all the EF-G(Q507) mutants (Fig. 22a). This indicates that mutations at residue Q507 do not affect the stabilization of the hybrid conformations at the beginning of translocation. This is in agreement with recent time-resolved cryo-EM studies that reveal high flexibility of domain 4 of EF-G before Pi release and stabilization after CHI state formation (Petrychenko et al., 2021) and ensemble kinetics studies reporting no significant difference at the binding and GTP hydrolysis rates of EF-G(Q507) mutants (Peng et al., 2019).

Next, we calculated the translocation rate using smFRET traces that show slow translocation via CHI states. To this end, we isolated the part of the traces between the first transition to FRET≤ 0.5 and the last transition to FRET 0.2 (P/P), extracted the dwell times and calculated the decay rates, which give an estimation of the translocation rate (Fig. 22b and Table 6). The average translocation rate was ~0.2±0.1 s^{-1} in all cases (Fig. 22b, Table 6). This value is two orders of magnitude lower than the translocation rate on non-slippery mRNA (≥ 30 s^{-1}), indicating that translocation is slowed down for a fraction of ribosomes.

We then investigated the structural dynamics of pept-tRNA^{Lys}-Cy5 during slow translocation on slippery mRNA. To do this, we quantified the transitions between the FRET 0.8 (A/A and A/P), 0.6 (A/P*), 0.4 (CHI) and 0.2 (P/P) states as a percentage to the total number of transitions and compared to transitions in PRE complex (Fig. 22c). The transition frequency gives an estimate of the stage in the translocation reaction coordinate that is severely impeded (Adio et al., 2015; Wasserman et al., 2016). The PRE complex in the absence of EF-G contains exclusively transitions between A/A, A/P and A/P* states, while transitions that involve CHI or P/P states are not observed (Fig. 22c) (Adio et al., 2015). In contrast, during EF-G—induced

slow translocation, very few transitions between A/A, A/P and A/P* states are observed, indicating that EF-G—induced translocation proceeds via the hybrid A/P* state allowing transitions to lower FRET (i.e. progression towards the P site) but not to higher FRET states (Fig. 22c) (Adio et al., 2015). In all cases, transitions between CHI and P/P states are more abundant compared to transitions between A/P* and CHI states (Fig. 22c and Table 6). This suggests that on a fraction of ribosomes, translocation on slippery mRNA by EF-G(wt) and EF-G(Q507) mutants is delayed, because pept-tRNA fluctuates between CHI and P/P states, instead of irreversibly transiting to the P site. To our knowledge, this is the first single molecule study reporting that ribosome stalling is due to dynamic behavior of pept-tRNA on slippery mRNA.

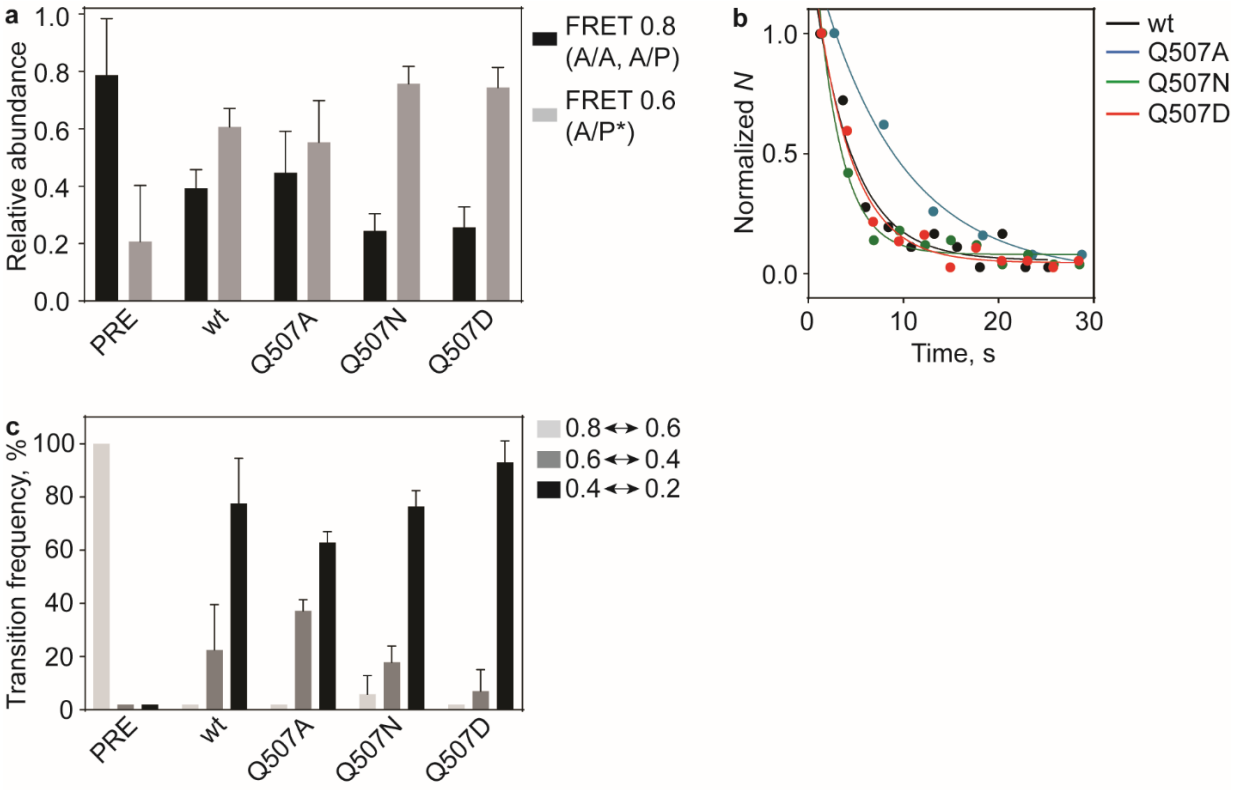

Figure 22. Systematic analysis of pept-tRNA^{Lys} translocation on slippery mRNA. (a) Relative abundance of FRET states 33 ms prior to translocation by EF-G(wt), EF-G(Q507A), EF-G(Q507N) and EF-G(Q507D), compared to PRE complex. Data are shown as mean values and error bars represent the standard deviation. (b) Dwell-time distribution of the translocation phase on slippery mRNA by EF-G(wt) (black), EF-G(Q507A) (blue), EF-G(Q507N) (green) and EF-G(Q507D) (red). Solid lines in respective colors are single exponential fit (Table 6). (c) Quantification of transitions between different FRET states during translocation of pept-tRNA^{Lys} on slippery mRNA (Table 6).

Table 6. Kinetics of pept-tRNA^{Lys} fluctuations during translocation on slippery mRNA.

EF-G	k_{TL}, s^{-1} (*N*)	FRET, μ±s.d.	Transition rates during translocation *k*, s^{-1} (n) 0.6→0.4 0.4→0.6	0.4→0.2 0.2→0.4
wt	0.2±0.1 (102)	0.6±0.1 0.4±0.1 0.2±0.1	n.d. (64) n.d (61)	2.6±0.6 (186) 2.7±1.4 (148)
Q507A	0.1±0.1 (110)	0.6±0.1 0.4±0.1 0.2±0.1	3.9±0.7 (79) 5.8±1.9 (83)	2.9±1.2 (152) 2.8±0.6 (138)
Q507N	0.2±0.1 (106)	0.6±0.1 0.4±0.1 0.2±0.1	n.d. (61) n.d. (64)	3.6±0.6 (261) 3.7±1.1 (228)
Q507D	0.3±0.1 (90)	0.6±0.1 0.4±0.1 0.2±0.1	n.d. (22) n.d. (21)	2.7±0.2 (324) 3.6±0.2 (315)

Next, we asked the question whether the population of ribosomes that show slow translocation of the pept-tRNA^{Lys} correlates with frameshifting. To do this, we measured spontaneous frameshifting during translation of the slippery mRNA using EF-G(wt) and the three frameshifting-promoting EF-G(Q507) mutants by quantifying the 0- and –1-frame translation products (Fig. 23a). The slippery mRNA encodes for the peptides fMet-Gly-Lys-Phe (fMGKF) in 0 frame and fMet-Gly-Lys-Val (fMGKV) in –1 frame. Purified initiation complexes (IC) were mixed with TC carrying [^{14}C]Gly-tRNA^{Gly}, Lys-tRNA^{Lys}, Phe-tRNA^{Phe} and Val-tRNA^{Val} in equal concentration, the EF-G variant and GTP and incubated for 2 min at 22°C (same temperature as the smFRET experiments, Fig. 23a). EF-G was added in 10-fold excess over ribosomes (Methods) to avoid EF-G depletion-triggered frameshifting, as reported during translation of slippery mRNA with EF-G/ribosome ratio < 1 (Peng et al., 2019). After translation, chemical peptide hydrolysis using KOH and HPLC separation of the peptides allow quantification of the translation products because 0-frame fMGKF peptides show higher retention time in reverse-phase column compared to –1-frame fMGKV peptides, due to higher hydrophobicity of Phe over Val (Fig. 23b) (Methods and (Peng et al., 2019)). By using [^{14}C]Gly (present in both 0- and –1-frame translation products), we were able to identify the eluted fractions that contain the expected translation products and quantify them (Fig. 23b). Frameshifting efficiency is then calculated as the ratio of –1-frame fMGKV peptide to the total amount of 0-frame fMGKF and –1-frame fMGKV peptides. Comparison of the frameshifting efficiency of each EF-G variant with the percentage of the ribosomes that show CHI during

translocation shows a correlation coefficient close to 1, indicating that frameshifting is at a large extent the result of slow translocation (Fig. 23c).

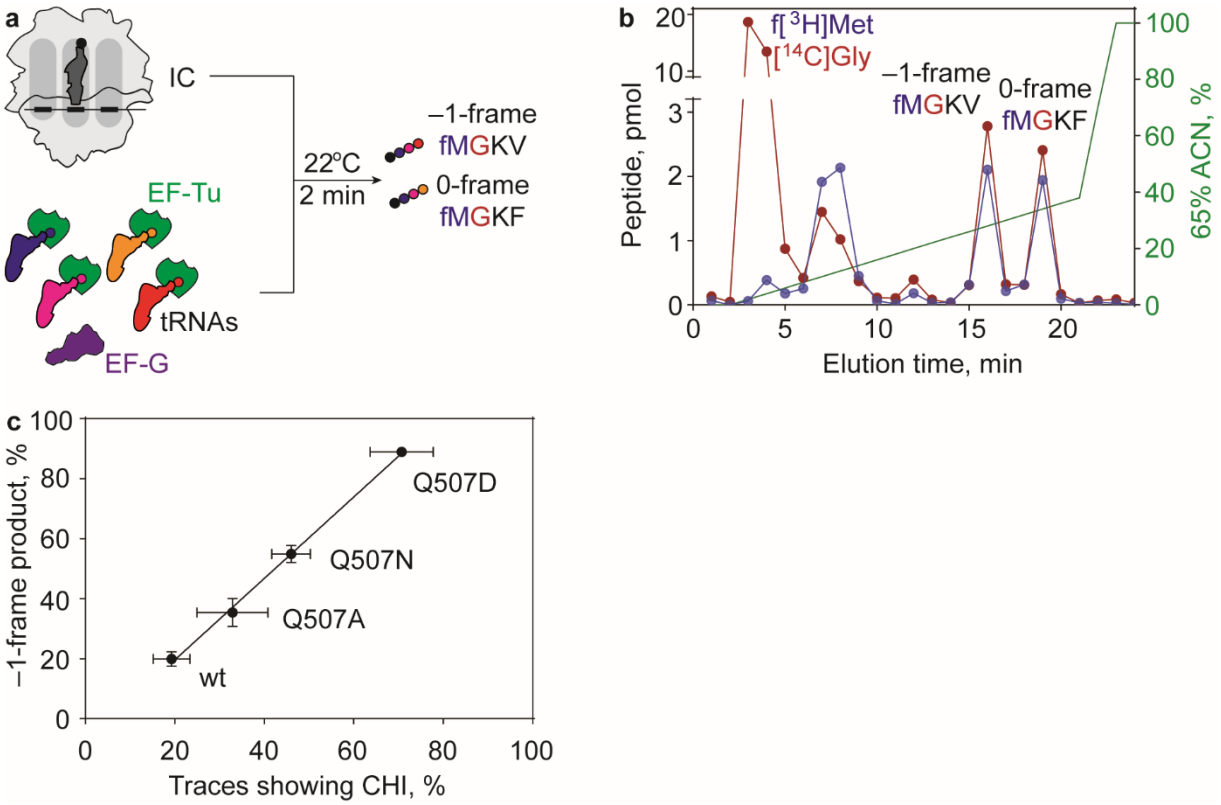

Figure 23. Quantification of spontaneous frameshifting and correlation with slow translocation. (a) Schematic of the frameshifting assay to measure spontaneous –1 frameshifting. 0-frame $tRNA^{Gly}$ is shown in blue, 0-frame $tRNA^{Lys}$ in magenta, 0-frame $tRNA^{Phe}$ in red and –1-frame $tRNA^{Val}$ in orange. (b) Representative elution profile after HPLC separation of the 0- (fMGKF) and –1- (fMGKV) frame products after translation using EF-G(Q507N). The ACN gradient is shown in green. Scintillation counts of [^{3}H]fMet (blue) and [^{14}C]Gly (red) are shown. (c) Correlation between frameshifting efficiency and the fraction of ribosomes that show slow translocation on slippery mRNA. Black line is linear fit with slope of 1.3±0.1, R^2=0.9982.

In order to unequivocally show that slow pept-tRNA translocation results in spontaneous frameshifting, we used a dual-FRET system to monitor, on the same ribosome, translocation of pept-tRNA^{Lys} and the incorporation of the –1-frame tRNA^{Val}. For this purpose, we used tRNA^{Lys} labeled with Black Hole Quencher 2 (BHQ2) (Fig. 24a), which is a strong quencher of Cy3 fluorescence, suitable for smFRET studies (Chen et al., 2014; Chen et al., 2012; Choi et al., 2020), and used the L11-Cy3/pept-tRNA^{Lys}-BHQ2 FRET pair to assign changes in Cy3 fluorescence intensity (FI) to tRNA conformations (Fig. 24b-d). POST L11-Cy3 complexes carrying pept-tRNA^{Gly} in the P site (POST1) show a stable Cy3 FI (Fig. 24b). Addition of TC carrying Lys-tRNA^{Lys}-BHQ2 results in drop of Cy3 FI and transient excursions to higher Cy3 FI values, presumably representing the fluctuations between A/A, A/P and A/P* states in the PRE1 complex (Fig. 24c), similar to the fluctuations seen with L11-Cy3/tRNA-Cy5 FRET (Fig. 17c, d). One-frame increase in Cy3 FI represents photobleaching of the BHQ2 quencher followed by photobleaching of Cy3 (Fig. 24c). Addition of EF-G(wt) results in the formation of POST2 complex carrying pept-tRNA^{Lys}-BHQ2 in the P site, which is characterized by high Cy3 FI (P/P) before photobleaching of the BHQ2 quencher (Fig. 24d).

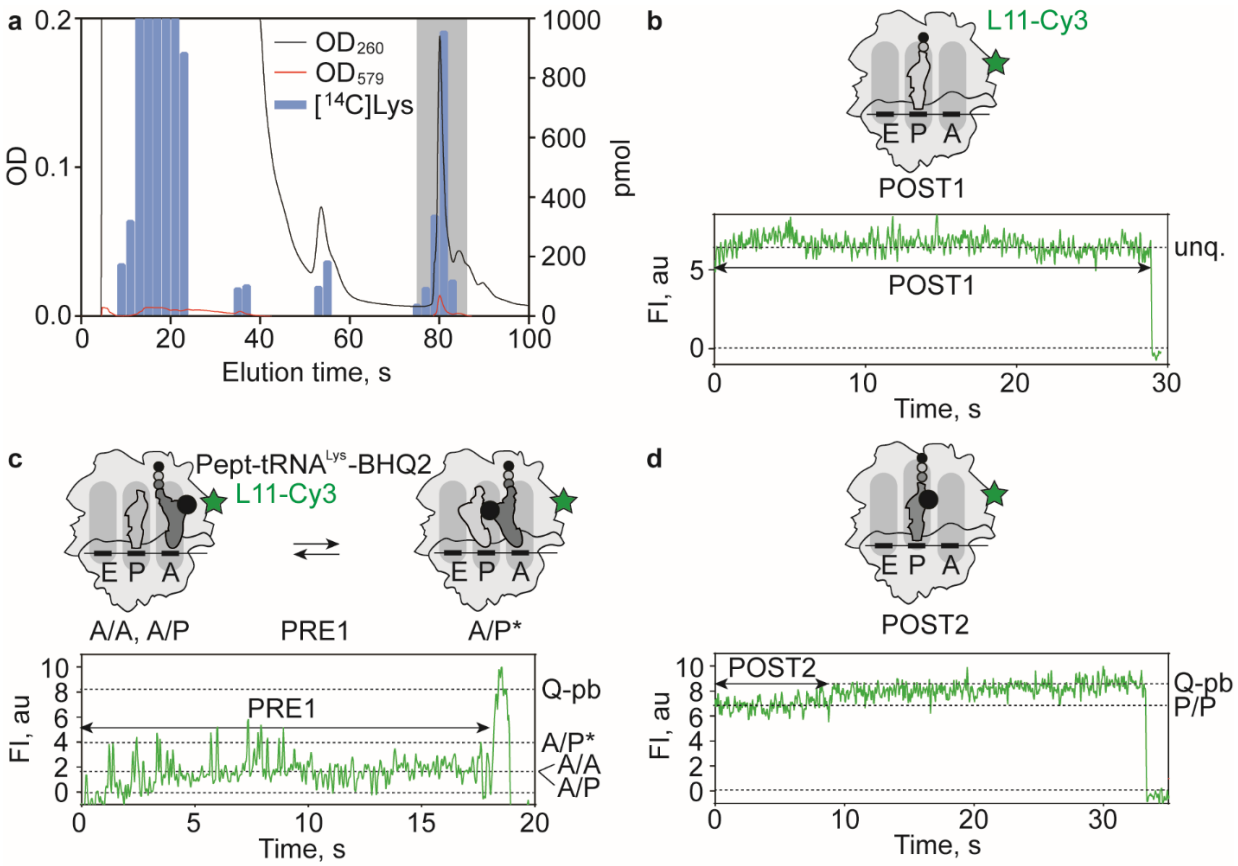

◄Figure 24. Assignment of L11-Cy3 fluorescence intensity levels to pept-tRNA^{Lys}-BHQ2 states. (a) HPLC chromatogram showing the elution time (grey shade) of [^{14}C]Lys-tRNA^{Lys}-BHQ2. OD_{260} is shown in black line, OD_{579} in red line and scintillation counting of [^{14}C]Lys as blue bars. (b) Schematic of the L11-Cy3 POST1 complex with pept-tRNA^{Gly} in the P site and representative time trace of L11-Cy3 FI. unq, unquenched FI of L11-Cy3. (c) Schematic of the L11-Cy3 PRE1 complex with pept-tRNA^{Lys}-BHQ2 (black circle) in the A site and deacylated tRNA^{Gly} in the P site and time trace of L11-Cy3 showing fluorescence fluctuations between A/A, A/P or A/P*. Q-pb, BHQ2 photobleaching. (d) Schematic of the L11-Cy3 POST2 complex with pept-tRNA^{Lys}-BHQ2 in the P site and time trace of L11-Cy3 FI in the P/P state.

Next, we immobilized POST1 complexes assembled on non-slippery mRNA and injected simultaneously EF-Tu—GTP—Lys-tRNA^{Lys}-BHQ2 and EF-G(wt) (Fig. 25a). We observed the drop of Cy3 FI (PRE1) and direct transition to high Cy3 FI (POST2) within one frame (Fig. 25b). When we repeated the experiment on slippery mRNA using EF-G(Q507D), we observed traces that showed intermediate Cy3 FI before transition to higher Cy3 FI (Fig. 25c), similar to the CHI state using the L11-Cy3/pept-tRNA^{Lys}-Cy5 FRET pair (Fig. 21e, f). In conclusion, the L11-Cy3/tRNA-BHQ2 FRET pair can recapitulate pept-tRNA translocation from the A to the P site in an analogous way as the L11-Cy3/tRNA-Cy5 pair.

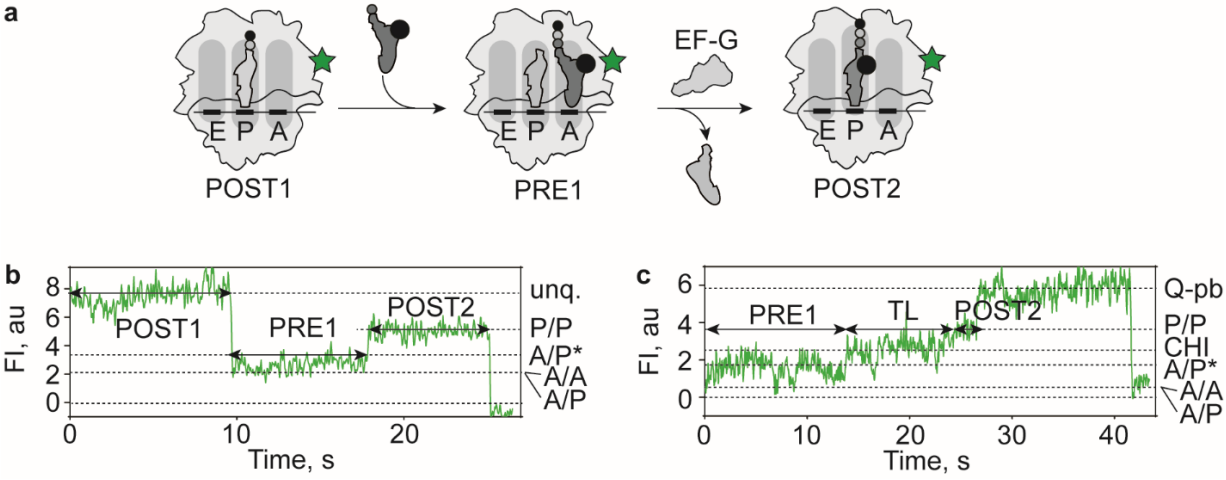

Figure 25. Monitoring translocation in real time by smFRET between L11-Cy3 and pept-tRNA^{Lys}-BHQ2. (b) Schematic of pept-tRNA^{Lys}-BHQ2 binding to POST1 complexes and translocation from the A to the P site by EF-G(wt). (b) Time trace of pept-tRNA^{Lys}-BHQ2 translocation from the A to the P site by EF-G(wt) on non-slippery mRNA. (c) Time trace of pept-tRNA^{Lys}-BHQ2 translocation from the A to the P site by EF-G(Q507D) on slippery mRNA. TL, translocation.

Next, we monitored translocation of pept-tRNA^{Lys} and incorporation of the next tRNA on the same ribosome. First, we monitored translocation of pept-tRNA^{Lys}-BHQ2 from the A to the P site on non-slippery mRNA and incorporation of the next 0-frame Phe-tRNA^{Phe}-Cy5, which reads the 0-frame UUC codon in the A site (Fig. 26a). PRE1 complexes on non-slippery mRNA were immobilized, followed by injection of EF-G(wt) and Phe-tRNA^{Phe}-Cy5. Translocation of pept-tRNA^{Lys} was rapid (within one frame) and without discernible intermediates. The arrival of the 0-frame Phe-tRNA^{Phe}-Cy5 was monitored as increase in Cy5 fluorescence (Fig. 26b). Phe-tRNA^{Phe}-Cy5 accommodation occurred in two steps: one showing high FRET and a subsequent step showing fluctuations between lower FRET states (Fig. 26b, c). Previous studies using L11-tRNA FRET identified the high FRET step as the codon reading (CR) and/or GTPase activation (GA) state, while the lower FRET states represent the accommodation of tRNA into the A site and have the same FRET efficiency as the A/A, A/P and A/P* states (Fig. 26c, d and Fig. 17d) (Geggier et al., 2010). FRET distribution after appearance of Cy5 FI and FRET revealed three Gaussian distributions (Fig. 26d). The FRET 0.9 state corresponds to the CR state, which rapidly resolves into the two lower states with FRET 0.8 and 0.5, corresponding to the A/A, A/P and A/P* tRNA conformations respectively (Fig. 26c-d and Fig. 17d). The decay rate of FRET is 0.2 s^{-1} (Fig. 26e), indicating a stable accommodation of the tRNA^{Phe}-Cy5 into the ribosome. Therefore, this experiment shows that cognate 0-frame Phe-tRNA^{Phe} is incorporated after rapid translocation of pept-tRNA^{Lys}.

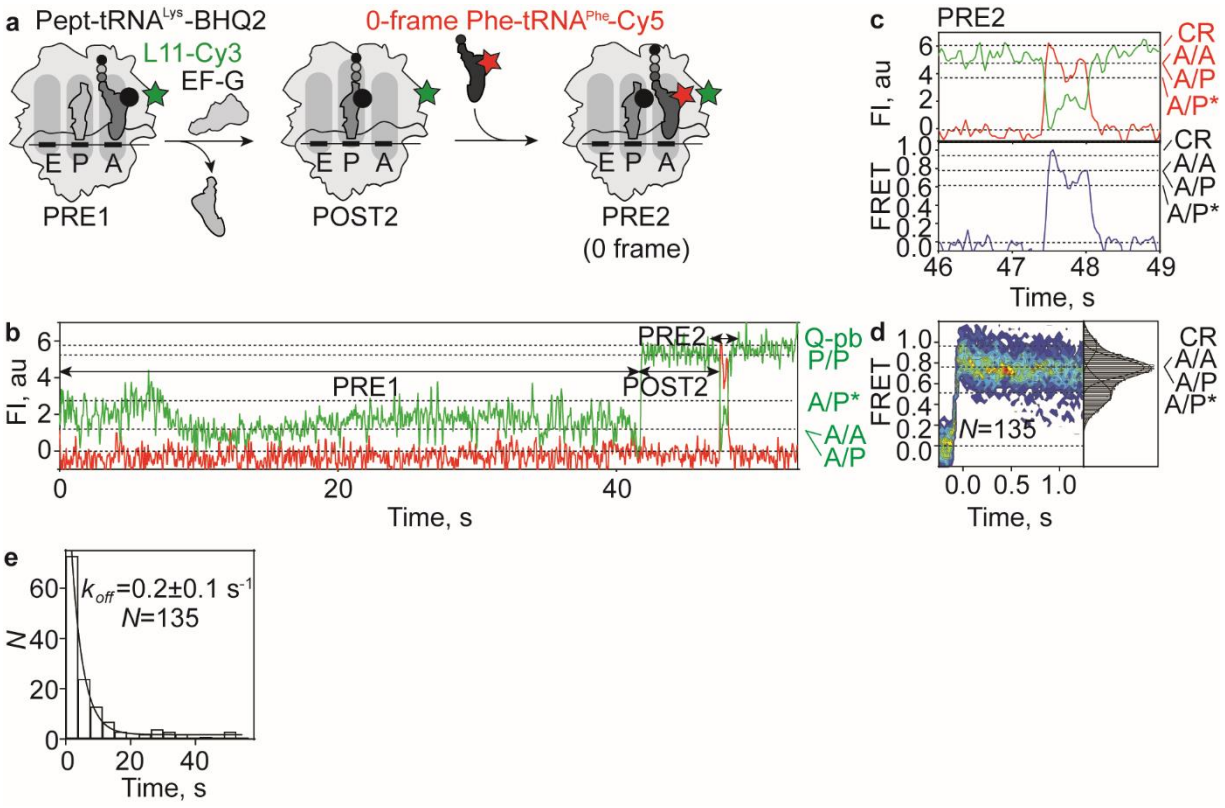

Figure 26. Translocation of pept-tRNA^{Lys}-BHQ2 on non-slippery mRNA by EF-G(wt) and incorporation of cognate 0-frame Phe-tRNA^{Phe}-Cy5. (a) Schematic of translocation of pept-tRNA^{Lys}-BHQ2 from the A to the P site on non-slippery mRNA by EF-G(wt) and subsequent accommodation of the cognate 0-frame Phe-tRNA^{Phe}-Cy5 (red star). (b) Representative time trace of pept-tRNA^{Lys}-BHQ2 movement and accommodation of Phe-tRNA^{Phe}-Cy5 (box) (*N*=42). (c) Zoom-in showing Cy3 and Cy5 FI and calculated FRET of Phe-tRNA^{Phe}-Cy5 binding to POST2 forming PRE2 complexes. The FRET changes are consistent with previously characterized steps of codon recognition (CR) and tRNA accommodation in the A site (Geggier et al., 2010). Phe-tRNA^{Phe}-Cy5 accommodation results in rapid peptide bond formation followed by fluctuations of pept-tRNA^{Phe}-Cy5 between A/A, A/P and A/P* states. (d) Contour plot showing FRET distribution after Phe-tRNA^{Phe}-Cy5 incorporation into the POST2 complex forming PRE2. Traces were synchronized to the point with FRET> 0. Histogram at the right shows FRET distribution after post-synchronization. (e) Dwell-time distribution of pept-tRNA^{Phe}-Cy5 accommodated on PRE2 complexes. Black line is single exponential fit.

In contrast, when we repeated the same experiment using Val-tRNA^{Val}-Cy5 (Fig. 27a), we observed only transient binding events without progression towards tRNA accommodation (Fig. 27b-c). 2D FRET distribution showed one Gaussian distribution, corresponding to the initial binding (IB) of Val-tRNA^{Val}-Cy5 without progression to stable tRNA incorporation into the A site (Fig. 27d). Additionally, the decay rate of FRET is 22 s^{-1} (Fig. 27e), indicating rapid dissociation of Val-tRNA^{Val}-Cy5 without progression to accommodation. Transient binding characterizes

decoding attempts of non-cognate tRNAs, such as the non-cognate –1-frame Val-tRNA^{Val}-Cy5 (Geggier et al., 2010). These results indicate that, using the dual-FRET pair, we can distinguish between productive and non-productive tRNA incorporation, which provides information about the codon that is exposed at the A site and therefore the translational reading frame.

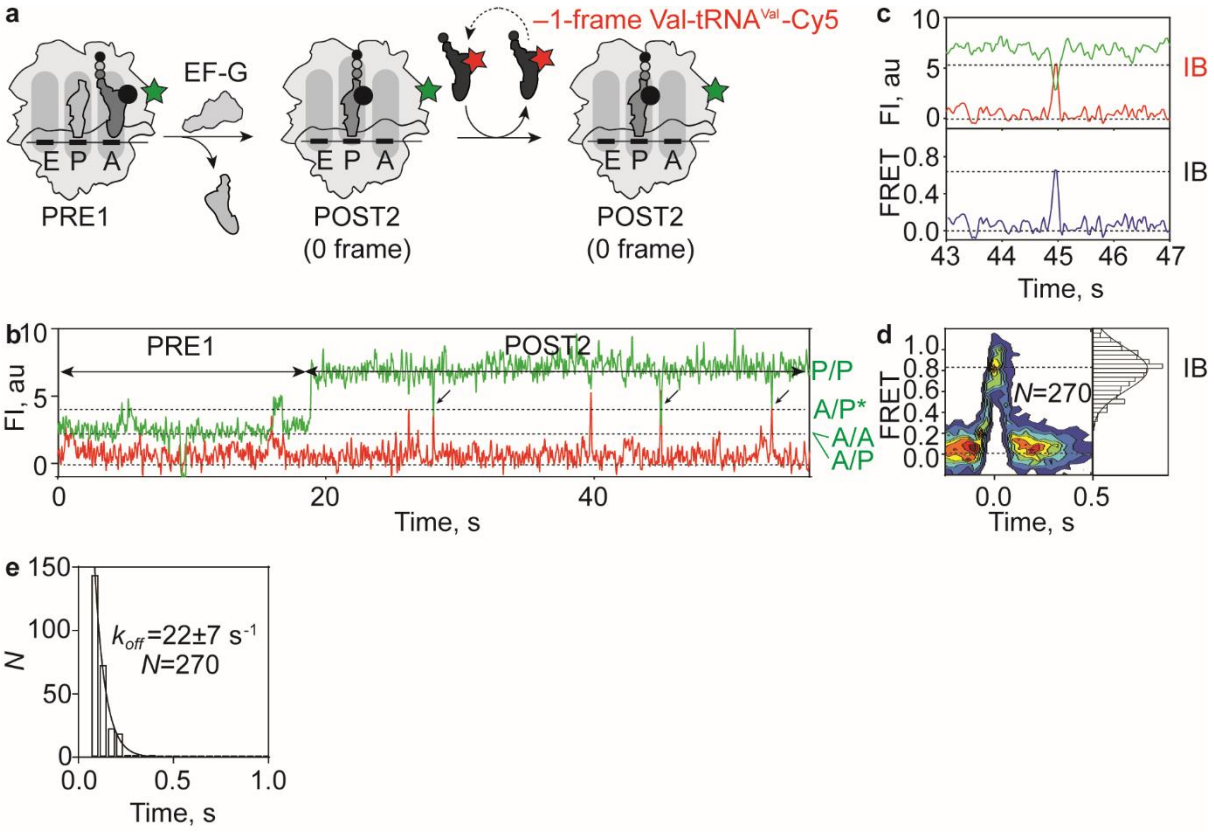

Figure 27. Translocation of pept-tRNA^{Lys}-BHQ2 on non-slippery mRNA by EF-G(wt) and binding attempts of non-cognate –1-frame Val-tRNA^{Val}-Cy5. (a) Schematic of translocation of pept-tRNA^{Lys}-BHQ2 from the A to the P site on non-slippery mRNA by EF-G(wt) and sampling of POST2 complexes by the non-cognate –1-frame Val-tRNA^{Val}-Cy5 (red star). (b) Representative time trace of pept-tRNA^{Lys}-BHQ2 translocation and subsequent sampling of POST2 complexes by the near-cognate –1-frame tRNA^{Val}-Cy5 (arrows) (*N*=68). (c) Zoom-in into Fig. 27b showing Cy3 and Cy5 FI and calculated FRET of initial binding (IB) without accommodation of –1-frame Val-tRNA^{Val}-Cy5 to POST2 complexes. (d) Contour plot showing distribution of FRET values during Val-tRNA^{Val}-Cy5 sampling of POST2 complexes. (e) Dwell-time distribution of transient binding of Val-tRNA^{Val}-Cy5 on POST2 complexes formed on non-slippery mRNA with EF-G(wt). Black line is single exponential fit.

The next question is whether the accommodation of the –1-frame Val-tRNA^{Val}-Cy5 follows slow translocation of the pept-tRNA^{Lys} on slippery mRNA. The experiment was repeated using PRE1 complexes assembled on slippery mRNA and translocation was induced by addition of EF-G(wt) (Fig. 28a). The majority of traces showed fast (within one frame) translocation and

did not accommodate the –1-frame Val-tRNA^{Val}-Cy5 (Fig. 28b), similar to the non-slippery mRNA (Fig. 27b, c). FRET distribution analysis revealed one Gaussian distribution (Fig. 28c, d) and the dissociation rate is 18 s^{-1} (Fig. 28e), similar to the dissociation rate on non-slippery mRNA (Fig. 27e).

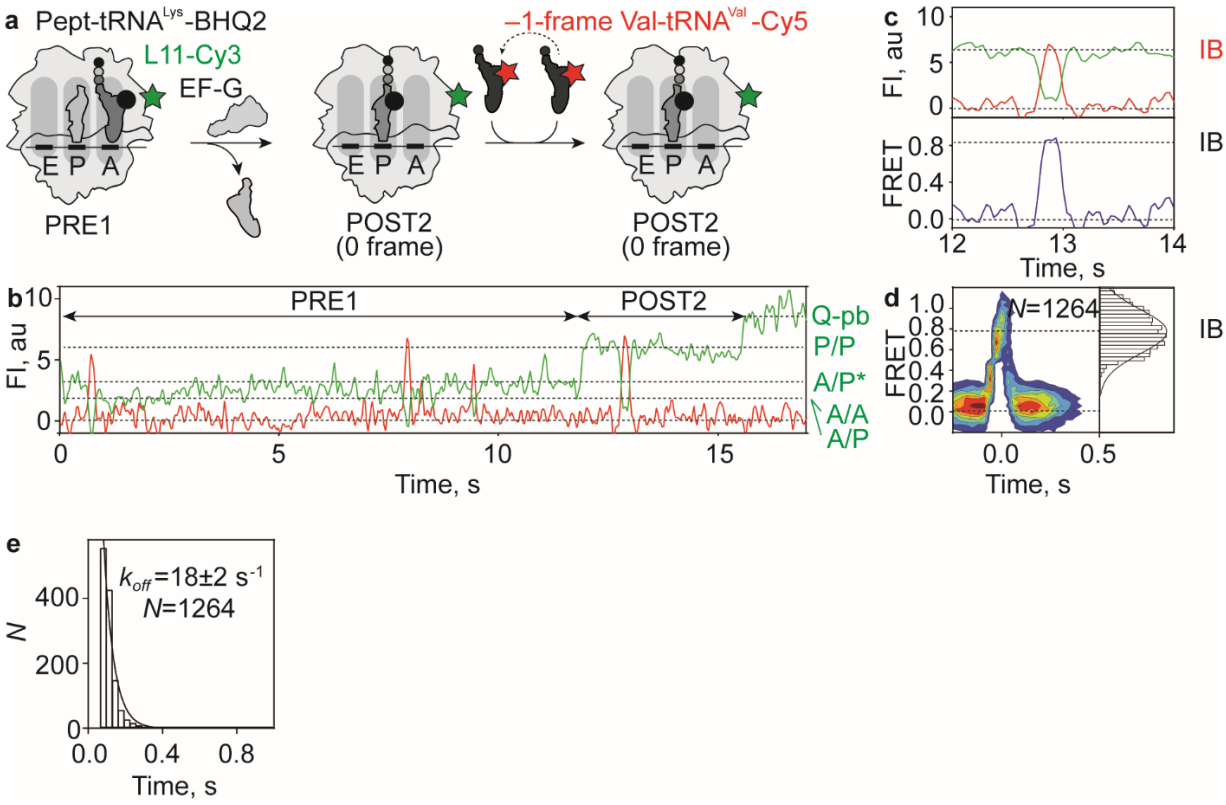

Figure 28. Translocation of pept-tRNA^{Lys}-BHQ2 on slippery mRNA by EF-G(wt) and binding attempts of non-cognate –1-frame Val-tRNA^{Val}-Cy5. (a) Schematic of pept-tRNA^{Lys}-BHQ2 translocation on slippery mRNA by EF-G(wt), without –1 frameshifting. The near-cognate –1-frame Val-tRNA^{Val}-Cy5 (red star) samples POST2 complexes without accommodating in the A site. (b) Representative time trace of pept-tRNA^{Lys}-BHQ2 movement and subsequent sampling of POST2 complexes by Val-tRNA^{Val}-Cy5 (*N*=89). (c) Zoom-in into Fig. 28b showing Cy3 and Cy5 FI and calculated FRET of the initial binding (IB) without accommodation of –1-frame Val-tRNA^{Val}-Cy5 on POST2 complexes. (d) Contour plot showing FRET distribution after synchronization during –1-frame Val-tRNA^{Val}-Cy5 sampling of POST2 complexes. (e) Dwell-time distribution of Val-tRNA^{Val}-Cy5 on POST2 complex formed on slippery mRNA after rapid translocation with EF-G(wt). Black line is single exponential fit.

However, on a fraction of ribosomes, we observed slow translocation via CHI state and subsequent accommodation of –1-frame Val-tRNA^{Val}-Cy5 (Fig. 29a, b). Similarly to the accommodation of the 0-frame Phe-tRNA^{Phe}-Cy5 on non-slippery mRNA (Fig. 26c, d), Val-tRNA^{Val}-Cy5 progresses from the CR state to fluctuations between A/A, A/P and A/P* states

(Fig. 29c, d). FRET distribution revealed three Gaussian distributions, corresponding to the CR, A/A and A/P and A/P* states (Fig. 29d). The decay rate of FRET is 0.1 s^{-1} (Fig. 29e), indicating a stable accommodation of the $tRNA^{Val}$-Cy5 into the ribosome. This experiment shows that slow translocation of pept-$tRNA^{Lys}$ by EF-G(wt) on slippery mRNA is followed by accommodation of the –1-frame Val-$tRNA^{Val}$-Cy5.

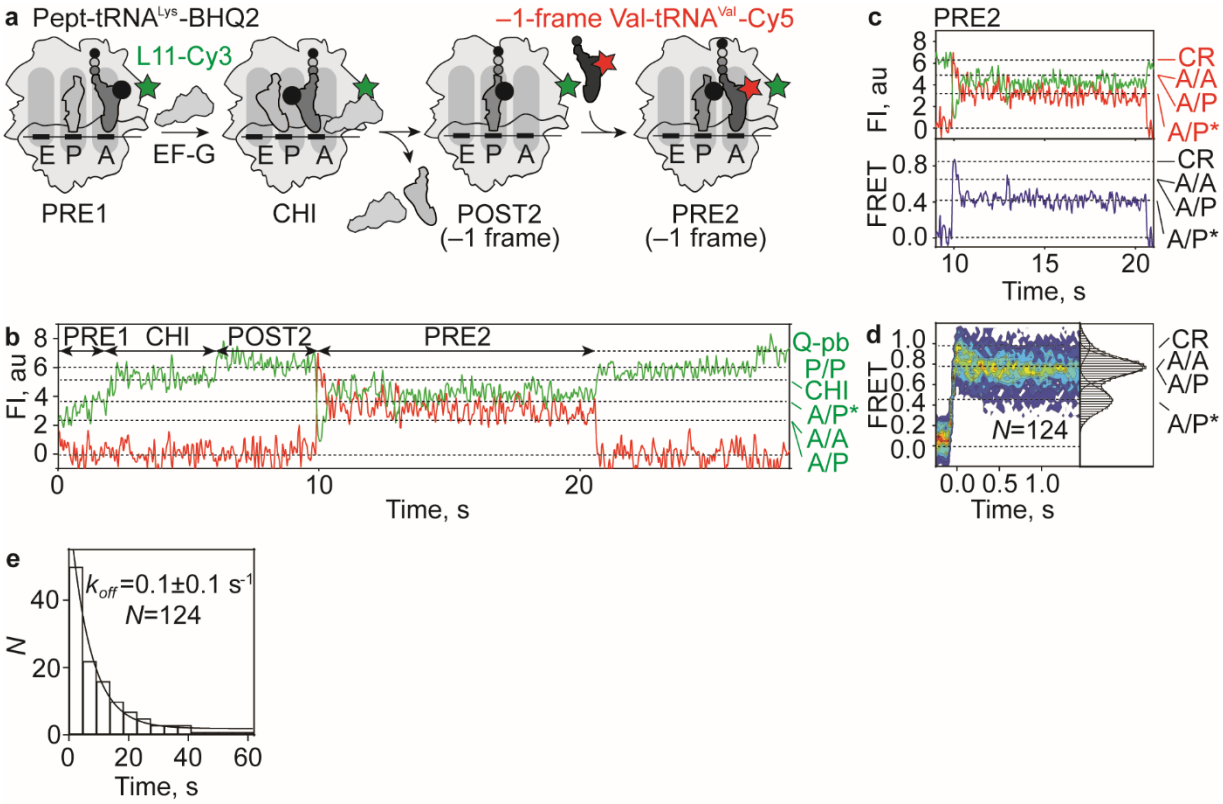

Figure 29. Translocation of pept-$tRNA^{Lys}$-BHQ2 on slippery mRNA by EF-G(wt) and incorporation of cognate –1-frame Val-$tRNA^{Val}$-Cy5. (a) Schematic of pept-$tRNA^{Lys}$-BHQ2 translocation on slippery mRNA by EF-G(wt), with –1 frameshifting. Val-$tRNA^{Val}$-Cy5 (red star) can bind to its cognate –1-frame codon and be accommodated into the A site. (b) Representative time trace of pept-$tRNA^{Lys}$-BHQ2 translocation and accommodation of –1-frame Val-$tRNA^{Val}$-Cy5 (*N*=57). (c) Zoom-in into Fig. 29b showing Cy3 and Cy5 FI and calculated FRET of Val-$tRNA^{Val}$-Cy5 binding to POST2 forming PRE2 complexes. The FRET changes are consistent with previously characterized steps of codon reading (CR) and tRNA accommodation (Geggier et al., 2010). Val-$tRNA^{Val}$-Cy5 CR state is followed by fluctuations of pept-$tRNA^{Val}$-Cy5 between A/A, A/P and A/P* states. (d) Contour plot showing FRET distribution after synchronization of Val-$tRNA^{Val}$-Cy5 accommodation on POST2 complex forming PRE2. (e) Dwell-time distribution of pept-$tRNA^{Val}$-Cy5 on PRE2 complexes formed on slippery mRNA after slow translocation with EF-G (wt). Black line is single exponential fit.

To validate this result, we monitored translocation on slippery mRNA with EF-G(Q507D) (Fig. 30a), which showed the highest level of frameshifting (Fig. 23c). Upon arrival of EF-G(Q507D), Cy3 FI on PRE1 complexes increased to intermediate FI levels (corresponding to CHI state) before reaching high FI level (POST2), indicating that in the presence of EF-G(Q507D) translocation of pept-tRNA^{Lys} is slow (Fig. 30b). Cy5 fluorescence increases indicating arrival of the –1-frame Val-tRNA^{Val}-Cy5 (Fig. 30b, c). Val-tRNA^{Val}-Cy5 does not dissociate, but instead progresses from the CR state towards full tRNA accommodation and ends in fluctuations between A/A, A/P and A/P* states (Fig. 30c, d, decay rate 0.1 s^{-1}, Fig. 30e). This is similar to the behavior of Phe-tRNA^{Phe}-Cy5 on non-slippery mRNA (Fig. 26c-e) and Val-tRNA^{Val}-Cy5 on slippery mRNA after translocation by EF-G(wt) (Fig. 29c-e). This result confirms that the –1-frame codon GUU is exposed in the A site, showing that the ribosome has shifted to the –1 frame. Taken together, slow translocation by both EF-G(wt) and EF-G(Q507D) results in –1 frameshifting due to subsequent incorporation of the –1-frame Val-tRNA^{Val}-Cy5 in the A site.

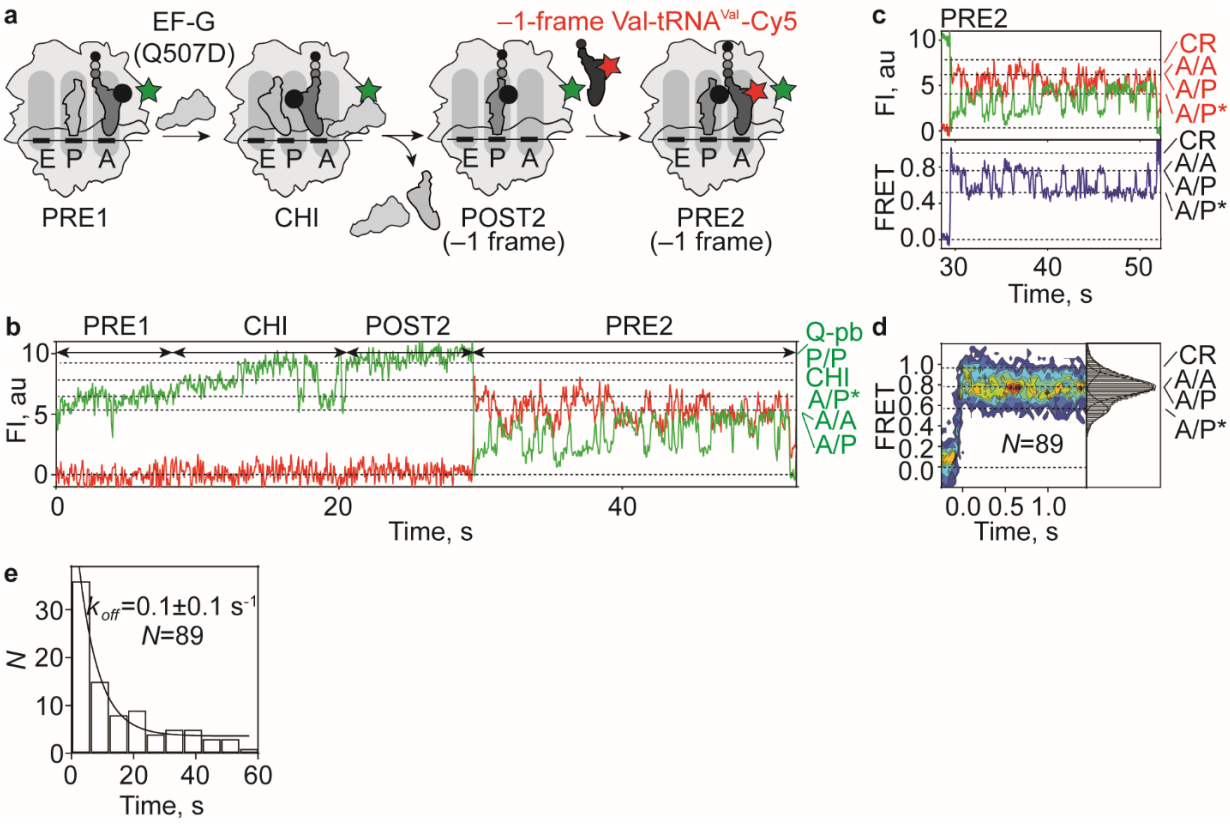

Figure 30. Translocation of pept-tRNA^{Lys}-BHQ2 on slippery mRNA by EF-G(Q507D) and incorporation of cognate –1-frame Val-tRNA^{Val}. (a) Schematic of pept-tRNA^{Lys}-BHQ2 translocation on slippery mRNA by EF-G(Q507D), with –1 frameshifting. Val-tRNA^{Val}-Cy5 (red star) can bind to its cognate –1-frame codon and be accommodated into the A site. (b) Representative time trace of pept-tRNA^{Lys}-BHQ2 translocation and subsequent accommodation of –1-frame Val-tRNA^{Val}-Cy5 (*N*=46). (c) Zoom-in into Fig. 30b showing Cy3 and Cy5 FI and calculated FRET of Val-tRNA^{Val}-Cy5 binding to POST2 complex, leading to CR and subsequent fluctuations between A/A, A/P and A/P* states. (d) Contour plot showing FRET distribution after synchronization of Val-tRNA^{Val}-Cy5 accommodation on POST2 complex. (e) Dwell-time distribution of pept-tRNA^{Val}-Cy5 on PRE2 complexes formed on slippery mRNA after slow translocation with EF-G(Q507D). Black line is single exponential fit.

5.2. Translocation of deacylated tRNA

Next, we asked the question whether the trajectory of the deacylated tRNA from the P to the E site is also affected by the slippery mRNA. Translocation was monitored by FRET efficiency change between ribosomal protein S13 of the SSU head domain and the P-site deacylated tRNA (Fig. 31a) (Belardinelli et al., 2016a; Cunha et al., 2013; Wasserman et al., 2016). S13-tRNA FRET has been previously used in ensemble and smFRET kinetics experiments to characterize the translocation from the P to the E site (Belardinelli et al., 2016a; Wasserman et al., 2016). Translocation from the P to the E site and tRNA dissociation from the ribosome leads to increase in S13-tRNA distance (Fischer et al., 2010) and simultaneous decrease to FRET 0 (Fig. 31a, b) (Belardinelli et al., 2016a). Thus, the S13-tRNA FRET pair is a suitable FRET pair to study the full translocation trajectory from the P to the E site.

A single-Cys S13 variant was labeled with the donor fluorophore Cy3 at the engineered Cys112 (Belardinelli et al., 2016a; Cunha et al., 2013) and $tRNA^{Lys}$ was labeled at the elbow region with the acceptor fluorophore Cy5 (Fig. 31c). For these experiments, we used a different set of mRNAs, one carrying the heptameric slippery sequence A AAA AAG and a non-slippery control mRNA, where the A AAA AAG sequence is replaced by U AAG AAG (Fig. 31d). On the slippery mRNA, the fMet-Ala-Lys-Lys-$tRNA^{Lys}$ (pept-$tRNA^{Lys}$) can base pair with the AAG in the 0 frame and AAA in the –1 frame, an identical shift as on the G GGA AAG slippery mRNA used for the pept-tRNA/L11 FRET experiments (Fig. 31d). Because frameshifting is determined by the free energy difference of codon-anticodon interactions in 0 and –1 frame (Bock et al., 2019), the frameshifting efficiency after translation of the A AAA AAG slippery mRNA is similar (Fig. 31e, f) to the frameshifting efficiency of G GGA AAG slippery mRNA (Fig. 23c). Respectively, frameshifting is prevented in the non-slippery mRNA because base pairing of the pept-$tRNA^{Lys}$ with the –1-frame GAA is thermodynamically unfavorable due to first-position G•U mismatch (Fig. 31d, f) (Bock et al., 2019). We purified S13-Cy3 POST complexes programmed with these mRNAs and carrying pept-$tRNA^{Ala}$ in the P site and mixed them with EF-Tu—GTP—Lys-$tRNA^{Lys}$-Cy5 and EF-G(wt). Incorporation of the Lys-$tRNA^{Lys}$-Cy5 in the A site, peptide bond formation and translocation leads to the formation of the POST complex carrying pept-$tRNA^{Lys}$-Cy5 in the P site and empty A site. This complex was immobilized on coverslip and excess of $tRNA^{Lys}$-Cy5 and EF-G(wt) was washed away. The POST complex was the start point of the experiments.

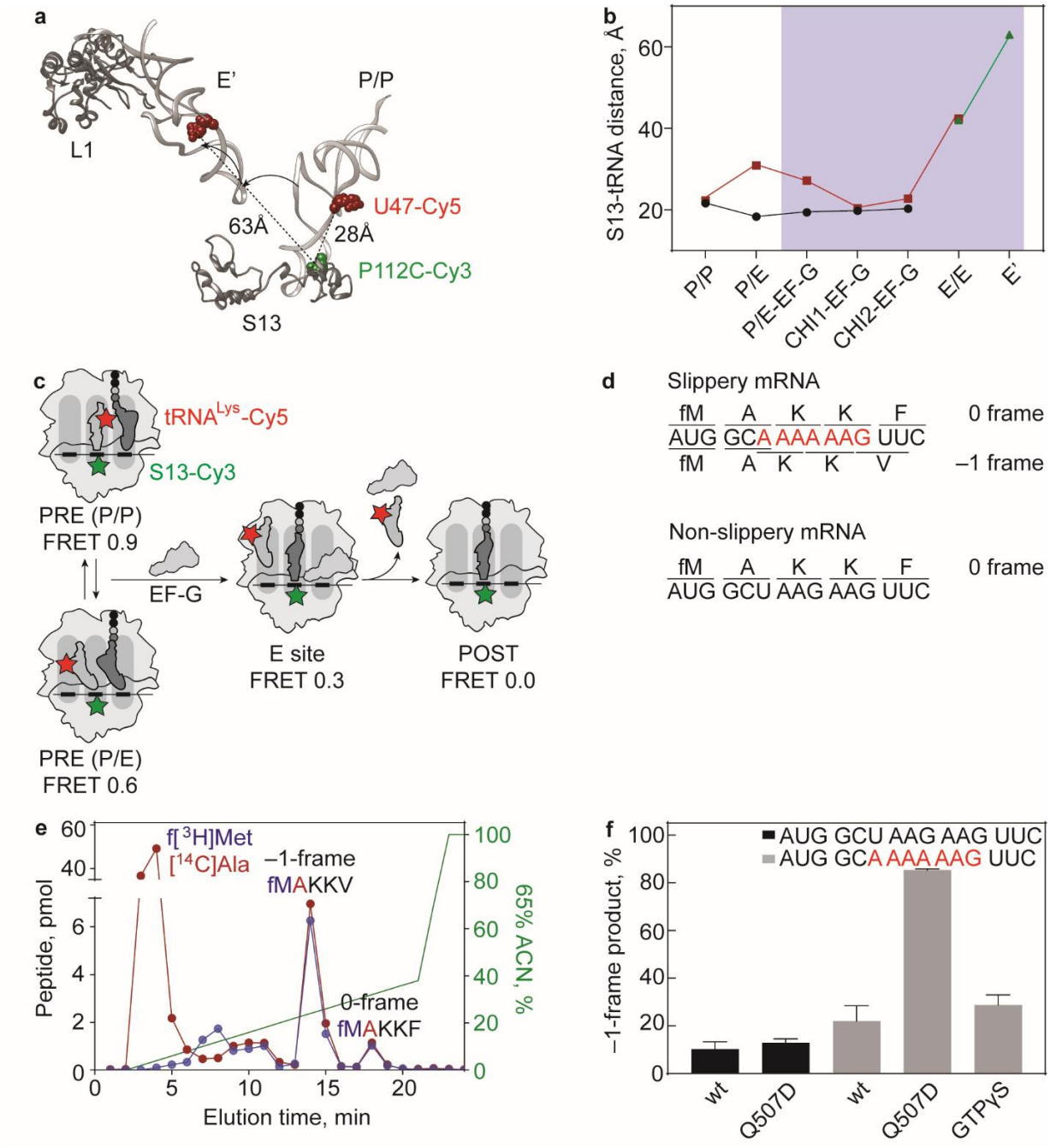

Figure 31. FRET pair and mRNAs used to monitor translocation of the deacylated tRNA. (a) Comparison of S13-tRNA distance in the P/P and E' tRNA conformations. The positions at S13 and tRNA where the fluorophores are attached are indicated in green (for Cy3) and red (for Cy5). The figure was adapted from PDB 4V79 (Fischer et al., 2010). (b) S13-tRNA distance change during translocation. The translocation phase is shown in blue shade. The distances were measured between the engineered Cys112 of S13 and U47 of tRNA and is adapted from (Fischer et al., 2010) (green triangles and connecting line), (Petrychenko et al., 2021) (black circles and connecting line) and (Carbone et al., 2021) (maroon squares and connecting line). (c) Schematic of the S13-tRNA FRET pair used to monitor translocation of the deacylated tRNA. (d) mRNAs used in this study. The slippery mRNA carries a slippery sequence (red)

◄encoding for fMAKKF peptide in 0 frame and fMAKKV peptide in –1 frame. Non-slippery mRNA does not allow translation in the –1 frame due to replacement of A AAA AAG with U AAG AAG. (e) Representative elution profile after HPLC separation of the 0- (fMAKKF) and –1- (fMAKKV) frame products after translation using EF-G(Q507D). The ACN gradient is shown in green. Scintillation counting of f[^{3}H]Met (blue) and [^{14}C]Ala (red) is shown. (f) Frameshifting efficiency during translation of the non-slippery (black bars) and slippery (grey bars) sequence by EF-G(wt), EF-G(Q507D) and EF-G(wt)—GTPγS.

Pept- and deacylated tRNA conformations in the P site

To characterize FRET efficiency in the P/P state, we determined smFRET of the pept-tRNA^{Lys}-Cy5 on POST complexes formed on the slippery mRNA in the absence of EF-G (Fig. 32a). The majority of traces show stable high FRET signals with FRET 0.92±0.09 (Fig. 32b, c). A minor population (<10%), which shows FRET 0.61±0.12 (Fig. 32c), presumably represents tRNAs in the P/E conformation as a result of spontaneous deacylation of the pept-tRNA^{Lys}-Cy5.

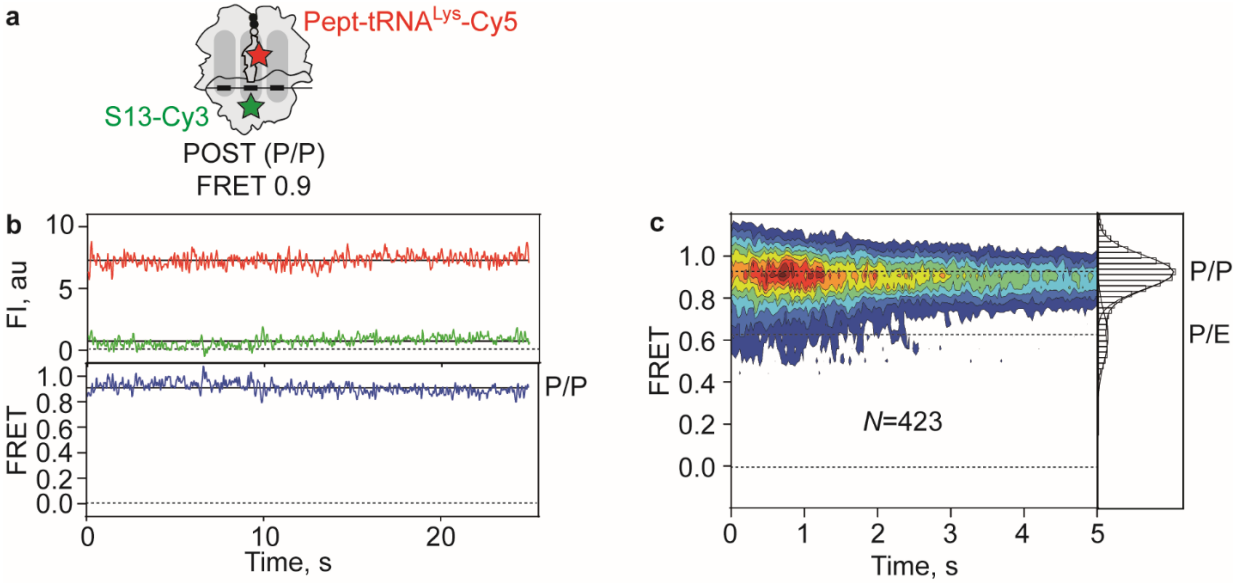

Figure 32. S13-tRNA smFRET in POST complex. (a) Schematic of pept-tRNA^{Lys}-Cy5 in P/P conformation in POST complex. (b) Representative smFRET trace showing donor and acceptor FI, calculated FRET and HMM fit, corresponding to the P/P conformation. (c) Contour plot showing FRET distribution in the POST complex. Histogram at the right reveals a major state with FRET 0.92±0.09 and a minor state with FRET 0.61±0.12. Data was obtained in at least three independent experiments.

In order to validate that the lower FRET population corresponds to the P/E conformation, we repeated the experiment in the presence of puromycin (Pmn). Pmn is an antibiotic that mimics the CCA end of tRNAs and binds to the A site in LSU, catalyzing the hydrolysis and release of the nascent peptide and the deacylation of the peptidyl-tRNA (Fig. 33a) (Semenkov

et al., 1992). In Pmn-treated POST complexes (POST-Pmn), two main types of smFRET traces were observed. The first type shows stable high FRET values (0.92±0.08) without transitions to higher or lower FRET states, similar to the traces observed in POST complexes (Fig. 32b). The second type of traces shows stable low FRET values (0.63±0.11, Fig. 33b, c). In POST-Pmn complexes, the amplitude of the FRET 0.6 state is larger (~30%) compared to the untreated POST complexes, indicating that more tRNAs entered the P/E hybrid conformation due to Pmn-catalyzed deacylation (Fig. 33c). The relative abundance of the P/E state is similar to the abundance of the A/P* state using the L11-tRNA FRET pair, indicating that the occupancy of hybrid conformations is a tRNA-specific feature, as reported in previous studies (Adio et al., 2015; Sharma et al., 2016). However, in contrast to the pept-tRNA dynamics in PRE as monitored by the L11-tRNA FRET, which exhibits 5.5±0.7 transitions per trace, the deacylated tRNA in POST-Pmn complex shows restricted movement with only 0.4±0.1 transitions per trace (Fig. 33d). This indicates that, in PRE complex, pept-tRNA is highly dynamic while the deacylated tRNA is found in either P/P or P/E conformation with low probability of interconversion, consistent with earlier studies that report low transition probability and low transition rates between P/P and P/E states (Munro et al., 2007). Taken together, the FRET 0.9 state corresponds to the P/P tRNA conformation and the FRET 0.6 state corresponds to the P/E tRNA conformation. Characterization of the tRNA conformations in the respective POST complex with deacylated $tRNA^{Lys}$-Cy5 in the E site and fMet-Ala-Lys-Lys-$tRNA^{Lys}$ in the P site is not feasible in steady-state conditions due to the low affinity of the deacylated tRNA to the E site that results in fast and spontaneous tRNA release from the ribosome and, thus, loss of FRET (Adio et al., 2015; Lill et al., 1986; Petropoulos and Green, 2012; Semenkov et al., 1996; Uemura et al., 2010; Wasserman et al., 2016).

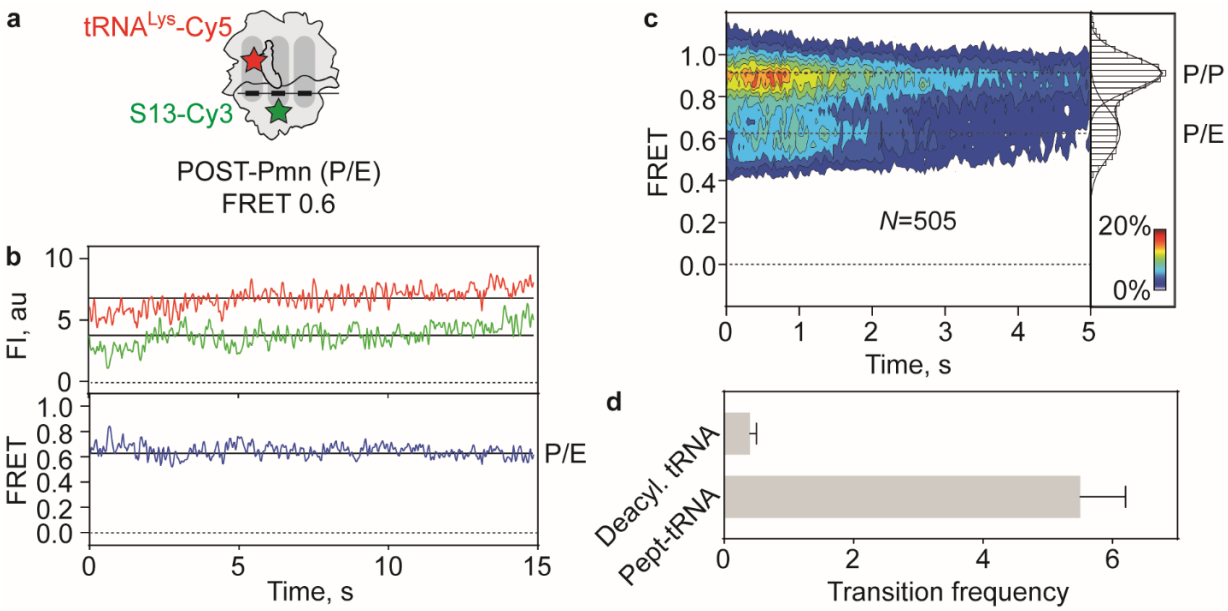

Figure 33. S13-tRNA smFRET in POST-Pmn complex. (a) Schematic of deacylated tRNA^{Lys}-Cy5 (red stars) in POST complex in the presence of Pmn. (b) Representative smFRET trace showing donor and acceptor FI, calculated FRET and HMM fit corresponding to P/E tRNA conformation. (c) Contour plot showing FRET distribution in the POST-Pmn complex. Histogram at the right reveals two states with FRET 0.92±0.08 and 0.63±0.11. Data was obtained in at least three independent experiments. (d) Transition frequency (transitions per trace) for the pept-tRNA^{Lys}-Cy5 in PRE (L11-tRNA FRET) and deacylated tRNA^{Lys}-Cy5 in POST-Pmn complex (S13-tRNA FRET).

Translocation of deacylated tRNA on slippery mRNA

In order to monitor translocation of the deacylated tRNA from the P to the E site and dissociation from the ribosome, we prepared S13-Cy3 ribosome complexes carrying a deacylated $tRNA^{Lys}$-Cy5 in the P site and pept-$tRNA^{Lys}$ in the A site. Translocation was first monitored on the non-slippery mRNA by EF-G(wt) as a decrease in FRET from 0.9 (P/P) or 0.6 (P/E) to lower FRET followed by loss of FRET (Fig. 34a). Synchronization of the traces at the time point where transition to FRET≤ 0.5 is observed and population distribution of the FRET values after the synchronization point revealed one Gaussian distribution with FRET 0.32±0.10 (Fig. 34b). In order to investigate whether the FRET 0.3 state represents the transient binding of the deacylated tRNA in the E site, we repeated the experiment in the presence of fusidic acid (FA). FA is an antibiotic that binds at the interface of EF-G domains 1, 2 and 3 (Fig. 34c) and prevents structural rearrangements that drive the dissociation of EF-G from the ribosome after translocation (Gao et al., 2009; Ramrath et al., 2013; Rundlet et al., 2021). FA does not prevent translocation from the P to the E site but blocks the dissociation of the deacylated tRNA and EF-G from the ribosome (Belardinelli and Rodnina, 2017; Wasserman et al., 2016). Translocation in the presence of FA leads to a long-lived state with FRET 0.31±0.11, indicating that the FRET 0.3 state represents the binding of the deacylated tRNA in the E site (Fig. 34d). Loss of FRET following the FRET 0.3 state can occur either due to tRNA dissociation from the ribosome or photobleaching. To clarify this, we compared the decay rate of the FRET 0.3 state in the absence and presence of FA. In the absence of FA, the decay rate of the FRET 0.3 state is 0.9±0.1 s^{-1} (Fig. 34b and Table 7), similar to tRNA dissociation rates from previous studies (Belardinelli and Rodnina, 2017; Belardinelli et al., 2016a; Wasserman et al., 2016) and in agreement with studies reporting spontaneous tRNA release (Adio et al., 2015; Chen et al., 2011b; Chen et al., 2013b; Choi and Puglisi, 2017; Lill et al., 1986; Petropoulos and Green, 2012; Semenkov et al., 1996; Uemura et al., 2010; Wasserman et al., 2016). In the presence of FA, the decay rate decreases significantly (Fig. 34e and Table 7). In order to assign the FRET 0.3 state to a structural state of the ribosome, we used the study by Fischer et al., 2010, the only time-resolved study of translocation that does not involve antibiotics and provides insights into tRNA dissociation, i.e. the transition from E/E into the E' state and tRNA dissociation (Fischer et al., 2010). In the E' state, the S13-tRNA distance increases (~63Å, corresponding to FRET 0.3). Furthermore, ensemble kinetic studies show that, in the presence of FA, the transition from the E' state to tRNA dissociation is severely affected (~200 fold slower) and the E' state is prolonged (Belardinelli and Rodnina, 2017). Therefore, we assign

the FRET 0.3 state to the transient binding of the deacylated tRNA in the E site, plausibly the E' state.

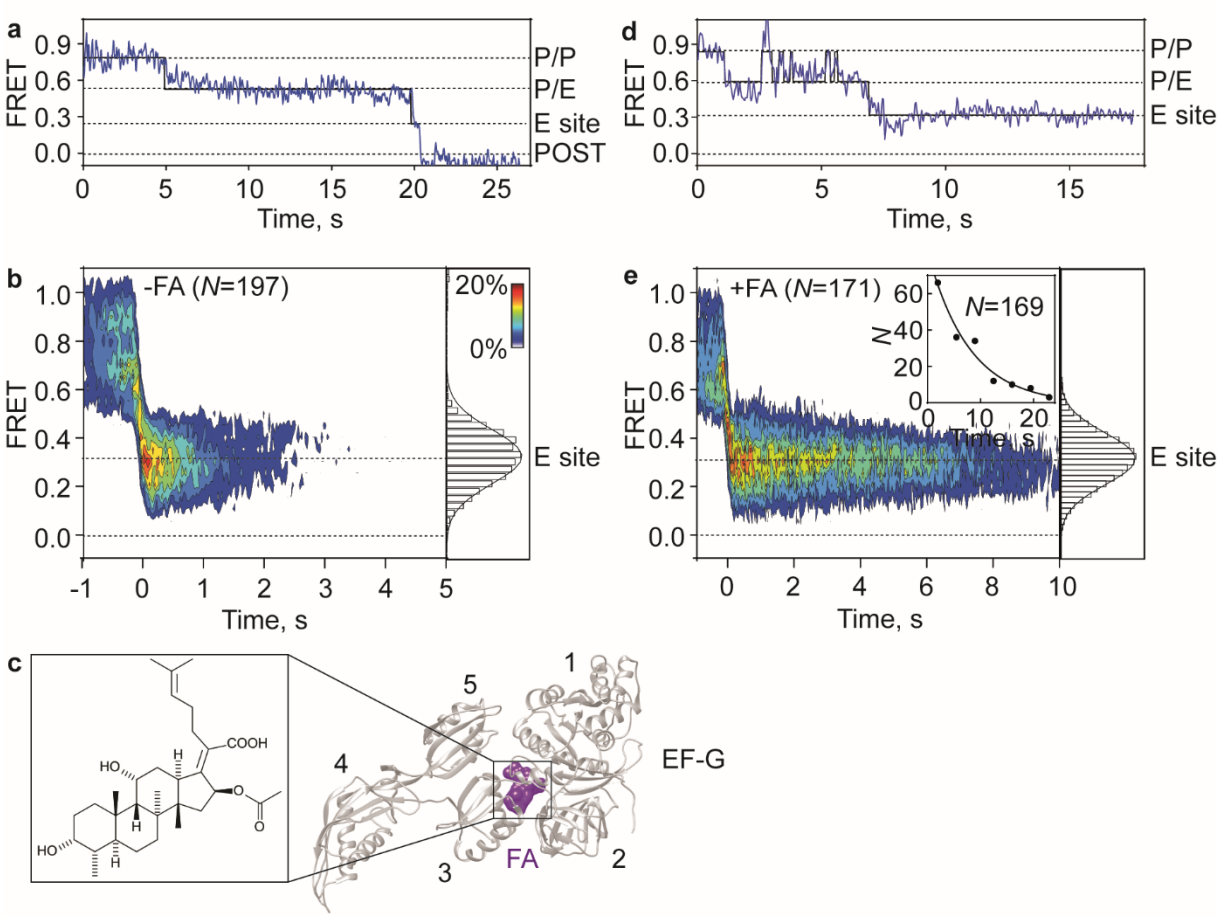

Figure 34. Translocation of the deacylated tRNA^{Lys} in the absence and presence of FA. (a) Representative smFRET trace corresponding to tRNA^{Lys} translocation by EF-G(wt) on non-slippery mRNA in the absence of FA. (b) Contour plot showing FRET distribution after synchronization during tRNA^{Lys} translocation on non-slippery mRNA mediated by EF-G(wt) in the absence of FA. Data was obtained in at least three independent experiments. (c) Crystal structure of FA (purple) bound to EF-G (grey). Zoom-in shows the chemical structure of FA. The figure was modified from PDB 4V5F (Gao et al., 2009). (d) Representative smFRET trace showing tRNA^{Lys} translocation by EF-G(wt) on non-slippery mRNA in the presence of FA. (e) Contour plot showing FRET distribution after synchronization during tRNA^{Lys} translocation on non-slippery mRNA mediated by EF-G(wt) in the presence of FA. Inset shows dwell-time distribution of the FRET 0.3 state (Table 7). Black line is single exponential fit.

However, in order to ensure that the photobleaching of the dyes does not affect the dwell time of the FRET 0.3 state, we determined the photobleaching rate of Cy3 and Cy5 attached to double-stranded DNA (Fig. 35a) (Ha et al., 2002), where one strand is 18-mer covalently attached to Cy5 at the 5' end followed by a unique sequence attached to 3'-biotin. A complementary 18-mer DNA strand carries Cy3 in its 5' end (Fig. 35a). Hybridization of the two strands leads to Cy3/Cy5-double labelled DNA so that the Cy3-Cy5 distance is ~60Å (Fig. 35a). FRET distribution of time traces showed a single Gaussian distribution with FRET 0.39±0.12 (Fig. 35b, c) and the photobleaching rate was as low as 0.03±0.01 s^{-1} (Fig. 35d). Therefore, the photobleaching of the FRET dyes does not significantly affect the dissociation rate of the deacylated tRNA.

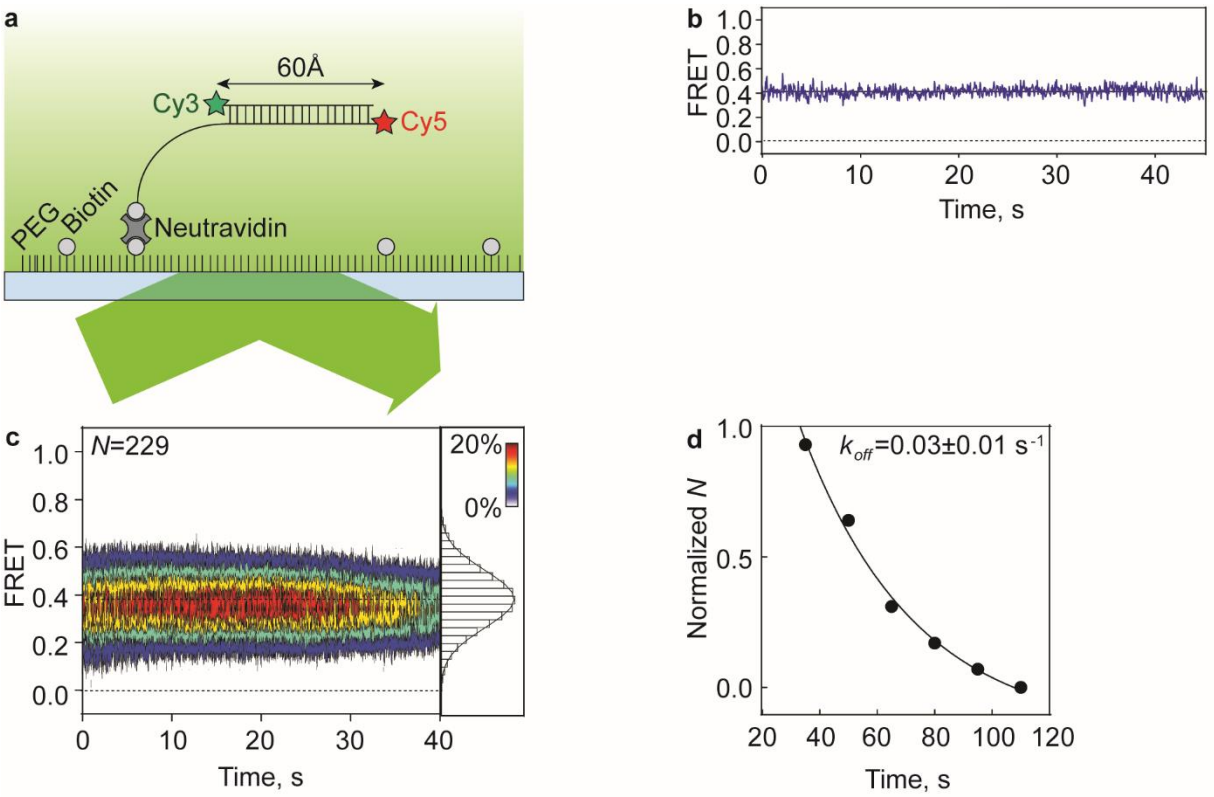

Figure 35. Photostability of the Cy3-Cy5 FRET pair. (a) smFRET setup to monitor the photobleaching rate of Cy3-Cy5 FRET. One DNA strand is 3'-biotinylated and labelled at the 5' end with acceptor Cy5 (red star) while the complementary strand is labelled at the 5' end with donor Cy3 (green star). (b) Representative smFRET trace of the Cy3-Cy5 double-labeled DNA. (c) Contour plot showing FRET distribution of the Cy3-Cy5 double-labelled DNA. (d) Dwell-time distribution of the smFRET traces. Black line is single exponential fit.

Next, we tested whether the slippery mRNA affects the trajectory of the deacylated tRNA from the P to the E site. We performed the experiment on the slippery mRNA and induced translocation by EF-G(wt) (Fig. 36a). smFRET traces showed the same pattern of transition from FRET 0.9 (P/P) or 0.6 (P/E) to FRET 0.3 state (E site) followed by loss of FRET (tRNA dissociation), as on non-slippery mRNA. FRET distribution after synchronization revealed a single state with FRET 0.3 (Fig. 36a). The decay rate of FRET 0.3 state was identical to non-slippery mRNA (1.0±0.1 s^{-1}, Fig. 36a and Table 7). Therefore, the slippery sequence has no effect on the trajectory of the deacylated tRNA from the P to the E site and dissociation from the ribosome. The next step is to investigate whether translocation of deacylated induced by EF-G(Q507D), the mutant that showed the highest frameshifting (Fig. 23c) and lowest translocation rate (Niblett et al., 2021; Peng et al., 2019), differs from translocation by EF-G(wt). tRNA trajectories during translocation by EF-G(Q507D) show transition from FRET 0.9 (P/P) or 0.6 (P/E) to FRET 0.3 (E site) followed by loss of FRET (tRNA dissociation, Fig. 36b, c). The pattern is identical on non-slippery and slippery mRNA (Fig. 36b, c) and, surprisingly, the decay rates of the FRET 0.3 state were not affected and were at the same range to EF-G(wt) (Fig. 36c and Table 7). Interestingly, when we quantified the transitions between FRET 0.9/0.6 and 0.3 states, we observed only forward transitions from FRET 0.9/0.6 to 0.3 state and no backward transitions from FRET 0.3 to 0.9/0.6 state, in all cases (Fig. 36d). This indicates directional unperturbed translocation of the deacylated tRNA from the P to the E site and dissociation from the ribosome. In conclusion, the slippery mRNA and EF-G(Q507D) do not affect the trajectory of the deacylated tRNA from the P to the E site. However, the dissociation rates in all cases (Table 7) are ~3-5-fold higher than the translocation rate of the pept-tRNA in the ribosomes that show slow translocation (~0.2 s^{-1}, Table 6). This indicates that, for a fraction of ribosomes, the movement of the two tRNAs is uncoupled: while the deacylated tRNA translocates and dissociates fast from the ribosome, the pept-tRNA is trapped in fluctuations between CHI and P/P states. Such fluctuations may lead to frameshifting because the –1-frame codon becomes available for binding of pept-tRNA.

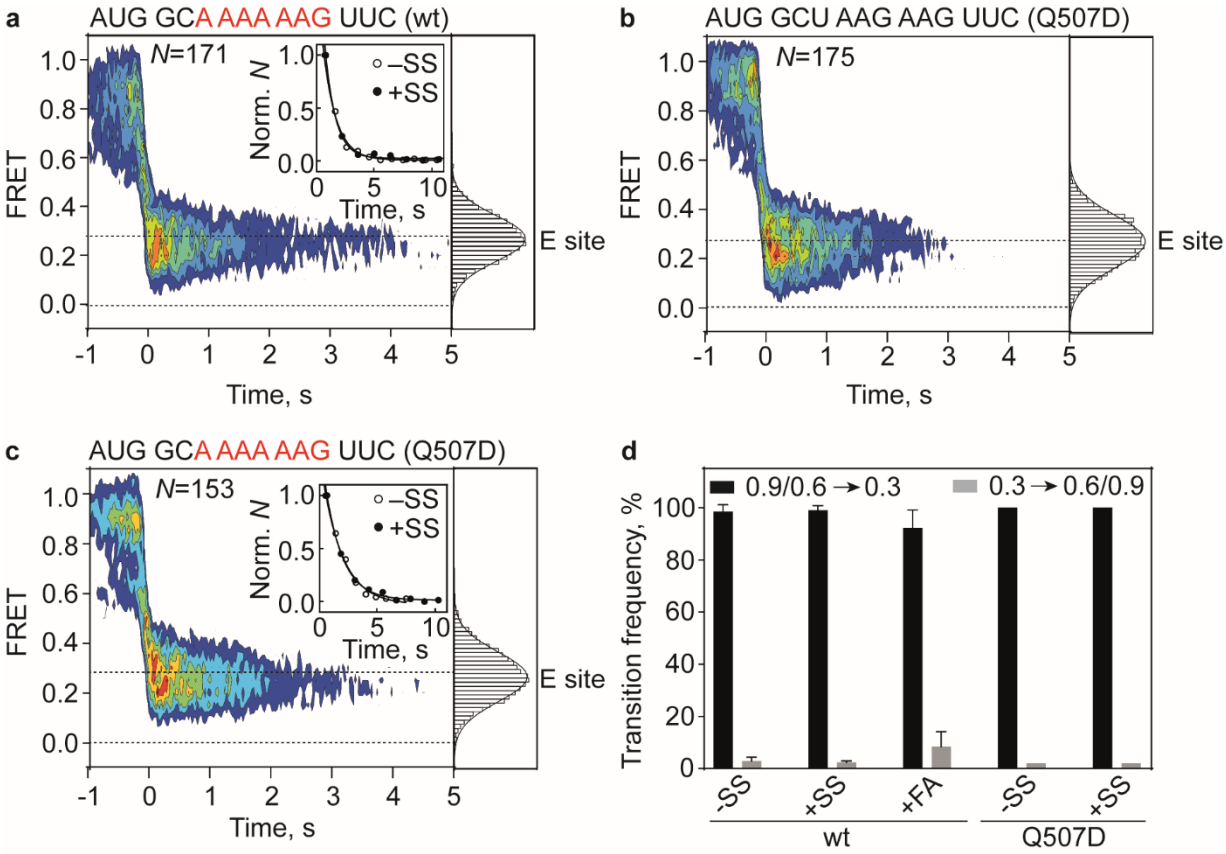

Figure 36. Translocation of deacylated tRNA^{Lys} by EF-G(wt) and EF-G(Q507D). (a) Contour plot showing FRET distribution after synchronization during tRNA^{Lys} translocation on slippery mRNA mediated by EF-G(wt). Inset is the dwell-time distribution of the FRET 0.3 (E site) state during translocation on slippery (closed circles) and non-slippery (open circles) mRNA mediated by EF-G(wt). (b) Contour plot showing FRET distribution after synchronization during tRNA^{Lys} translocation on non-slippery mRNA by EF-G(Q507D). (c) Contour plot showing FRET distribution after synchronization during tRNA^{Lys} translocation on slippery mRNA by EF-G(Q507D). Inset is the dwell-time distribution of the FRET 0.3 (E site) state during translocation on slippery (closed circles) and non-slippery (open circles) mRNA mediated by EF-G(Q507D). (d) Quantification of forward (FRET 0.9/0.6→0.3, black) and backward (FRET 0.3→0.6/0.9, grey) transitions during translocation of deacylated tRNA^{Lys}.

Table 7. Kinetics of deacylated tRNA^{Lys} dissociation from the E site.

EF-G	Dissociation rate from E site, s^{-1} (*N*)	
	U AAG AAG (non-slippery)	A AAA AAG (slippery)
wt	0.9±0.1 (196)	1.0±0.1 (169)
Q507D	0.6±0.1 (175)	0.5±0.1 (152)
wt–FA	0.1±0.1 (169)	n.d.

5.3. Timing and key transitions of frameshifting

In order to further understand the correlation between slow translocation and spontaneous frameshifting, we studied whether a delay in translocation at a stage prior to CHI formation also promotes frameshifting. To make translocation slow, we used GTPγS and the antibiotic spectinomycin (Spc), which are both inhibitors that impede the tRNA progression from the PRE to the CHI state (Adio et al., 2015; Belardinelli et al., 2016a; Belardinelli et al., 2021; Wasserman et al., 2016).

Translocation on slippery mRNA by EF-G–GTPγS

GTPγS is a GTP analog, in which one oxygen atom in the γ-phosphate group is replaced by sulfur (Fig. 37a). This impedes the attack of the nucleophile (water) on the covalent bond between β- and γ-phosphate groups, thus slowing down GTP hydrolysis by EF-G to a rate of ~0.005 s^{-1} (Rodnina et al., 1997). GTPγS has the same affinity and engages in the same interactions as GTP in the nucleotide-binding pocket of translational GTPases (Fig. 37b) (Kuhle and Ficner, 2014). Therefore, GTPγS is an authentic GTP analog that stalls translocation at stage before CHI formation (Adio et al., 2015; Belardinelli et al., 2016a).

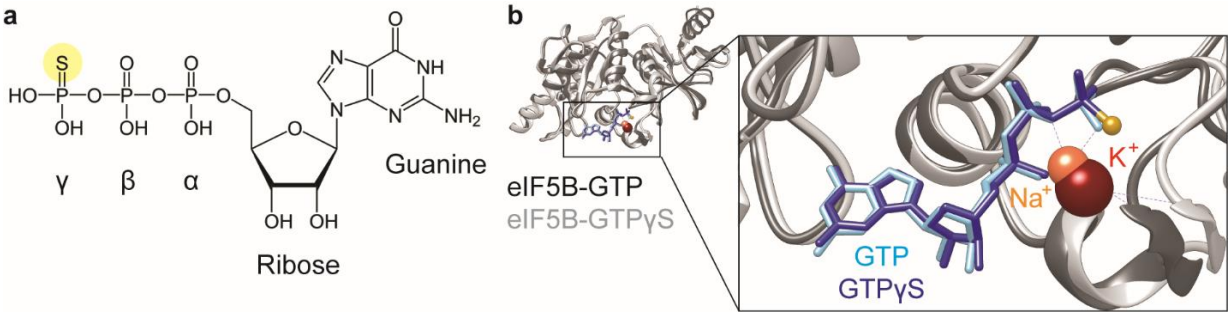

Figure 37. GTPγS structure and conformation in the nucleotide-binding pocket of the translational GTPase eIF5B. (a) Chemical structure of GTPγS. The replaced sulfur atom is shown in yellow. (b) Superimposition of crystal structures of the translational GTPase eIF5B bound to GTP (dark grey) or GTPγS (light grey). Zoom-in shows the GTP-binding pocket with GTP (light blue) or GTPγS (dark blue). The monovalent ions Na^+ (orange) and K^+ (red) are shown as spheres. The figure is adapted from PDB 4TMZ and 4NCN (Kuhle and Ficner, 2014).

Slow hydrolysis of GTPγS by EF-G slows down translocation to rates of ~0.5-0.7 s^{-1} (based on puromycin reactivity), ~50-fold slower than translocation rate in the presence of GTP (Adio et al., 2015; Belardinelli et al., 2016a; Katunin et al., 2002; Rodnina et al., 1997). Interestingly, this rate is in the same range with the translocation rate of EF-G(Q507D) (~0.8 s^{-1}, Fig. 38a) (Niblett et al., 2021; Peng et al., 2019) but the efficiency of spontaneous frameshifting in the

presence of GTPγS is as low as with EF-G(wt)—GTP (Fig. 38a). This indicates that slow translocation alone is not sufficient to induce spontaneous frameshifting. This prompted us to investigate how the tRNA trajectories on slippery mRNA in the presence of GTPγS differ compared to the highly error-prone translocation by EF-G(Q507D).

First, we followed the trajectory of the pept-tRNA^{Lys}-Cy5 during translocation on slippery mRNA by EF-G(wt)—GTPγS using the L11-tRNA FRET pair (Fig. 38b). The majority of smFRET traces (72%) showed translocation to FRET 0.2 state (P/P) via CHI-like states (Fig. 38b, c and Table 8). The CHI-like state corresponds to the off-pathway translocation intermediate in the presence of GTPγS and is different from the authentic CHI state in the presence of GTP (Carbone et al., 2021; Petrychenko et al., 2021). We then systematically analyzed the translocation trajectory. EF-G(wt)—GTPγS stabilizes the hybrid A/P* tRNA conformation (Fig. 38d), similarly to EF-G(Q507D) (Fig. 23a). However, transition frequency analysis after synchronization shows increased fluctuations between A/P* and CHI-like states (Fig. 38e, f), in drastic contrast to EF-G(wt)—GTP and EF-G(Q507D) (Fig. 23c). Therefore, in the presence of GTPγS, pept-tRNA^{Lys}-Cy5 is trapped in fluctuations between A/P* and CHI-like states.

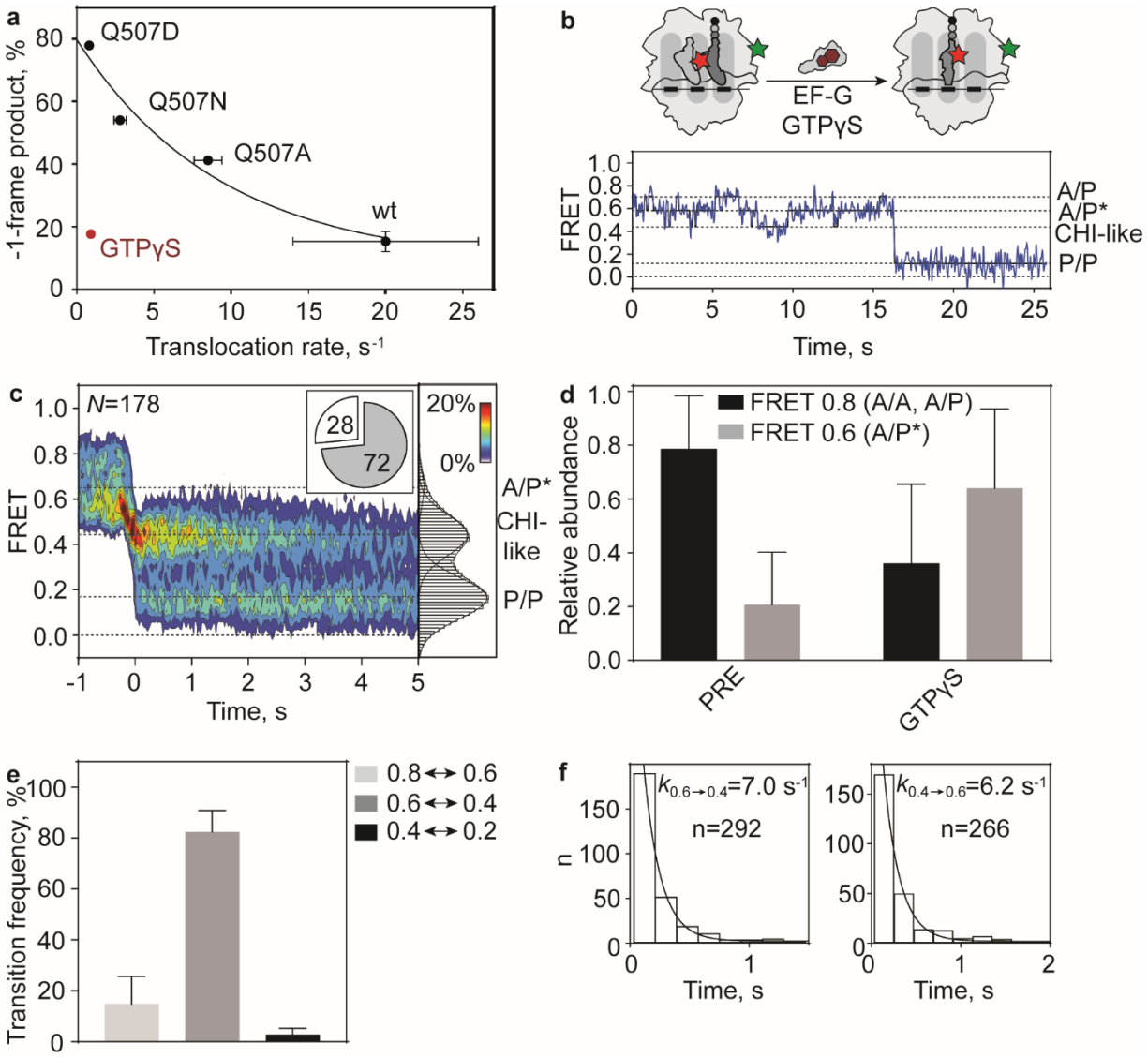

Figure 38. Translocation of pept-tRNA^{Lys} on slippery mRNA in the presence of GTPγS. (a) Correlation between frameshifting and the translocation rate at 37°C. Translocation rates are from (Peng et al., 2019) for EF-G(wt) and EF-G(Q507) mutants and from (Katunin et al., 2002) for GTPγS. (b) Schematic and representative smFRET trace corresponding to pept-tRNA^{Lys}-Cy5 translocation from A to P site on slippery mRNA mediated by EF-G(wt)—GTPγS. GTPγS is shown as maroon hexagons inside EF-G. (c) Contour plot showing FRET distribution after synchronization during translocation on slippery mRNA mediated by EF-G(wt)—GTPγS. Pie chart indicates the fraction of smFRET traces showing slow during translocation (grey). (d) Relative abundance of the FRET states 33 ms prior to translocation mediated by EF-G(wt)—GTPγS, compared to PRE complex. (e) Transition frequency between different FRET states during translocation on slippery mRNA in the presence of GTPγS. (f) Dwell-time distribution of the major transitions during translocation on slippery mRNA mediated by EF-G(wt)—GTPγS. Black line is single exponential fit.

Table 8. Kinetics of pept-tRNA^{Lys} fluctuations during translocation on slippery mRNA in the presence of GTPγS.

EF-G	k_{TL}, s^{-1} (*N*)	FRET, μ±s.d.	Transition rates during translocation *k*, s^{-1} (n) 0.6→0.4 0.4→0.6	0.4→0.2 0.2→0.4
wt–GTPγS	0.2±0.1 (128)	0.6±0.1 0.4±0.1 0.2±0.1	7.0±0.9 (292) 6.2±0.9 (266)	n.d. (9) n.d. (9)

Next, we tested how the trajectory of the deacylated tRNA during translocation on slippery mRNA is affected by GTPγS using the S13-tRNA FRET pair (Fig. 39). The smFRET traces showed transition from FRET 0.9 (P/P) or 0.6 (P/E) to FRET 0.3 (E site) followed by loss of FRET (tRNA dissociation, Fig. 39a). Synchronization at the point where the first transition with FRET≤ 0.5 is observed and FRET population distribution after the synchronization point revealed one Gaussian distribution (FRET 0.31±0.11 for non-slippery and 0.27±0.10 for slippery mRNA, Fig. 39b, c). The dissociation of deacylated tRNA occurred at the same rate on non-slippery (0.2±0.1 s^{-1}) and slippery mRNA (0.3±0.1 s^{-1}, Fig. 39c), but ~2-3-fold lower than tRNA dissociation in the presence of EF-G(wt)—GTP and EF-G(Q507D)—GTP. Interestingly, during translocation by EF-G—GTPyS, deacylated tRNA and pept-tRNA translocate at comparable speed implying that the movement of the two tRNAs is slow but coupled.

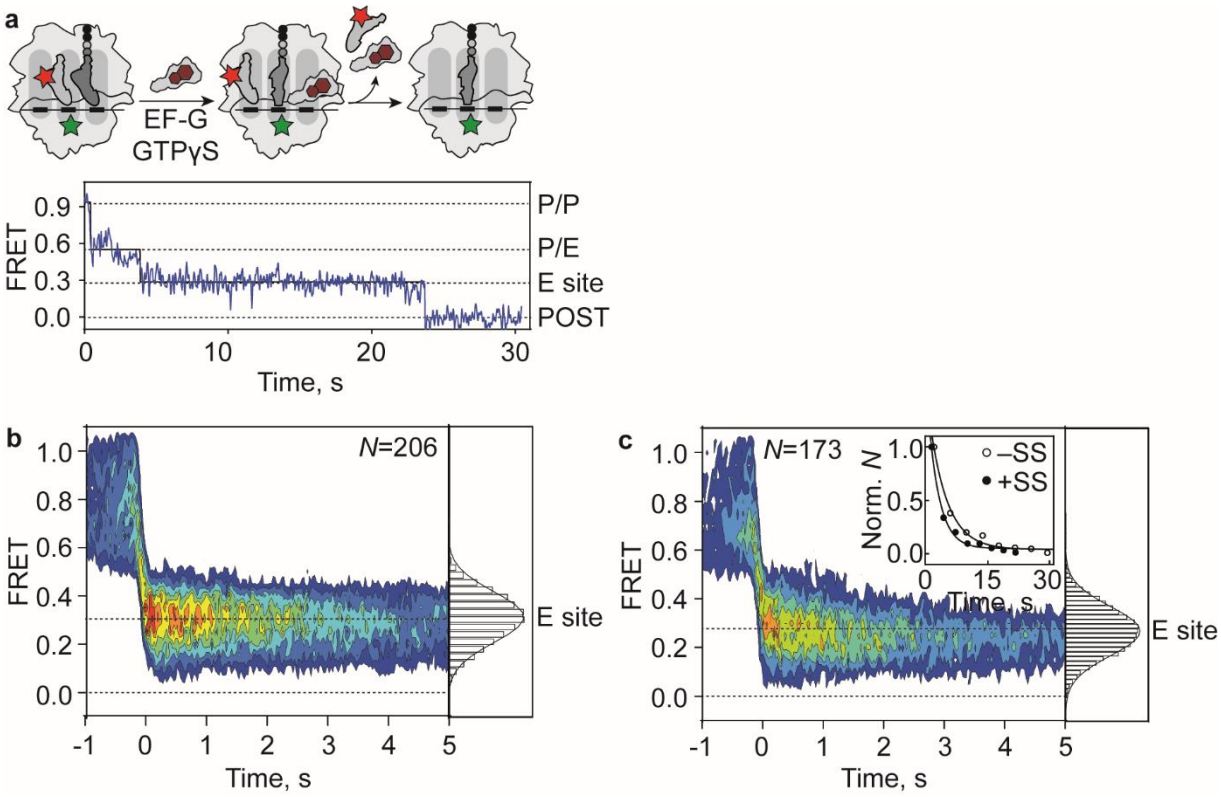

Figure 39. Translocation of the deacylated tRNA^{Lys} in the presence of GTPγS. (a) Schematic and representative smFRET trace corresponding to translocation of the deacylated tRNA^{Lys}-Cy5 from P to E site on slippery mRNA in the presence of GTPγS. (b-c) Contour plot showing FRET distribution after synchronization during translocation on non-slippery (b) and slippery (c) mRNA in the presence of GTPγS. Inset in (c) is dwell-time distribution of the FRET 0.3 (E site) state during translocation on non-slippery (open circles, 0.2±0.1 s^{-1}) and slippery (closed circles, 0.3±0.1 s^{-1}) mRNA in the presence of GTPγS. Black line is single exponential fit.

Translocation on slippery mRNA in the presence of Spc

To further understand the key transitions that lead to spontaneous frameshifting, we repeated the experiments in the presence of the antibiotic spectinomycin (Spc), which binds to 16S rRNA helix 34 (h34) between the SSU body and head domains close to the P site (Fig. 40a) (Borovinskaya et al., 2007; Rundlet et al., 2021). In the presence of EF-G, Spc induces ~5.9° swiveling of the SSU head domain that potentially allows movement of the pept-tRNA in SSU out of the A site towards a CHI-like state (Rundlet et al., 2021). However, ensemble kinetics and smFRET studies reported that Spc prevents unlocking of the ribosome, thus stalling the complex prior to authentic CHI state formation (Belardinelli et al., 2021; Wasserman et al., 2016). The translocation rate in the presence of Spc is in the same range to the rate with EF-G(Q507D) and EF-G(wt)—GTPγS (Fig. 40b) (Katunin et al., 2002; Peng et al., 2019; Peske et al., 2004). However, the frameshifting efficiency in the presence of Spc was only slightly higher than frameshifting by EFG(wt)—GTPγS, but significantly lower than frameshifting by EF-G(Q507D) (Fig. 40b). This result confirms that delay in translocation prior to CHI state formation does not lead to frameshifting.

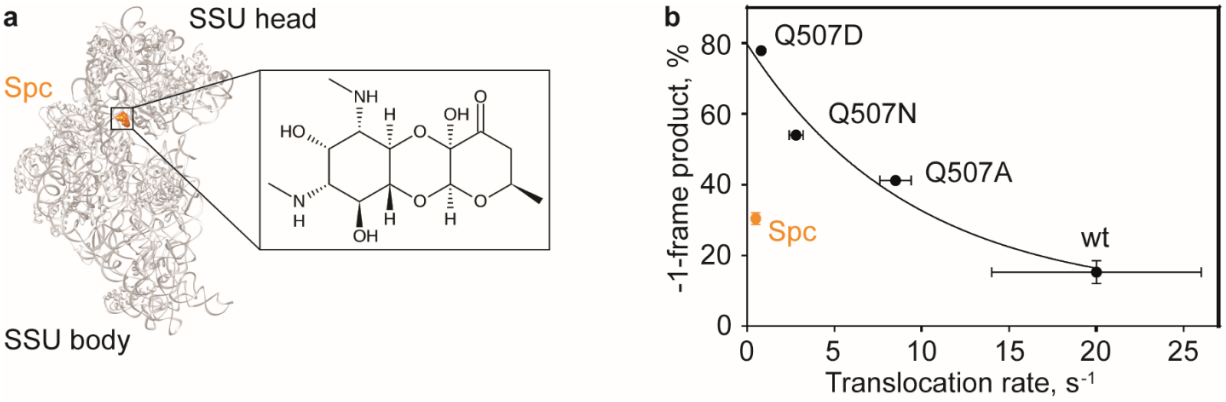

Figure 40. Spontaneous –1 frameshifting in the presence of Spc. (a) Crystal structure of Spc (orange) bound to SSU (grey). Zoom-in shows the chemical structure of Spc. The figure is adapted from PDB 4V56 (Borovinskaya et al., 2007). (b) Correlation between frameshifting and the translocation rate at 37°C. Translocation rates are from (Peng et al., 2019) for EF-G(wt) and EF-G(Q507) mutants and from (Peske et al., 2004) for EF-G(wt) in presence of 1mM Spc.

When we followed the trajectory of the pept-tRNA^{Lys}-Cy5 during translocation on slippery mRNA by EF-G(wt) in the presence of Spc using the L11-tRNA FRET pair, the majority of smFRET traces (81%) show translocation via CHI-like states (Fig. 41a, b). The POST state was not reached in the time course of the experiment, indicating that translocation rate was very low and limited by the photobleaching of the dyes (Fig. 41a, b). 19% show direct transition from PRE to POST states, probably due to the fact that Spc was not bound to these complexes (Fig. 41b), as indicated by previous studies (Peske et al., 2004). Spc does not affect the ability of EF-G(wt) to stabilize the A/P* tRNA conformation (Fig. 41c), similar to EF-G(wt)—GTPγS (Fig. 38d), EF-G(wt)—GTP and EF-G(Q507D) (Fig. 23a). Transition frequency analysis after synchronization shows enhanced fluctuations between A/A, A/P and A/P* and between A/P* and CHI-like states (Fig. 41d, e and Table 9), as observed during translocation by EF-G(wt)—GTPγS (Fig. 38d) but in drastic contrast to translocation by EF-G(wt)—GTP and EF-G(Q507D), where fluctuations between CHI and P/P states were enhanced (Fig. 22c). Thus, Spc traps pept-tRNA in fluctuations between A/A, A/P, A/P* and CHI-like states, which again shows that fluctuations between early translocation intermediates do not enhance frameshifting.

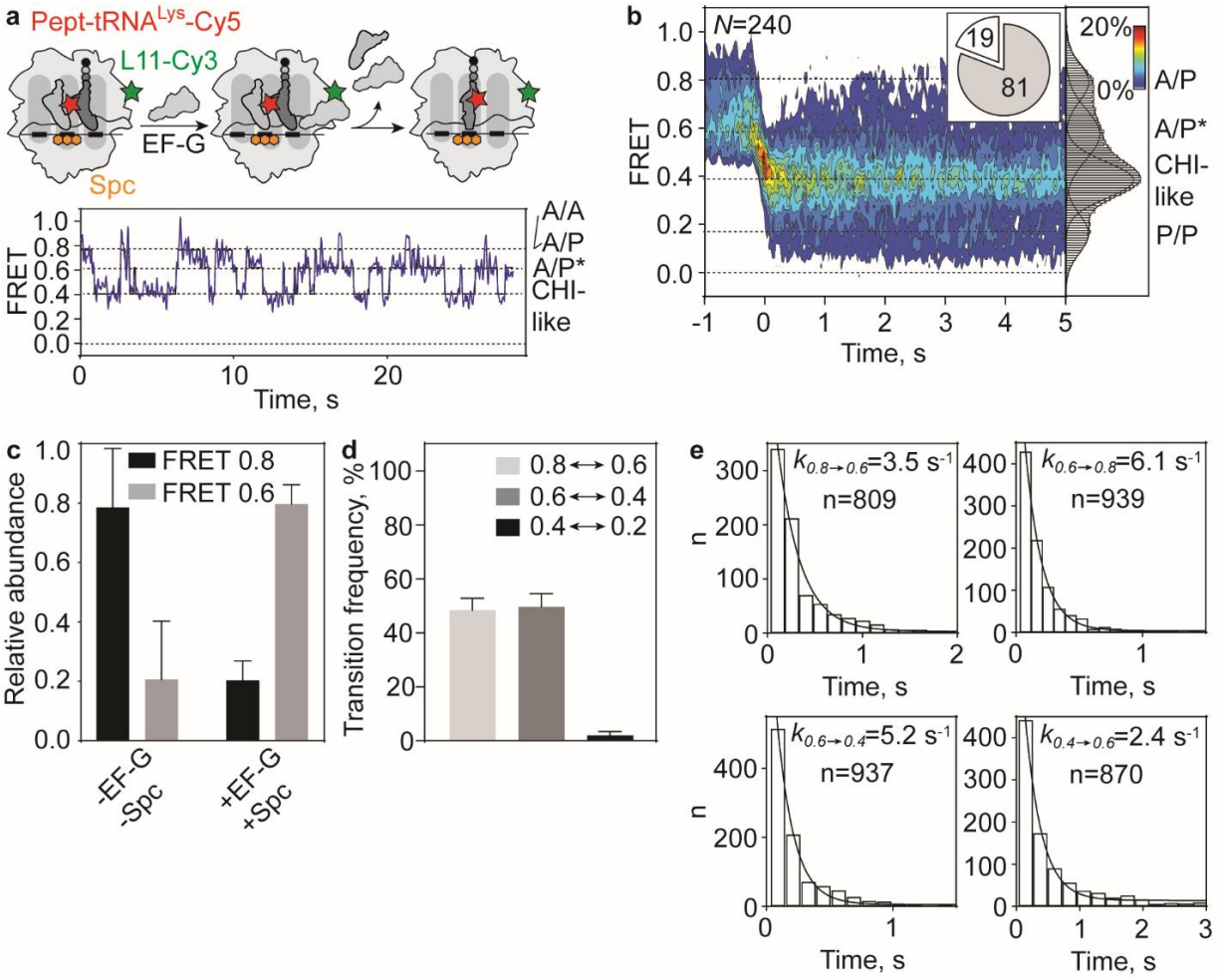

Figure 41. Translocation of pept-tRNA^{Lys} on slippery mRNA in the presence of Spc. (a) Schematic and representative smFRET trace corresponding to pept-tRNA^{Lys}-Cy5 translocation from the A to the P site by EF-G(wt) in the presence of Spc (orange hexagons). (b) Contour plot showing FRET distribution after synchronization during translocation on slippery mRNA mediated by EF-G(wt) in the presence of Spc. Pie chart indicates the fraction of smFRET traces showing slow translocation (grey). (c) Relative abundance of the FRET states 33 ms prior to translocation mediated by EF-G(wt) in the presence of Spc, compared to PRE complex in the absence of Spc. (d) Transition frequency between different FRET states during translocation of pept-tRNA^{Lys}-Cy5 on slippery mRNA in the presence of Spc. (e) Dwell-time distribution of the major transitions during translocation on slippery mRNA in the presence of Spc. Black line is single exponential fit.

Table 9. Kinetics of pept-tRNA^{Lys} fluctuations during translocation on slippery mRNA in the presence of Spc.

EF-G	FRET, μ±s.d	Transition rates during translocation *k*, s^{-1} (n)		
		0.8→0.6 0.6→0.8	0.6→0.4 0.4→0.6	0.4→0.2 0.2→0.4
wt-Spc	0.8±0.1			
	0.6±0.1	3.5±0.4 (809)	5.2±1.2 (937)	n.d. (39)
	0.4±0.1	6.1±1.2 (939)	2.4±0.2 (870)	n.d. (29)
	0.2±0.1			

The effect of Spc on deacylated tRNA translocation was studied using the S13-tRNA FRET pair (Fig. 42a). The smFRET traces showed transition from FRET 0.9 (P/P) or 0.6 (P/E) to FRET 0.3 (E site) followed by loss of FRET (tRNA dissociation, Fig. 42a). Synchronization at the point where the first transition to FRET≤ 0.5 is observed and FRET population distribution after the synchronization point revealed one Gaussian distribution (FRET 0.3) corresponding to the binding of the deacylated tRNA in the E site (Fig. 42b). The decay rate of the FRET 0.3 state (0.3±0.1 s^{-1}, Fig. 42c) is similar to the rate by EF-G(wt)—GTPγS (0.3±0.1 s^{-1}, Fig. 39c) and ~2-3-fold lower than the respective rates induced by EF-G(wt)—GTP and EF-G(Q507D) (Fig. 36a, c). This signifies that the movement of the two tRNAs in the presence of Spc is slow but coupled, similar to EF-G(wt)—GTPγS. In conclusion, the experiments with GTPγS and Spc demonstrate that coupled tRNA movement and fluctuations of pept-tRNA between A/P* and CHI states do not lead to frameshifting, while uncoupled tRNA movement resulting in fast dissociation of the deacylated tRNA and the fluctuations of the pept-tRNA between CHI and P/P states seem to be the hallmark of spontaneous frameshifting.

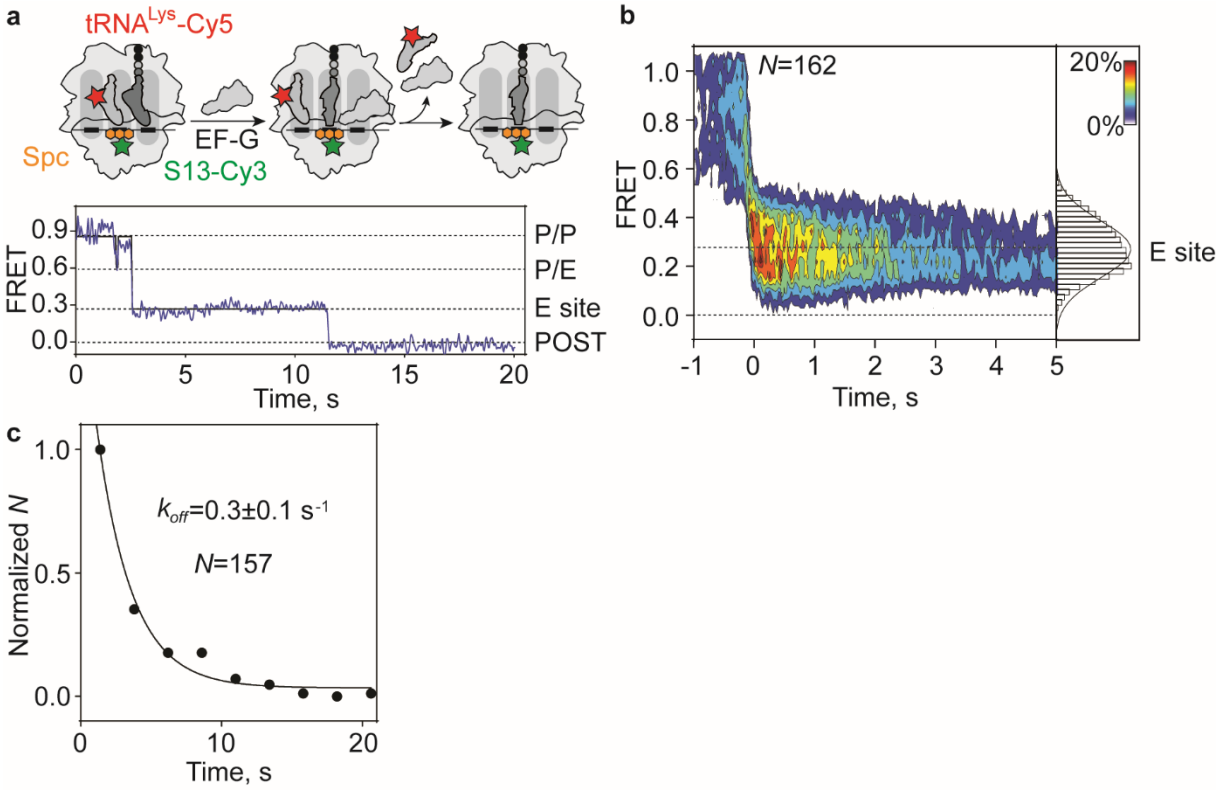

Figure 42. Translocation of deacylated tRNA^{Lys} on slippery mRNA in the presence of Spc. (a) Schematic and representative smFRET trace corresponding to tRNA^{Lys}-Cy5 translocation from the P to the E site by EF-G(wt) in the presence of Spc. (b) Contour plot showing FRET distribution after synchronization during translocation on slippery mRNA mediated by EF-G(wt) in the presence of Spc. (c) Dwell-time distribution of the FRET 0.3 state during translocation of the deacylated tRNA on slippery mRNA by EF-G(wt) in the presence of Spc (0.3±0.1 s^{-1}). Black line is single exponential fit.

5.4. SSU head swiveling during translocation

Next, we studied the motions of the mobile elements of the ribosome, as they have distinct roles in translocation and their actions are orchestrated towards fast and accurate movement of the two tRNAs (Belardinelli et al., 2016b; Carbone et al., 2021; Petrychenko et al., 2021; Wasserman et al., 2016). While the pathway from the A to the P site in SSU is structurally unobstructed (Schuwirth et al., 2005), the opening of the pathway from the P to the E site is regulated by the SSU head domain (Ratje et al., 2010). The 16S rRNA residues A790 and G1338-U1341 form a structural constriction between the P and E site in SSU, known as the P gate (Fig. 43a) (Schuwirth et al., 2005). The P gate is ~17Å wide in the N state of the SSU head and therefore sterically blocks the ~20Å-wide double-stranded tRNA ASL to pass through towards the E site (Jenner et al., 2005; Schuwirth et al., 2005). Ribosome unlocking facilitates widening of the P gate via SSU head domain swiveling, thereby driving forward tRNA movement (Fig. 43b) (Belardinelli et al., 2016a; Carbone et al., 2021; Guo and Noller, 2012; Nishima et al., 2022; Petrychenko et al., 2021; Wasserman et al., 2016). Given that the –1-frame codon resides in the E site in SSU at the end of translocation and uncoupled tRNA movement is a prerequisite for frameshifting, the SSU head domain dynamics may provide an explanation for the undisturbed and fast tRNA dissociation and the high positional uncertainty of the pept-tRNA during spontaneous frameshifting.

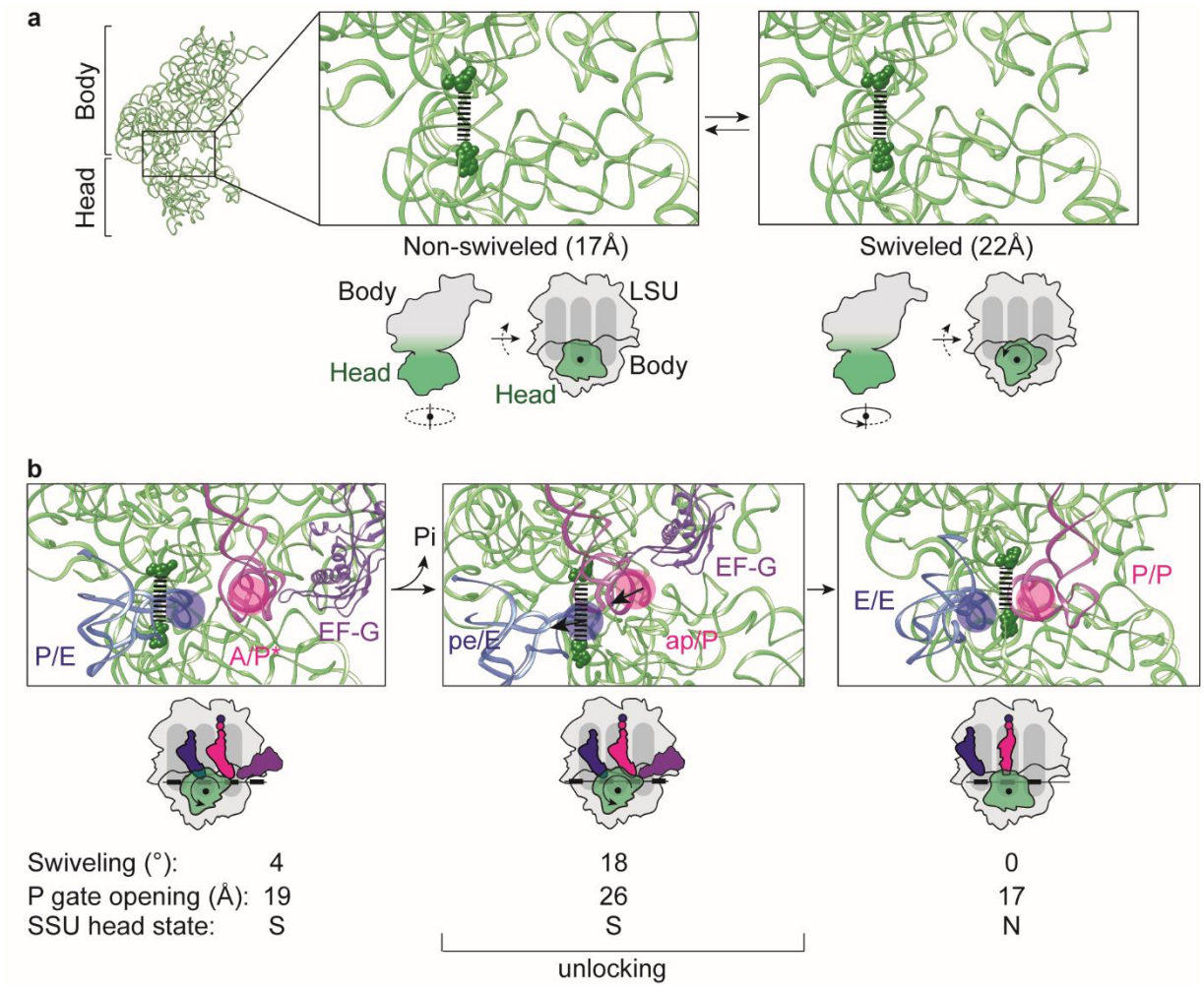

Figure 43. Structural rearrangements of SSU head domain during translocation. (a) Spontaneous swiveling of the SSU head domain in PRE complex. 16S rRNA is shown as light green ribbon. Dotted line indicates the distance between the 16S rRNA bases A790 and G1338-U1341 (dark green spheres) that demarcate the P gate. In the cartoon, SSU head domain is shown in green and the rest of the ribosome in grey. The figure is adapted from PDB 7N1P and 7N30 (Rundlet et al., 2021). (b) Regulation of SSU head domain swiveling by EF-G during translocation. EF-G (purple) stabilizes the swiveled state (left panel). GTP hydrolysis and Pi release drives ribosome unlocking and further opening of the P gate, thus allowing the pept- (magenta) and deacylated (blue) tRNAs to move towards the P and E site, respectively (middle panel). At the POST state, the P gate closes via SSU head back swiveling to the N state (right panel). The swiveling degree (°) and the P gate opening (Å) are shown for each structure. Arrows indicate the direction of tRNA movement. The figure is adapted from PDB 7PJW (PRE—EF-G), 7PJY (unlocking) (Petrychenko et al., 2021) and 7N31 (POST) (Rundlet et al., 2021).

To that end, we monitored FRET using a validated FRET pair between ribosomal protein S13 of the SSU (labeled with Cy3) and protein L33 of the LSU (labeled with Cy5, Fig. 44a) (Belardinelli et al., 2016a). S13 is located at the SSU head domain and L33 is located close to the P site in LSU (Fig. 44a). Swiveling of the SSU head domain leads to decrease in S13-L33 distance and increase in FRET (Fig. 44a, b). We prepared S13-Cy3/L33-Cy5 PRE complexes carrying pept-tRNA^{Lys} in the A site and deacylated tRNA^{Gly} in the P site (Fig. 44c).

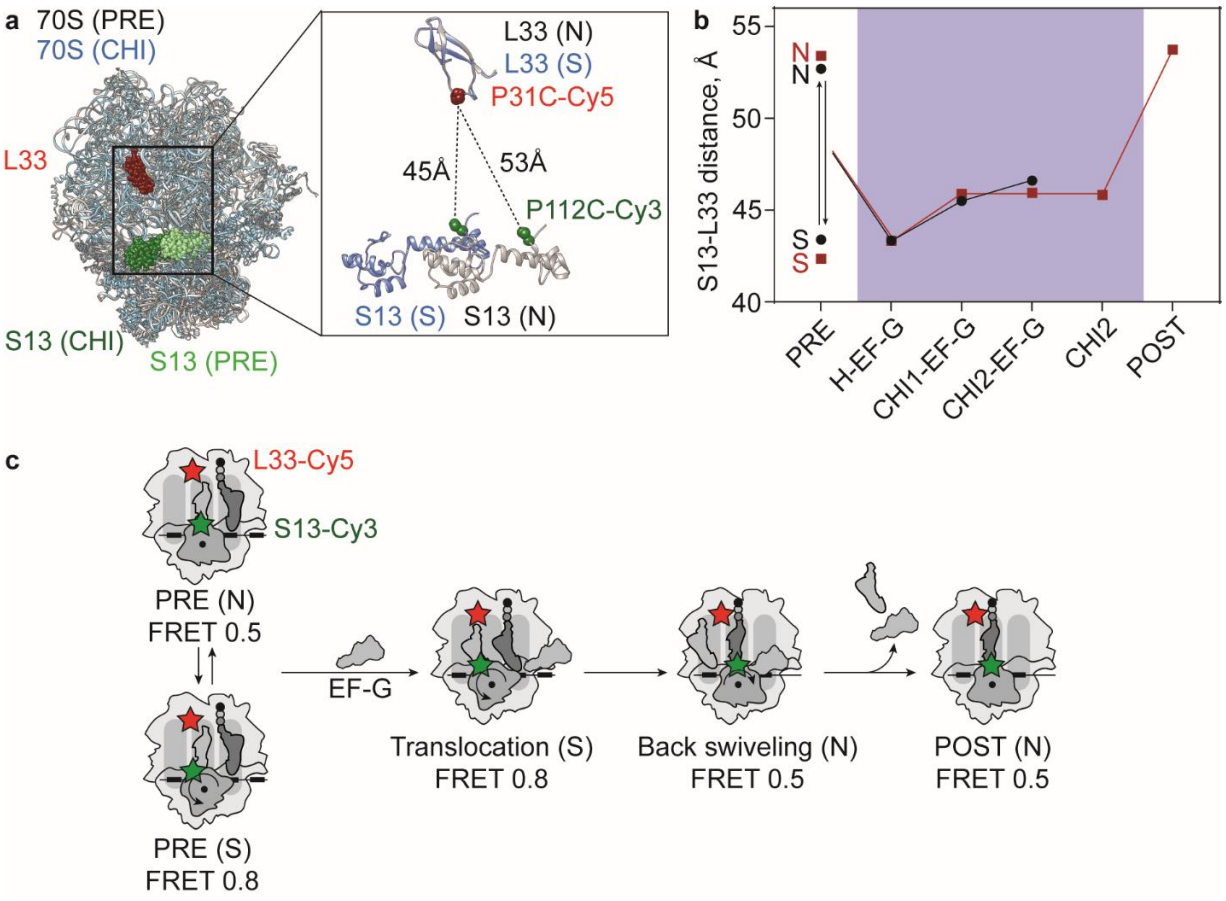

Figure 44. S13-L33 FRET during translocation. (a) Superimposed cryo-EM structures of complexes in PRE state (grey), where the SSU head is in the N state (light green), and CHI state (blue), where the SSU head is in the S state (dark green). Zoom-in shows the distance change between S13 and L33 as a result of SSU head swiveling during translocation. The figure was adapted from PDB 7PJS and 7PJY (Petrychenko et al., 2021). (b) S13-L33 distance change during translocation. The translocation time window is shown in blue shade. The figure is adapted from (Petrychenko et al., 2021) (black circles and connecting line) and (Carbone et al., 2021) (maroon squares and connecting line). (c) smFRET experiment scheme of SSU head swiveling during translocation. The ribosomal protein S13 is labeled with Cy3 (green stars) and L33 with Cy5 (red stars).

SSU head dynamics in PRE and POST complex

To validate the experimental approach, we first monitored smFRET between S13-Cy3 and L33-Cy5 in the PRE complex on the G GGA AAG slippery mRNA in the absence of EF-G (Fig. 45a). smFRET traces show fluctuations between high and lower FRET values (Fig. 45b). FRET population distribution histogram of smFRET traces revealed two Gaussian distributions with FRET values of 0.75±0.12 and 0.54±0.07 (Fig 45c). The transition rate from the FRET 0.5 to 0.8 state ($k_{0.5\rightarrow0.8}$) and the reverse rate from the FRET 0.8 to 0.5 state ($k_{0.8\rightarrow0.5}$) have similar values (Fig. 45d). These results indicate that, in the PRE complex, the SSU head spontaneously interconverts between N and S conformations.

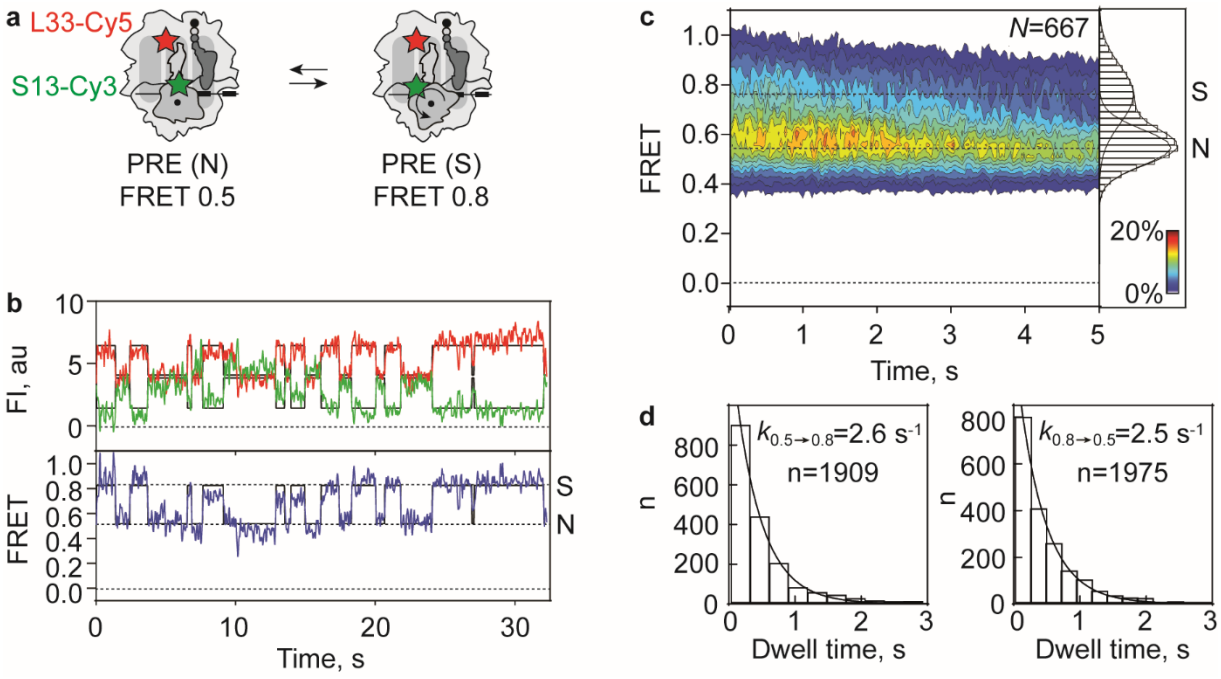

Figure 45. S13-L33 smFRET in PRE complex. (a) Schematic of the PRE complex. S13-Cy3 is shown as green star and L33-Cy5 as red star. (b) Representative smFRET trace showing donor and acceptor FI, calculated FRET and HMM fit, corresponding to SSU head domain fluctuations between the non-swiveled (N) and swiveled (S) states in the PRE complex. (c) Contour plot showing FRET distribution in the PRE complex. (d) Dwell-time distribution of the FRET 0.5 state before transition to the FRET 0.8 state (left, 2.6±0.3 s^{-1}) and of the FRET 0.8 state before transition to the FRET 0.5 state (right, 2.5±0.2 s^{-1}). Black line is single exponential fit.

To determine which FRET states correspond to the N and S conformations of the SSU head domain, we monitored S13-L33 smFRET of POST complexes carrying pept-tRNA^{Lys} in the P site, in which the SSU head domain is expected to be predominantly in the N state (Fig. 46a) (Carbone et al., 2021; Gao et al., 2009; Rundlet et al., 2021). smFRET traces show stable low FRET signal (Fig. 46b). Population distribution of FRET values shows the same FRET states as seen for the PRE complex with FRET 0.52±0.07 and 0.75±0.09 (Fig 46c). However, in this case, the FRET 0.5 population is dominant (Fig. 46c). Therefore, the FRET 0.5 state corresponds to the N state and the FRET 0.8 state corresponds to the S state of the SSU head domain.

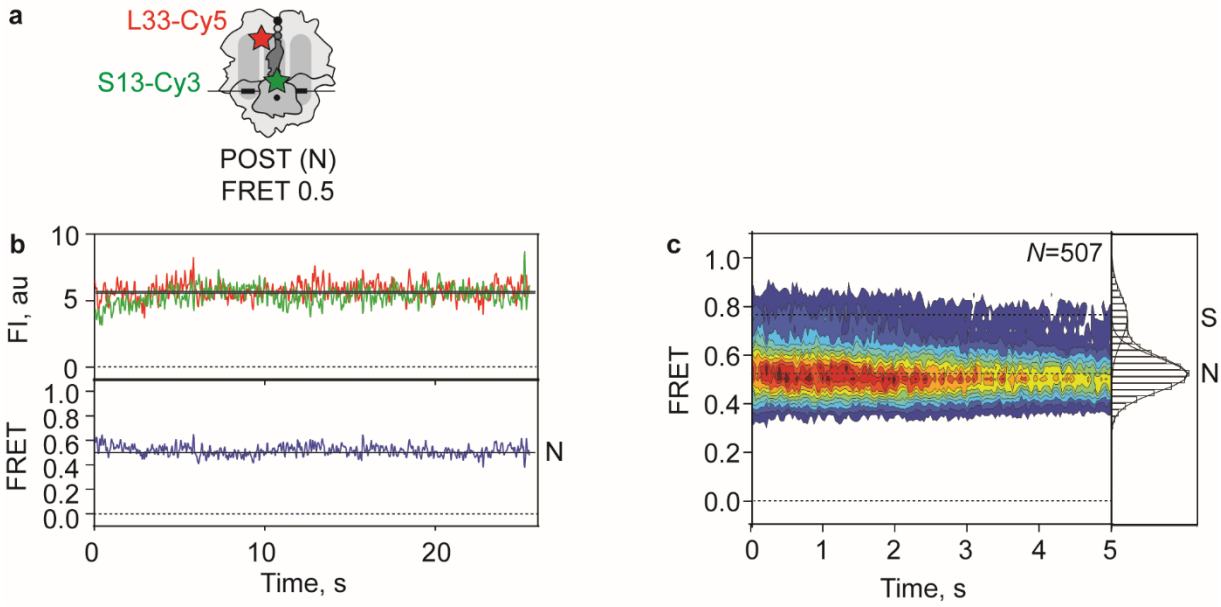

Figure 46. S13-L33 smFRET in POST complex. (a) Schematic of the POST complex. (b) smFRET trace showing donor and acceptor FI, calculated FRET and HMM fit, corresponding to SSU head domain non-swiveled (N) state in the POST complex. (c) Contour plot showing FRET distribution in the POST complex.

SSU head swiveling during translocation by EFG(wt)

Next, we followed SSU head domain swiveling during translocation in real time. The decay rate of the last S state before a long-lived N state gives an estimation of the translocation rate, because the back swiveling of the SSU head is among the last kinetic steps during translocation (Fig. 47a) (Belardinelli et al., 2016a; Nishima et al., 2022; Peng et al., 2019; Wasserman et al., 2016). On the non-slippery mRNA, the majority of smFRET traces (85%) were fluctuating between FRET 0.8 (S) and 0.5 (N) states before transition to a stable FRET 0.5 (N) state, which signifies completion of translocation. A small fraction (15%) showed a long-lived S state without transition to N state, signifying failure to complete SSU head back swiveling within the observation window of the experiment (Fig. 47a). Synchronization of the traces at the time point where the last transition to S state is observed and population distribution of the FRET values after the synchronization point revealed two Gaussian distributions with FRET 0.78±0.11 (EF-G-induced S state) and 0.51±0.08 (N state of the POST complex) (Fig. 47b).

On the slippery sequence and with EF-G(wt), the majority of smFRET traces (87%) were fluctuating between FRET 0.8 (S) and 0.5 (N) states before transition to a stable FRET 0.5 (N), while a small fraction (13%) show slow translocation, similar to the situation on the non-slippery mRNA. Synchronization of the traces at the time point where the last transition to S state is observed and population distribution of the FRET values after the synchronization point revealed two Gaussian distributions with FRET 0.78±0.10 (EF-G-induced S state) and 0.51±0.07 (N state of the POST complex, Fig. 47c). Respectively, the decay rate of the last S state (1.9±0.1 s^{-1}) is similar to the rate on the non-slippery mRNA (2.2±0.3 s^{-1}, Fig. 47d). This result indicates that the slippery sequence does not affect the dynamics and timing of the SSU head domain swiveling during translocation. Additionally, EF-G(wt) drives fast back swiveling of the SSU head domain, thus locking the pept-tRNA in the P site, for the majority of ribosomes. The rate of the back swiveling of the SSU head domain by EF-G(wt) is at the same range with the dissociation rate of the deacylated tRNA from the E site, indicating that the latter occurs at the same time or shortly after the completion of translocation, as previously reported (Belardinelli et al., 2016a; Peng et al., 2019; Wasserman et al., 2016).

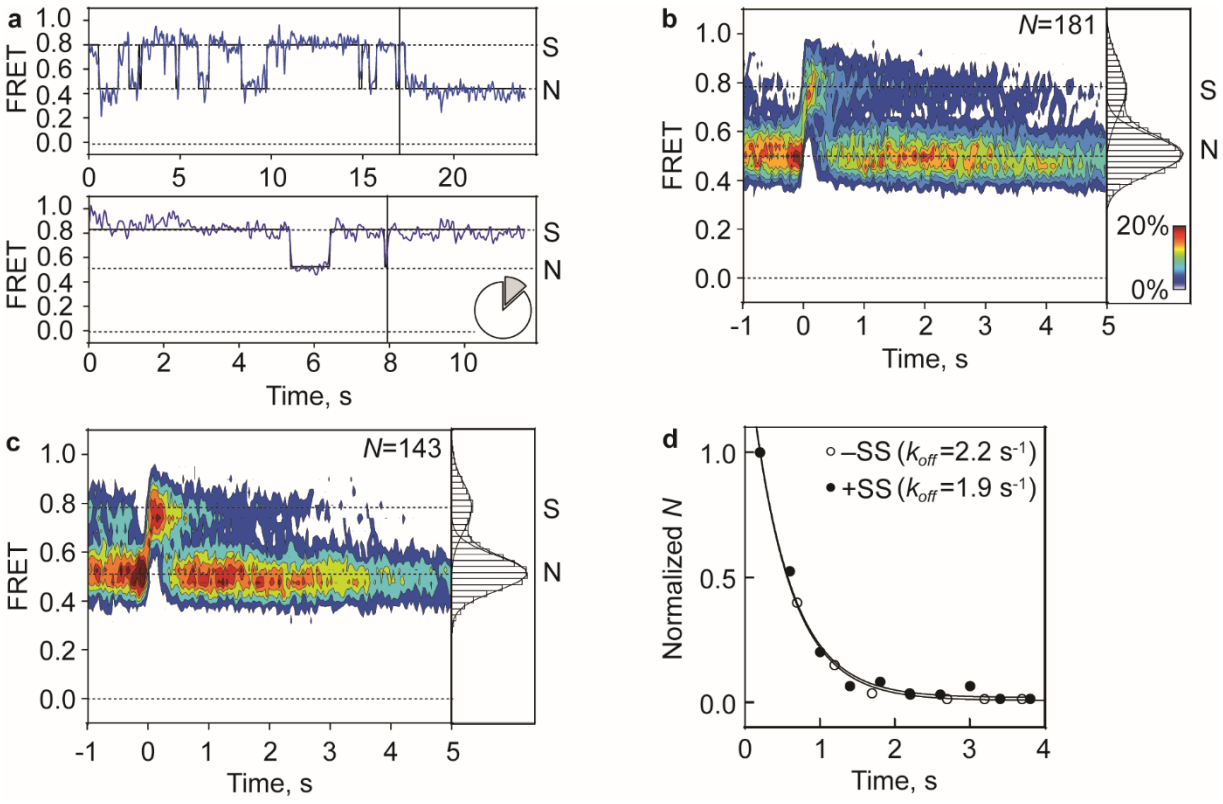

Figure 47. SSU head swiveling during translocation by EF-G(wt). (a) Representative smFRET traces corresponding to SSU head domain dynamics during translocation on slippery mRNA by EF-G(wt). Traces are synchronized to the point indicated by the vertical solid line. (b-c) Contour plot showing FRET distribution after synchronization during translocation on non-slippery (b) and slippery (c) mRNA mediated by EF-G(wt). (d) Dwell-time distribution of the last S state before transition to long-lived N state during translocation on slippery (closed circles) and non-slippery (open circles) mRNA by EF-G(wt). Black line is single exponential fit.

SSU head swiveling during translocation by EF-G(Q507D)

Finally, we monitored the SSU head domain dynamics during translocation on slippery mRNA by EF-G(Q507D). In contrast to EF-G(wt), only a small fraction (13%) of the smFRET traces reached a stable FRET 0.5 (N). The majority (87%) showed a long-lived S state without transition to N before photobleaching (Fig. 48a). Synchronization of the traces at the time point where the last transition to S state is observed and population distribution of the FRET values after the synchronization point revealed two Gaussian distributions (Fig. 48b). The prevalent state showed FRET 0.79±0.09 (EF-G-induced S) and the minor state 0.49±0.09 (N state of the complexes that swiveled back in the time course of the experiment). The decay rate of the last long-lived S state was ~17-fold lower (0.11±0.1 s^{-1}, Fig. 48c) than that observed with EF-G(wt) and represents the upper limit of the actual translocation rate (Fig. 48c). This result indicates that EF-G(Q507D) causes a delay in the back swiveling of the SSU head domain, compared to EF-G(wt), consistent with previous reports (Niblett et al., 2021; Peng et al., 2019).

Notably, the rate of the SSU head back swiveling is similar to the translocation rate of the pept-tRNA from the A to the P site, but ~5-fold lower than the dissociation rate of the deacylated tRNA from the E site. This indicates that the late steps of SSU head back swiveling and tRNA dissociation, which are coupled during translocation by EF-G(wt) (Belardinelli et al., 2016a; Peng et al., 2019; Wasserman et al., 2016), become uncoupled by EF-G(Q507D). The delay in the SSU head back swiveling does not affect the fast and undisturbed dissociation of the deacylated tRNA. However, it may account for the high positional uncertainty of the pept-tRNA during translocation because the tRNA-ribosome interactions in the P site are not developed. During this state, the –1-frame codon is unoccupied by tRNA and the pept-tRNA can freely sample the 0- and –1-frame codons, thus shifting the reading frame. It is important to note that the rotation of the SSU body domain most likely does not contribute appreciably to spontaneous –1 frameshifting, as both forward and reverse SSU body rotation are complete prior to progression of the tRNAs to the CHI state (Belardinelli et al., 2016a; Carbone et al., 2021; Petrychenko et al., 2021; Savelsbergh et al., 2003).

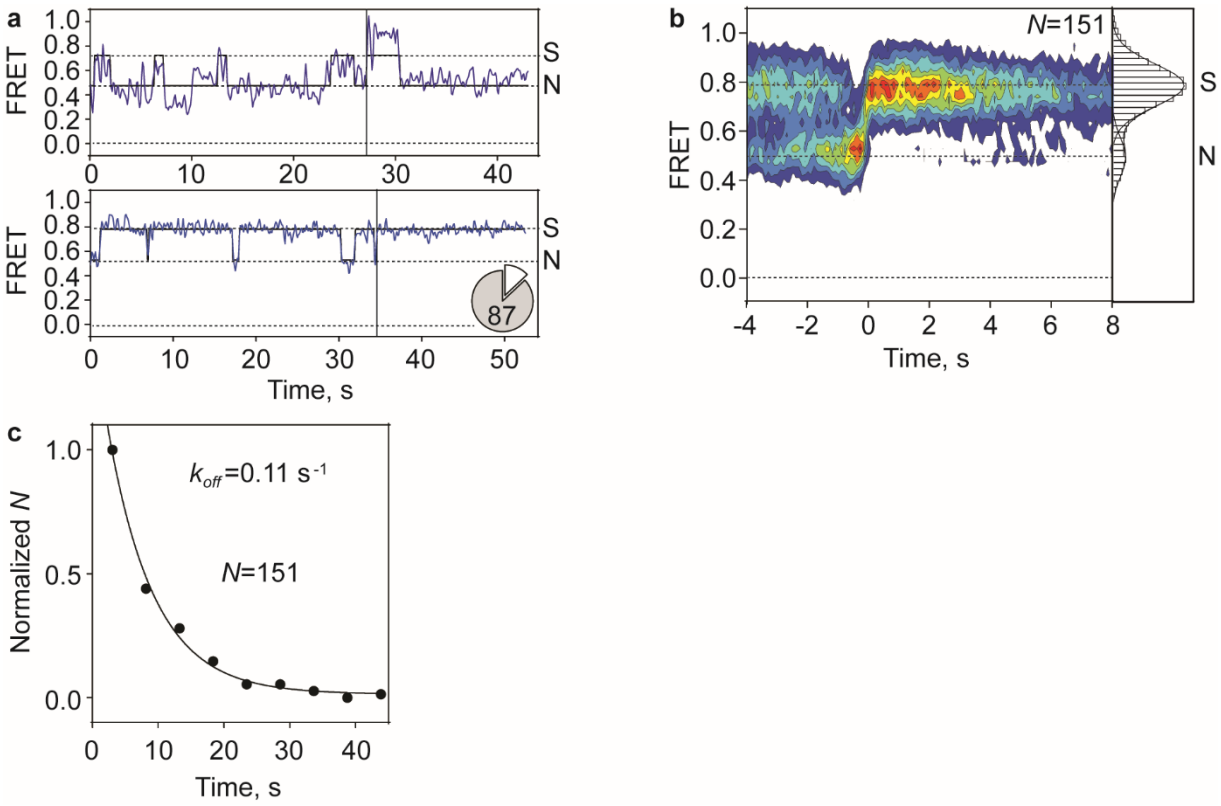

Figure 48. SSU head swiveling during translocation on slippery mRNA by EF-G(Q507D). (a) Representative smFRET time traces corresponding to SSU head domain dynamics during translocation by EF-G(Q507D). Traces are synchronized to the point indicated by the vertical solid line. (b) Contour plot showing FRET distribution after synchronization during translocation on slippery mRNA mediated by EF-G(Q507D). (c) Dwell-time distribution of the last S state during translocation by EF-G(Q507D) on slippery mRNA. Black line is single exponential fit.

6. Discussion

Part of the discussion of the study has been published (Poulis et al., 2022). No reuse/reprint permission required by authors.

6.1. Choreography of translocation on slippery mRNA

In this study, we characterized the molecular mechanism of the error-prone pathway of spontaneous frameshifting, providing new insights into mRNA sequence-specific regulation of translation. The slippery mRNA does not seem to affect the dynamics of the PRE complex prior to translocation. Previous studies using L11-tRNA FRET monitored dynamics of PRE complex assembled on non-slippery sequences and carrying various tRNA species in the A site and reported similar results as in the present study (Adio et al., 2015). Differences in the occupancy of classical and hybrid states and the transition rates are attributed to the tRNA species (Sharma et al., 2016). Taken together, the results of the present and previous studies demonstrate that the slippery mRNA sequence does not affect the dynamics of the peptidyl-tRNA in PRE complex.

However, the slippery mRNA affects the order and timing of events during translocation. Although during translocation on non-slippery mRNA all ribosomes behave in quasi-uniform way (within the time resolution of our experiments) with both peptidyl- and deacylated tRNAs translocating rapidly and driving rapid relocking of the SSU head domain (Fig. 49a), on a slippery mRNA we observe two distinct ribosome populations. In the first population, the peptidyl- and deacylated tRNAs translocate rapidly, while, in the other, peptidyl-tRNA translocates slowly (Fig. 49a). The fraction of ribosomes that show slow translocation in the population correlates with the frameshifting efficiency of EF-G(wt) and error-prone EF-G(Q507) mutants (Fig. 49a). Furthermore, we show that slow translocation is followed by –1-frame tRNA incorporation. On slow ribosomes, both tRNAs rapidly move from the hybrid into their respective CHI states and, subsequently, the deacylated tRNA dissociates rapidly from the ribosome (Fig. 49b). However, the peptidyl-tRNA fluctuates between CHI and P/P states (Fig. 49b). Respectively, the back swiveling of the SSU head, which would normally lock peptidyl-tRNA in the P site, is also delayed (Fig. 49b). Given that, often on slippery sequences, base pairing of the peptidyl-tRNA anticodon with the –1-frame codon is thermodynamically favored over the 0-frame codon (Bock et al., 2019), these fluctuations provide the time window for peptidyl-tRNA to slip to the –1 frame.

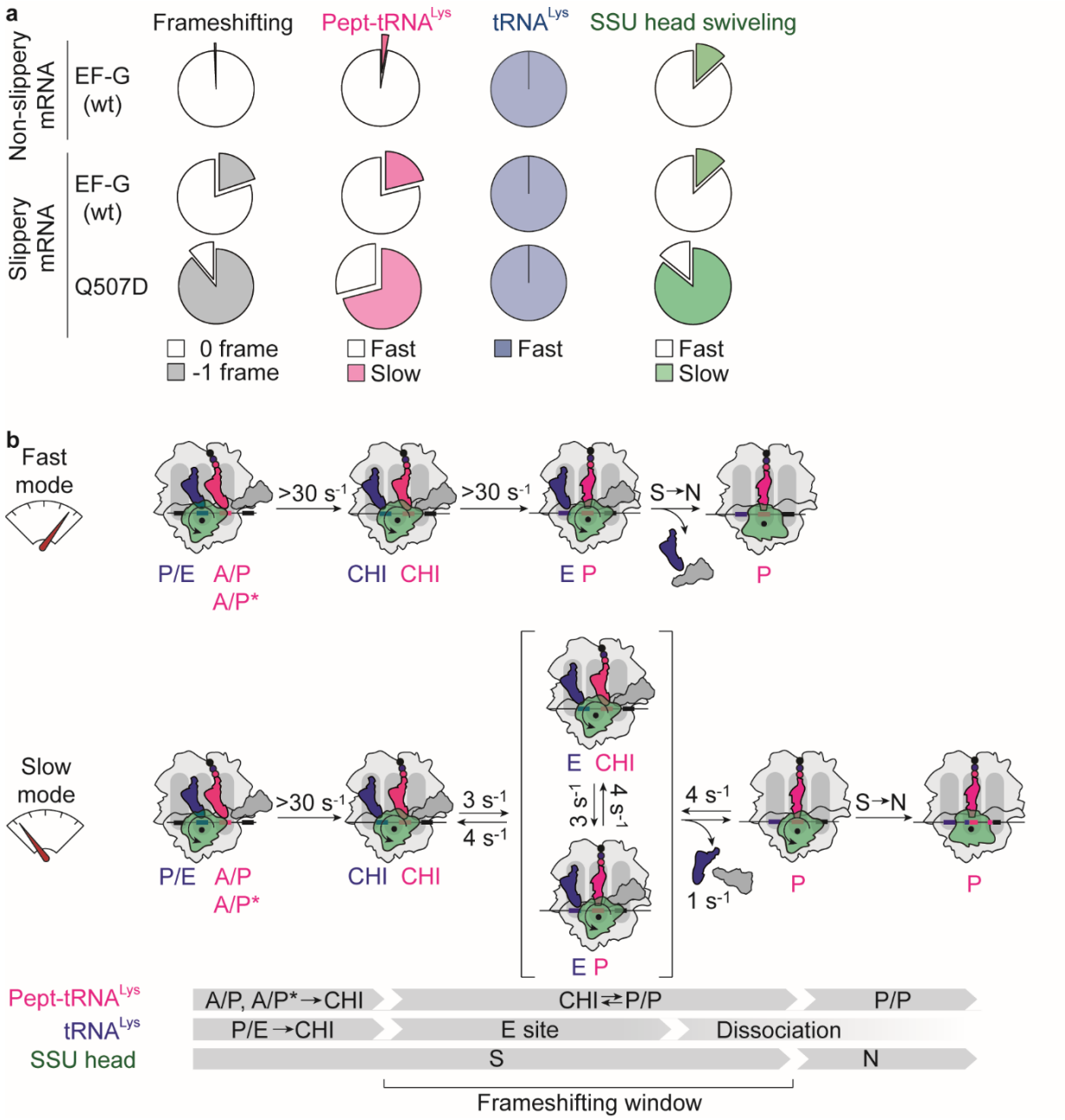

Figure 49. Translocation trajectories correlating with frameshifting. (a) Pie charts comparing the –1 spontaneous frameshifting efficiency (grey) with the translocation patterns of peptidyl- (magenta) and deacylated (blue) tRNAs and SSU head domain back swiveling (green) by EF-G(wt) and EF-G(Q507D). (b) Kinetic model of translocation on slippery mRNA. A fraction of ribosomes translocate rapidly with both tRNAs moving synchronously to the POST state, followed by back swiveling of the SSU head domain to complete translocation. Another fraction of ribosomes translocates in slow mode, where peptidyl-tRNA fluctuates between CHI and P/P. Deacylated tRNA translocates rapidly and dissociates from the ribosome, thus allowing pept-tRNA to sample 0- and –1-frame codons. SSU head back swiveling is delayed as a result of peptidyl-tRNA fluctuations. Rates of the elemental reactions are indicated.

Residues Q507 and H583 at the tip of EF-G domain 4 are crucial for reading frame maintenance, as shown in previous studies (Niblett et al., 2021; Peng et al., 2019). Recent time-resolved cryo-EM studies capturing translocating ribosomes prior to Pi release and CHI state formation suggest that EF-G domain 4 is flexible and most probably does not contribute to the stabilization of the codon-anticodon duplex at this stage (Petrychenko et al., 2021). This explains why the stabilization of the A/P* state prior to translocation is not impaired by mutations at Q507 residue. Instead, at this stage prior to Pi release, the codon-anticodon duplex is supported by residues of 16S rRNA h44, which is part of the SSU body (Carbone et al., 2021; Petrychenko et al., 2021). Upon Pi release and tRNA progression to the CHI state, the contacts of EF-G with the SSU body domain are abolished and tRNA anticodon has a propensity to disconnect from its 0-frame codon, as studies of spontaneous (EF-G-independent) transition of tRNAs to CHI state reported (Zhou et al., 2014, 2019). At this stage, EF-G residues Q507 and H583 stabilize the codon-anticodon duplex in its correct geometry, thereby maintaining the reading frame (Zhou et al., 2019). This is probably why mutations at residue Q507 impair the ability of EF-G to stabilize the codon-anticodon interactions after CHI state formation and, thus, peptidyl-tRNA fluctuates between CHI and P/P states. Previous studies report that mutations in the second key residue of EF-G domain 4, H583 (e.g. H583K), increase frameshifting (Peng et al., 2019) and allow fluctuations between CHI and P/P states during translocation (Adio et al., 2015), thus affecting translocation in a similar way as mutations in Q507.

6.2. Slow gears of translocation

In this study, we identify two alternative translocation pathways, one that shows rapid and coordinated movement of tRNAs in the 0 frame, and the other which progresses slowly and is prone to –1 spontaneous frameshifting. Recent single-molecule studies combining force (readout for ribosome progression) and fluorescence (readout for EF-G binding) measurements reported that ribosomes can operate in two alternative gears during translation in response to the mechanical barrier created by an mRNA secondary structure (Desai et al., 2019). In the slow gear, unwinding of the secondary structure occurred during the early (prior to Pi release) step of forward swiveling of the SSU head domain, suggesting that the speed of ribosome progression across the mRNA is reduced due to delays in steps prior to CHI state formation. At this stage, ribosomes engage in reversible sub-codon steps against the secondary structure, exploiting fluctuations on the mRNA to overcome the mechanical barrier. However, our data show that tRNA fluctuations between early translocation intermediates, i.e. prior to authentic CHI formation, e.g. in the presence of GTPγS instead of GTP or the presence of Spc, do not

confer –1 frameshifting. Therefore, there are different ways and translocation stages for the ribosome to switch gears, but –1 frameshifting is promoted only at a specific stage, i.e. when peptidyl-tRNA transits from CHI to P/P.

In this study, we show that, at given translocation conditions, some ribosomes follow a rapid route, whereas others switch into a slow mode. Previous molecular dynamics simulations revealed that translocation can proceed via almost 500,000,000 possible kinetic sequences and calculated, among them, the favored route of tRNA movement (Bock et al., 2013). Apparently, specific mRNA sequences, such as slippery sequences or secondary structures, can affect the canonical structural dynamics of the ribosome, set the course for ribosomes to deviate from the designated route and change into alternative, potentially error-prone, pathways ((Desai et al., 2019) and this study). Thus, the mRNA sequence appears to modulate the pace of the ribosome, not only by acting as a roadblock for the progression along the mRNA (reviewed in (Samatova et al., 2020)), but also in more subtle ways, where specific mRNA sequences are linked to alternative translocation outcomes that result in the synthesis of alternative peptides. Future work will elucidate why ribosomes switch to slow gears and what is their role in biological processes, such as co-translational folding of nascent peptides or the mRNA stability by ribosome loading.

6.3. Comparison with –1PRF, hungry and +1 frameshifting

The timing of events during spontaneous frameshifting shows similarities but also differences to programmed (PRF), hungry and +1 frameshifting. A hallmark of –1PRF is the reduction of translocation speed on the slippery sequence, stimulated by mRNA secondary structures. During stalling, the SSU head domain remains swiveled (Caliskan et al., 2014) and the SSU body is (hyper-)rotated (Chen et al., 2014; Choi et al., 2020; Kim et al., 2014), suggesting a key role of SSU motions both in –1PRF and spontaneous –1 frameshifting (Table 10) (this study and (Niblett et al., 2021; Peng et al., 2019)). Additionally, the positional uncertainty of the ribosome complex is a common feature between PRF and spontaneous –1 frameshifting. Previous studies of –1PRF on *dnaX* mRNA of *E. coli* using optical tweezers to monitor the position of ribosomes on the mRNA, show that stalled ribosomes make multiple translocation attempts sampling sequences upstream (–1 or –4 frames) or downstream (+2 frame) of the 0 frame (Yan et al., 2015). Here, we show that fluctuations of peptidyl-tRNA between CHI and P/P states allow ribosomes to explore alternative reading frames and eventually re-equilibrate in the most thermodynamically favored frame before resuming

translation. However, a fundamental difference between –1PRF and spontaneous –1 frameshifting is the timing of deacylated tRNA dissociation, which is rapid during spontaneous frameshifting (this study and (Peng et al., 2019)), but slow in previous studies of –1PRF where this was studied (Table 10) (Caliskan et al., 2014; Chen et al., 2013a; Kim et al., 2014). Thus, frameshifting can occur both with one or two tRNAs present in the ribosome, provided peptidyl-tRNA is trapped in fluctuations between CHI and P/P. –1 frameshifting can be also induced by the low availability of cognate aa-tRNAs, resulting in hungry frameshifting events (Caliskan et al., 2017). Hungry –1 frameshifting is also a slow process, but probably follows a distinct mechanism that involves spontaneous P-site tRNA slippage in the POST complex, rather than tRNA translocation (Table 10). Together, the present and previous studies highlighted several pathways that lead to –1 frameshifting, following either one- or two-tRNA mechanism. These aforementioned pathways show differences but share similarities, such as the slow translocation of the peptidyl-tRNA after CHI state formation and the prolonged swiveling of the SSU head.

Spontaneous –1 frameshifting is substantially different from the mechanism of +1 frameshifting. The most striking difference is that +1 frameshifting is alleviated by tRNA ASL modifications, while tRNA ASL modifications have no effect in –1 frameshifting (Hoffer et al., 2020; Urbonavicius et al., 2001; Urbonavicius et al., 2003). Additionally, +1 frameshifting has been reported to occur in the absence of EF-G, i.e. in POST and post-decoding complex, but also during translocation (Table 10). In POST complexes carrying the +1-frameshifting-prone slippery sequence C<u>CC U</u> in the P site and empty A site, peptidyl-tRNA^{Pro} unexpectedly adopts an e*/E conformation, where the ASL is located between the P and E site (Hoffer et al., 2020). The e*/E conformation is frameshifting-prone because it involves the constriction of mRNA +1 nucleotide into the P site and profound SSU head swiveling and tilting that resembles the open SSU conformation during decoding. This is in drastic contrast to the mechanism of –1 frameshifting, because steps prior to and after translocation are not affected by the slippery sequence (Table 10) (this study and (Caliskan et al., 2014)). Although decoding occurs in a canonical three-nucleotide manner (Gamper et al., 2021a), substantial differences are also observed even when the A site is occupied by tRNA. Proline exhibits low rate of peptide bond formation (Wohlgemuth et al., 2008), which is resolved by EF-P (Doerfel et al., 2013). Previous studies report that delay in peptide bond formation due to absence of EF-P contributes to +1 frameshifting on slippery mRNA (Gamper et al., 2015). Even after peptide bond formation, PRE complexes assembled on slippery mRNA exhibit a destabilizing frameshifting-prone open SSU conformation, observed only in near-cognate codon-anticodon interactions (Demo et al., 2021).

+1 frameshifting also occurs during translocation (Demo et al., 2021; Gamper et al., 2021a; Gamper et al., 2021b; Hoffer et al., 2020). SufB2, a +1-frameshifting-prone $tRNA^{Pro}$ containing a G37a insertion in the ASL is prone to shifts into the +1 frame during translocation. Recent smFRET studies using L1-L9 FRET (reporting on L1 stalk motion) as readout for translocation have shown that steps related to the transition to the POST state are slower with SufB2, compared to the canonical $tRNA^{Pro}$ (Gamper et al., 2021a). This indicates that +1 frameshifting during translocation is characterized by slow tRNA progression, as observed in spontaneous –1 frameshifting. However, if the L1 stalk motion via L1-L9 FRET is interpreted solely as a readout for dissociation of deacylated tRNA from the ribosome rather than the entire process of translocation, then translocation on the +1-frameshifting-prone mRNA causes significant delay in E-site tRNA dissociation from the ribosome. This indicates a two-tRNA slippage mechanism, in drastic contrast to the mechanism of –1 spontaneous frameshifting (Table 10) (this study and (Peng et al., 2019)). Additionally, the timing of +1 frameshifting during translocation is different from –1 spontaneous frameshifting. Visualization of +1 frameshifting by cryo-EM revealed that PRE complexes containing deacylated tRNA in the P site and a frameshifting-prone peptidy-$tRNA^{Pro}$ in the A site shift into the +1 frame upon addition of EF-G and the non-hydrolysable GTP analog GMPPCP (Demo et al., 2021). Our and previous studies have shown that translocation by EF-G bound to non-(or slowly) hydrolysable GTP analogs is stalled at early steps (Adio et al., 2015; Belardinelli et al., 2016a; Wasserman et al., 2016). Indeed, in this study, we show that translocation in the presence of GTPγS is stalled before the formation of the authentic CHI state and, thus, does not confer –1 frameshifting. If GMPPCP acts in a similar manner during translocation as GTPγS, the recent studies on +1 frameshifting suggest that it occurs before CHI state formation. This is clearly different to –1 spontaneous frameshifting, which occurs after CHI state formation and during transition to the POST state (Table 10).

In conclusion, a plethora of studies suggest multiple alternative translocation pathways that can lead to frameshifting, which share similarities but also differ in specific details, such as the number of frameshifting tRNAs and the timing of slippage. However, the slow translocation of the peptidyl-tRNA and the prolonged swiveling of SSU head that offers the unconstrained access to alternative-frame codons are universal determinants of the frameshifting-prone translocation pathways.

Table 10. Comparison of the molecular mechanisms of spontaneous (SRF), programmed (PRF), depletion-triggered (hungry) and +1 ribosome frameshifting.

	–1SRF[a]	–1PRF[b]	hungry –1RF[c]	+1 RF[d]
It occurs in POST and/or post-decoding complex.	No	No	Yes, POST	Yes
It occurs during translocation.	Yes	Yes	No	Yes
PRE complex is unstable.	No	No	No	Yes
Translocation of peptidyl-tRNA is slow.	Yes	Yes	n.a.[e]	Yes
Translocation of deacylated tRNA is slow.	No	Yes	n.a.	Yes
One- or two-tRNA slippage mechanism	One-	Two-	One-	One- Two-
Translocation is stalled after CHI state.	Yes	Yes	n.a.	No
The SSU head is swiveled during slippage.	Yes	Yes	n.d.[f]	Yes

[a]Information is from this study and (Peng et al., 2019).
[b]Information is from (Caliskan et al., 2014; Chen et al., 2013a; Kim et al., 2014).
[c]Information is from (Caliskan et al., 2017; Korniy et al., 2019).
[d]Information is from(Demo et al., 2021; Gamper et al., 2021a; Gamper et al., 2021b; Gamper et al., 2015; Hoffer et al., 2020).
[e]The feature is not applicable for this mechanism.
[f]The feature has not been studied for this mechanism.

6.4. Fine tune of reading frame maintenance in eukaryotes

The mechanics of translocation and the major structural dynamics of the ribosome, such as SSU body rotation and head swiveling, are highly conserved in all three domains of life, although slight mechanistic differences due to additional eukaryotic-specific motions were reported (Budkevich et al., 2014). The homologue of EF-G in eukaryotes, elongation factor 2 (eEF2), is structurally similar to the bacterial EF-G (Fig. 50a). However, eEF2 is post-translationally modified with diphthamide (Dph), a unique 2-[3-carboxyamido-3-(trimethylammonio)]propyl modification, which is exclusively found at key histidine residue of the tip of domain 4 (H699 in yeast *Saccharomyces cerevisiae* and H715 in mammals), in a similar position to the key residues Q507 and H583 of EF-G (Fig. 50a) (Djumagulov et al., 2021; Flis et al., 2018; Pellegrino et al., 2018). Due to the fact that the loop I of domain 4, where Q507 of EF-G and H715 of mammalian eEF2 are located, is shorter in eEF2 compared to EF-G (Fig. 50a), previous studies hypothesized that diphthamide extension compensates for that (Flis et al., 2018). Diphthamide is the molecular target of diphtheria exotoxin of the human pathogen *Corynebacterium diphtheriae* (Chung and Collier, 1977; Giovane et al., 1985), exotoxin A of *Pseudomonas aeruginosa* (Jorgensen et al., 2005) and cholera toxin of *Vibrio cholerae* (Jorgensen et al., 2008). The three toxins catalyze the ADP-ribosylation of diphthamide, thus impeding eEF2 binding to the ribosome and abolishing translocation (Burns et al., 1986; Davydova and Ovchinnikov, 1990; Marzouki et al., 1991; Montanaro et al., 1976; Nygard and Nilsson, 1990).

Several studies have suggested a role of diphthamide in reading frame maintenance during translocation. In crystal structures of yeast ribosomes stalled by the non-hydrolysable GTP analog GMPPCP and cryo-EM structures of mammalian (rabbit) ribosomes stalled by GDPNP, diphthamide interacts with the peptidy-tRNA and mRNA, acting as a pawl that prevents frameshifting (Fig. 50b) (Djumagulov et al., 2021; Flis et al., 2018). The conceptual insights provided by these structural studies are supported by genetic analysis. Point mutations at the key histidine residue and mutations or deletions of diphthamide biosynthesis enzymes in yeast, mouse and plant (*Arabidopsis thaliana*) models, as well as congenital diseases in humans, confer –1 frameshifting and are linked to developmental and growth abnormalities (Hawer et al., 2018; Kapur and Ackerman, 2018; Liu et al., 2012; Ortiz et al., 2006; Zhang et al., 2022). Although these studies have highlighted the connection between diphthamide and reading frame maintenance, future work will elucidate how diphthamide fine tunes the maintenance of

the translational reading frame during translocation in eukaryotes and what is the impact of diphthamide loss in development.

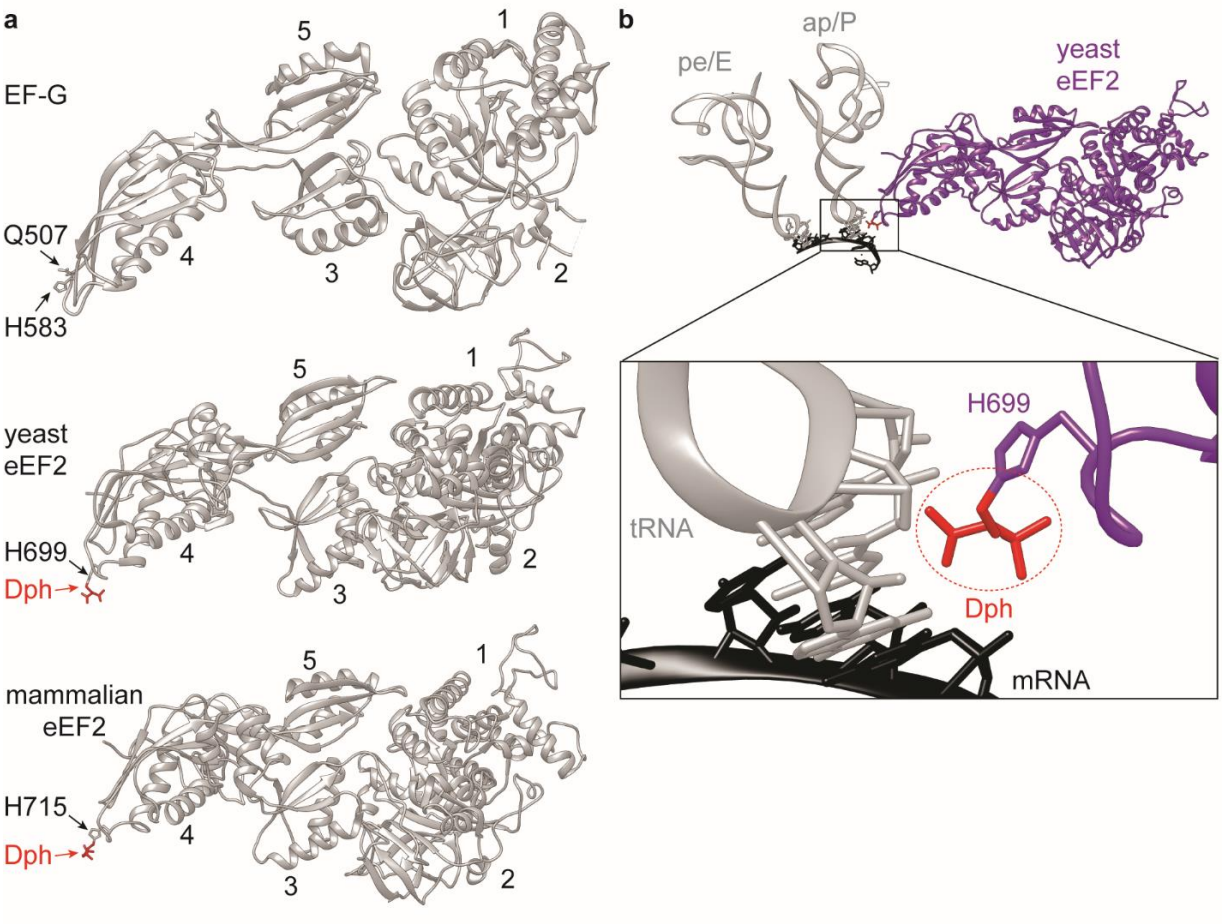

Figure 50. The role of diphthamide in reading frame maintenance in eukaryotes. (a) Structures of *E. coli* EF-G (PDB 7PJY) (Petrychenko et al., 2021), yeast eEF2 (PDB 7OSM) (Djumagulov et al., 2021) and mammalian (rabbit) eEF2 (PDB 6GZ3) (Flis et al., 2018). Shown are the domains 1, 2, 3, 4 and 5, the residues H583 and Q507 of EF-G and the H699 (yeast) and H715 (mammalian) residue of eEF2 modified with diphthamide (Dph, red). (b) Crystal structure of yeast ribosome stalled in intermediate stage of translocation. tRNAs are shown in grey, eEF2 in purple, mRNA in black. Zoom-in shows diphthamide (Dph, red) developing interactions with the peptidyl-tRNA and mRNA. The figure is adapted from PDB 7OSM (Djumagulov et al., 2021).

6.5. Future perspectives

We anticipate that our work will set the foundations for future research on the mechanism, biological significance and biomedical implications of spontaneous ribosome frameshifting. Although the mechanistic details of spontaneous frameshifting and its prevention in the cell are beginning to be elucidated, future research may focus on the fate and effect of the frameshifted peptides inside the cell. Given that –1-frame peptides represent ~20% of the total translation products even with EF-G(wt) (this study and (Caliskan et al., 2014; Chen et al., 2014; Peng et al., 2019)), erroneous frameshifted peptides are expected to be highly abundant in the cell. It remains obscure whether frameshifted peptides are either in principle tolerated in the cell, such as other translation errors (Drummond and Wilke, 2009), or rapidly eradicated by protein degradation machinery. In the case of the latter, it remains to be discovered if targeting and eradication of frameshifted peptides occurs co-translationally, due to the activation of ribosome quality control mechanisms by ribosome stalling on slippery mRNA sequences, or by conventional protein targeting and degradation machinery, due to failure to adopt a native fold. Future research will bridge the proximate (i.e. effect on the ribosome progression and protein synthesis) and ultimate (i.e. effect on the cell) effects of spontaneous frameshifting. Additionally, spontaneous frameshifting may serve as a framework for development of novel antibiotics. Previous studies identified a moonlighting function of LSU-binding antibiotics to promote –1 frameshifting (Dinman et al., 1997; Gupta et al., 2013). However, it remains unclear if and how antibiotic-induced frameshifting contributes to pathogen death. Future research will show whether frameshifted peptides is a causative factor for pathogen death and inspire development of frameshifting-promoting highly bactericidal antimicrobials for treating challenging bacterial infections.

Future research on translocation by the eukaryotic ribosome will reveal the mechanistic conservation of reading frame maintenance and the role of diphthamide and other eukaryotic-specific elements in it. Ensemble and single molecule kinetic studies, as well as time-resolved cryo-EM, will describe the dynamics of ribosome, tRNAs, mRNA and translation factors during translocation on slippery mRNA and reveal whether the canonical and frameshifting-prone pathways contain similarities and differences with the bacterial ribosome. Lastly, the effect of disease-relevant mutations in diphthamidation will link the error-prone pathway of the eukaryotic ribosome with pathological phenotypes. Collectively, knowledge on the molecular mechanism of reading frame maintenance in eukaryotes and its abolishment will inspire the design of frameshifting-suppressing (or -promoting) drugs to treat human diseases.

7. References

Adio, S., Senyushkina, T., Peske, F., Fischer, N., Wintermeyer, W., and Rodnina, M.V. (2015). Fluctuations between multiple EF-G-induced chimeric tRNA states during translocation on the ribosome. Nature communications *6*, 7442.

Advani, V.M., Belew, A.T., and Dinman, J.D. (2013). Yeast telomere maintenance is globally controlled by programmed ribosomal frameshifting and the nonsense-mediated mRNA decay pathway. Translation (Austin) *1*, e24418.

Agirrezabala, X., Lei, J., Brunelle, J.L., Ortiz-Meoz, R.F., Green, R., and Frank, J. (2008). Visualization of the hybrid state of tRNA binding promoted by spontaneous ratcheting of the ribosome. Mol Cell *32*, 190-197.

Allen, G.S., Zavialov, A., Gursky, R., Ehrenberg, M., and Frank, J. (2005). The cryo-EM structure of a translation initiation complex from Escherichia coli. Cell *121*, 703-712.

Altuntop, M.E., Ly, C.T., and Wang, Y. (2010). Single-molecule study of ribosome hierarchic dynamics at the peptidyl transferase center. Biophys J *99*, 3002-3009.

Arora, S., Bhamidimarri, S.P., Weber, M.H., and Varshney, U. (2013). Role of the ribosomal P-site elements of m(2)G966, m(5)C967, and the S9 C-terminal tail in maintenance of the reading frame during translational elongation in Escherichia coli. J Bacteriol *195*, 3524-3530.

Atkins, J.F., O'Connor, K.M., Bhatt, P.R., and Loughran, G. (2021). From Recoding to Peptides for MHC Class I Immune Display: Enriching Viral Expression, Virus Vulnerability and Virus Evasion. Viruses *13*.

Ayhan, F., Perez, B.A., Shorrock, H.K., Zu, T., Banez-Coronel, M., Reid, T., Furuya, H., Clark, H.B., Troncoso, J.C., Ross, C.A.*, et al.* (2018). SCA8 RAN polySer protein preferentially accumulates in white matter regions and is regulated by eIF3F. EMBO J *37*.

Ban, N., Nissen, P., Hansen, J., Moore, P.B., and Steitz, T.A. (2000). The complete atomic structure of the large ribosomal subunit at 2.4 A resolution. Science *289*, 905-920.

Bartok, O., Pataskar, A., Nagel, R., Laos, M., Goldfarb, E., Hayoun, D., Levy, R., Korner, P.R., Kreuger, I.Z.M., Champagne, J.*, et al.* (2021). Anti-tumour immunity induces aberrant peptide presentation in melanoma. Nature *590*, 332-337.

Belardinelli, R., and Rodnina, M.V. (2017). Effect of Fusidic Acid on the Kinetics of Molecular Motions During EF-G-Induced Translocation on the Ribosome. Sci Rep *7*, 10536.

Belardinelli, R., Sharma, H., Caliskan, N., Cunha, C.E., Peske, F., Wintermeyer, W., and Rodnina, M.V. (2016a). Choreography of molecular movements during ribosome progression along mRNA. Nature structural & molecular biology *23*, 342-348.

Belardinelli, R., Sharma, H., Peske, F., and Rodnina, M.V. (2021). Perturbation of ribosomal subunit dynamics by inhibitors of tRNA translocation. RNA *27*, 981-990.

Belardinelli, R., Sharma, H., Peske, F., Wintermeyer, W., and Rodnina, M.V. (2016b). Translocation as continuous movement through the ribosome. RNA biology *13*, 1197-1203.

Belew, A.T., Advani, V.M., and Dinman, J.D. (2011). Endogenous ribosomal frameshift signals operate as mRNA destabilizing elements through at least two molecular pathways in yeast. Nucleic Acids Res *39*, 2799-2808.

Belew, A.T., and Dinman, J.D. (2015). Cell cycle control (and more) by programmed -1 ribosomal frameshifting: implications for disease and therapeutics. Cell Cycle *14*, 172-178.

Belew, A.T., Hepler, N.L., Jacobs, J.L., and Dinman, J.D. (2008). PRFdb: a database of computationally predicted eukaryotic programmed -1 ribosomal frameshift signals. BMC Genomics *9*, 339.

Belew, A.T., Meskauskas, A., Musalgaonkar, S., Advani, V.M., Sulima, S.O., Kasprzak, W.K., Shapiro, B.A., and Dinman, J.D. (2014). Ribosomal frameshifting in the CCR5 mRNA is regulated by miRNAs and the NMD pathway. Nature *512*, 265-269.

Bhatt, P.R., Scaiola, A., Loughran, G., Leibundgut, M., Kratzel, A., Meurs, R., Dreos, R., O'Connor, K.M., McMillan, A., Bode, J.W.*, et al.* (2021). Structural basis of ribosomal frameshifting during translation of the SARS-CoV-2 RNA genome. Science.
Blanchard, S.C., Kim, H.D., Gonzalez, R.L., Jr., Puglisi, J.D., and Chu, S. (2004). tRNA dynamics on the ribosome during translation. Proceedings of the National Academy of Sciences of the United States of America *101*, 12893-12898.
Blinkowa, A.L., and Walker, J.R. (1990). Programmed ribosomal frameshifting generates the Escherichia coli DNA polymerase III gamma subunit from within the tau subunit reading frame. Nucleic Acids Res *18*, 1725-1729.
Boccaletto, P., Machnicka, M.A., Purta, E., Piatkowski, P., Baginski, B., Wirecki, T.K., de Crecy-Lagard, V., Ross, R., Limbach, P.A., Kotter, A.*, et al.* (2018). MODOMICS: a database of RNA modification pathways. 2017 update. Nucleic Acids Res *46*, D303-D307.
Bocchetta, M., Xiong, L., Shah, S., and Mankin, A.S. (2001). Interactions between 23S rRNA and tRNA in the ribosomal E site. RNA *7*, 54-63.
Bock, L.V., Blau, C., Schroder, G.F., Davydov, II, Fischer, N., Stark, H., Rodnina, M.V., Vaiana, A.C., and Grubmuller, H. (2013). Energy barriers and driving forces in tRNA translocation through the ribosome. Nature structural & molecular biology *20*, 1390-1396.
Bock, L.V., Blau, C., Vaiana, A.C., and Grubmuller, H. (2015). Dynamic contact network between ribosomal subunits enables rapid large-scale rotation during spontaneous translocation. Nucleic Acids Res *43*, 6747-6760.
Bock, L.V., Caliskan, N., Korniy, N., Peske, F., Rodnina, M.V., and Grubmuller, H. (2019). Thermodynamic control of -1 programmed ribosomal frameshifting. Nature communications *10*, 4598.
Borovinskaya, M.A., Shoji, S., Holton, J.M., Fredrick, K., and Cate, J.H.D. (2007). A steric block in translation caused by the antibiotic spectinomycin. ACS Chem Biol *2*, 545-552.
Brilot, A.F., Korostelev, A.A., Ermolenko, D.N., and Grigorieff, N. (2013). Structure of the ribosome with elongation factor G trapped in the pretranslocation state. Proceedings of the National Academy of Sciences of the United States of America *110*, 20994-20999.
Bronson, J.E., Fei, J., Hofman, J.M., Gonzalez, R.L., Jr., and Wiggins, C.H. (2009). Learning rates and states from biophysical time series: a Bayesian approach to model selection and single-molecule FRET data. Biophysical journal *97*, 3196-3205.
Budkevich, T.V., Giesebrecht, J., Behrmann, E., Loerke, J., Ramrath, D.J., Mielke, T., Ismer, J., Hildebrand, P.W., Tung, C.S., Nierhaus, K.H.*, et al.* (2014). Regulation of the mammalian elongation cycle by subunit rolling: a eukaryotic-specific ribosome rearrangement. Cell *158*, 121-131.
Burnett, B.J., Altman, R.B., Ferrao, R., Alejo, J.L., Kaur, N., Kanji, J., and Blanchard, S.C. (2013). Elongation factor Ts directly facilitates the formation and disassembly of the Escherichia coli elongation factor Tu.GTP.aminoacyl-tRNA ternary complex. J Biol Chem *288*, 13917-13928.
Burns, G., Abraham, A.K., and Vedeler, A. (1986). Nucleotide binding to elongation factor 2 inactivated by diphtheria toxin. FEBS Lett *208*, 217-220.
Caliskan, N., Katunin, V.I., Belardinelli, R., Peske, F., and Rodnina, M.V. (2014). Programmed -1 frameshifting by kinetic partitioning during impeded translocation. Cell *157*, 1619-1631.
Caliskan, N., Peske, F., and Rodnina, M.V. (2015). Changed in translation: mRNA recoding by -1 programmed ribosomal frameshifting. Trends in biochemical sciences *40*, 265-274.
Caliskan, N., Wohlgemuth, I., Korniy, N., Pearson, M., Peske, F., and Rodnina, M.V. (2017). Conditional Switch between Frameshifting Regimes upon Translation of dnaX mRNA. Molecular cell *66*, 558-567 e554.
Carbone, C.E., Loveland, A.B., Gamper, H.B., Jr., Hou, Y.M., Demo, G., and Korostelev, A.A. (2021). Time-resolved cryo-EM visualizes ribosomal translocation with EF-G and GTP. Nat Commun *12*, 7236.

Champagne, J., Pataskar, A., Blommaert, N., Nagel, R., Wernaart, D., Ramalho, S., Kenski, J., Bleijerveld, O.B., Zaal, E.A., Berkers, C.R.*, et al.* (2021). Oncogene-dependent sloppiness in mRNA translation. Mol Cell *81*, 4709-4721 e4709.
Chandler, M., and Fayet, O. (1993). Translational frameshifting in the control of transposition in bacteria. Mol Microbiol *7*, 497-503.
Chen, C., Cui, X., Beausang, J.F., Zhang, H., Farrell, I., Cooperman, B.S., and Goldman, Y.E. (2016). Elongation factor G initiates translocation through a power stroke. Proc Natl Acad Sci U S A *113*, 7515-7520.
Chen, C., Stevens, B., Kaur, J., Cabral, D., Liu, H., Wang, Y., Zhang, H., Rosenblum, G., Smilansky, Z., Goldman, Y.E.*, et al.* (2011a). Single-molecule fluorescence measurements of ribosomal translocation dynamics. Molecular cell *42*, 367-377.
Chen, C., Stevens, B., Kaur, J., Smilansky, Z., Cooperman, B.S., and Goldman, Y.E. (2011b). Allosteric vs. spontaneous exit-site (E-site) tRNA dissociation early in protein synthesis. Proc Natl Acad Sci U S A *108*, 16980-16985.
Chen, C., Zhang, H., Broitman, S.L., Reiche, M., Farrell, I., Cooperman, B.S., and Goldman, Y.E. (2013a). Dynamics of translation by single ribosomes through mRNA secondary structures. Nature structural & molecular biology *20*, 582-588.
Chen, J., Petrov, A., Johansson, M., Tsai, A., O'Leary, S.E., and Puglisi, J.D. (2014). Dynamic pathways of -1 translational frameshifting. Nature *512*, 328-332.
Chen, J., Petrov, A., Tsai, A., O'Leary, S.E., and Puglisi, J.D. (2013b). Coordinated conformational and compositional dynamics drive ribosome translocation. Nat Struct Mol Biol *20*, 718-727.
Chen, J., Tsai, A., Petrov, A., and Puglisi, J.D. (2012). Nonfluorescent quenchers to correlate single-molecule conformational and compositional dynamics. J Am Chem Soc *134*, 5734-5737.
Choe, Y.J., Park, S.H., Hassemer, T., Korner, R., Vincenz-Donnelly, L., Hayer-Hartl, M., and Hartl, F.U. (2016). Failure of RQC machinery causes protein aggregation and proteotoxic stress. Nature *531*, 191-195.
Choi, J., O'Loughlin, S., Atkins, J.F., and Puglisi, J.D. (2020). The energy landscape of -1 ribosomal frameshifting. Sci Adv *6*, eaax6969.
Choi, J., and Puglisi, J.D. (2017). Three tRNAs on the ribosome slow translation elongation. Proc Natl Acad Sci U S A *114*, 13691-13696.
Chung, B.Y., Firth, A.E., and Atkins, J.F. (2010). Frameshifting in alphaviruses: a diversity of 3' stimulatory structures. J Mol Biol *397*, 448-456.
Chung, D.W., and Collier, R.J. (1977). The mechanism of ADP-ribosylation of elongation factor 2 catalyzed by fragment A from diphtheria toxin. Biochim Biophys Acta *483*, 248-257.
Clark, M.B., Janicke, M., Gottesbuhren, U., Kleffmann, T., Legge, M., Poole, E.S., and Tate, W.P. (2007). Mammalian gene PEG10 expresses two reading frames by high efficiency -1 frameshifting in embryonic-associated tissues. J Biol Chem *282*, 37359-37369.
Clementi, N., Chirkova, A., Puffer, B., Micura, R., and Polacek, N. (2010). Atomic mutagenesis reveals A2660 of 23S ribosomal RNA as key to EF-G GTPase activation. Nat Chem Biol *6*, 344-351.
Cornish, P.V., Ermolenko, D.N., Noller, H.F., and Ha, T. (2008). Spontaneous intersubunit rotation in single ribosomes. Molecular cell *30*, 578-588.
Cornish, P.V., Ermolenko, D.N., Staple, D.W., Hoang, L., Hickerson, R.P., Noller, H.F., and Ha, T. (2009). Following movement of the L1 stalk between three functional states in single ribosomes. Proceedings of the National Academy of Sciences of the United States of America *106*, 2571-2576.
Cunha, C.E., Belardinelli, R., Peske, F., Holtkamp, W., Wintermeyer, W., and Rodnina, M.V. (2013). Dual use of GTP hydrolysis by elongation factor G on the ribosome. Translation (Austin) *1*, e24315.

Czworkowski, J., Wang, J., Steitz, T.A., and Moore, P.B. (1994). The crystal structure of elongation factor G complexed with GDP, at 2.7 A resolution. EMBO J *13*, 3661-3668.
Datta, P.P., Sharma, M.R., Qi, L., Frank, J., and Agrawal, R.K. (2005). Interaction of the G' domain of elongation factor G and the C-terminal domain of ribosomal protein L7/L12 during translocation as revealed by cryo-EM. Mol Cell *20*, 723-731.
Davies, J.E., and Rubinsztein, D.C. (2006). Polyalanine and polyserine frameshift products in Huntington's disease. J Med Genet *43*, 893-896.
Davydova, E.K., and Ovchinnikov, L.P. (1990). ADP-ribosylated elongation factor 2 (ADP-ribosyl-EF-2) is unable to promote translocation within the ribosome. FEBS Lett *261*, 350-352.
Demo, G., Gamper, H.B., Loveland, A.B., Masuda, I., Carbone, C.E., Svidritskiy, E., Hou, Y.M., and Korostelev, A.A. (2021). Structural basis for +1 ribosomal frameshifting during EF-G-catalyzed translocation. Nat Commun *12*, 4644.
Desai, V.P., Frank, F., Lee, A., Righini, M., Lancaster, L., Noller, H.F., Tinoco, I., Jr., and Bustamante, C. (2019). Co-temporal Force and Fluorescence Measurements Reveal a Ribosomal Gear Shift Mechanism of Translation Regulation by Structured mRNAs. Mol Cell *75*, 1007-1019 e1005.
Devaraj, A., Shoji, S., Holbrook, E.D., and Fredrick, K. (2009). A role for the 30S subunit E site in maintenance of the translational reading frame. RNA *15*, 255-265.
Diaconu, M., Kothe, U., Schlunzen, F., Fischer, N., Harms, J.M., Tonevitsky, A.G., Stark, H., Rodnina, M.V., and Wahl, M.C. (2005). Structural basis for the function of the ribosomal L7/12 stalk in factor binding and GTPase activation. Cell *121*, 991-1004.
Dinman, J.D., Ruiz-Echevarria, M.J., Czaplinski, K., and Peltz, S.W. (1997). Peptidyl-transferase inhibitors have antiviral properties by altering programmed -1 ribosomal frameshifting efficiencies: development of model systems. Proc Natl Acad Sci U S A *94*, 6606-6611.
Djumagulov, M., Demeshkina, N., Jenner, L., Rozov, A., Yusupov, M., and Yusupova, G. (2021). Accuracy mechanism of eukaryotic ribosome translocation. Nature *600*, 543-546.
Doerfel, L.K., Wohlgemuth, I., Kothe, C., Peske, F., Urlaub, H., and Rodnina, M.V. (2013). EF-P is essential for rapid synthesis of proteins containing consecutive proline residues. Science *339*, 85-88.
Drummond, D.A., and Wilke, C.O. (2009). The evolutionary consequences of erroneous protein synthesis. Nat Rev Genet *10*, 715-724.
Dunham, C.M., Selmer, M., Phelps, S.S., Kelley, A.C., Suzuki, T., Joseph, S., and Ramakrishnan, V. (2007). Structures of tRNAs with an expanded anticodon loop in the decoding center of the 30S ribosomal subunit. RNA *13*, 817-823.
Dunkle, J.A., Wang, L., Feldman, M.B., Pulk, A., Chen, V.B., Kapral, G.J., Noeske, J., Richardson, J.S., Blanchard, S.C., and Cate, J.H. (2011). Structures of the bacterial ribosome in classical and hybrid states of tRNA binding. Science *332*, 981-984.
Ermolenko, D.N., Majumdar, Z.K., Hickerson, R.P., Spiegel, P.C., Clegg, R.M., and Noller, H.F. (2007). Observation of intersubunit movement of the ribosome in solution using FRET. J Mol Biol *370*, 530-540.
Ermolenko, D.N., and Noller, H.F. (2011). mRNA translocation occurs during the second step of ribosomal intersubunit rotation. Nature structural & molecular biology *18*, 457-462.
Evarsson, A., Brazhnikov, E., Garber, M., Zheltonosova, J., Chirgadze, Y., al-Karadaghi, S., Svensson, L.A., and Liljas, A. (1994). Three-dimensional structure of the ribosomal translocase: elongation factor G from Thermus thermophilus. EMBO J *13*, 3669-3677.
Fei, J., Bronson, J.E., Hofman, J.M., Srinivas, R.L., Wiggins, C.H., and Gonzalez, R.L., Jr. (2009). Allosteric collaboration between elongation factor G and the ribosomal L1 stalk directs tRNA movements during translation. Proc Natl Acad Sci U S A *106*, 15702-15707.
Fei, J., Kosuri, P., MacDougall, D.D., and Gonzalez, R.L., Jr. (2008). Coupling of ribosomal L1 stalk and tRNA dynamics during translation elongation. Molecular cell *30*, 348-359.

Fischer, N., Konevega, A.L., Wintermeyer, W., Rodnina, M.V., and Stark, H. (2010). Ribosome dynamics and tRNA movement by time-resolved electron cryomicroscopy. Nature *466*, 329-333.
Fischer, N., Neumann, P., Bock, L.V., Maracci, C., Wang, Z., Paleskava, A., Konevega, A.L., Schroder, G.F., Grubmuller, H., Ficner, R.*, et al.* (2016). The pathway to GTPase activation of elongation factor SelB on the ribosome. Nature *540*, 80-85.
Fischer, N., Neumann, P., Konevega, A.L., Bock, L.V., Ficner, R., Rodnina, M.V., and Stark, H. (2015). Structure of the E. coli ribosome-EF-Tu complex at <3 A resolution by Cs-corrected cryo-EM. Nature *520*, 567-570.
Flis, J., Holm, M., Rundlet, E.J., Loerke, J., Hilal, T., Dabrowski, M., Burger, J., Mielke, T., Blanchard, S.C., Spahn, C.M.T.*, et al.* (2018). tRNA Translocation by the Eukaryotic 80S Ribosome and the Impact of GTP Hydrolysis. Cell reports *25*, 2676-2688 e2677.
Frank, J., and Agrawal, R.K. (2000). A ratchet-like inter-subunit reorganization of the ribosome during translocation. Nature *406*, 318-322.
Fu, C., and Parker, J. (1994). A ribosomal frameshifting error during translation of the argI mRNA of Escherichia coli. Mol Gen Genet *243*, 434-441.
Gallant, J., and Lindsley, D. (1993). Ribosome frameshifting at hungry codons: sequence rules, directional specificity and possible relationship to mobile element behaviour. Biochem Soc Trans *21*, 817-821.
Gamper, H., Li, H., Masuda, I., Miklos Robkis, D., Christian, T., Conn, A.B., Blaha, G., Petersson, E.J., Gonzalez, R.L., Jr., and Hou, Y.M. (2021a). Insights into genome recoding from the mechanism of a classic +1-frameshifting tRNA. Nat Commun *12*, 328.
Gamper, H., Mao, Y., Masuda, I., McGuigan, H., Blaha, G., Wang, Y., Xu, S., and Hou, Y.M. (2021b). Twice exploration of tRNA +1 frameshifting in an elongation cycle of protein synthesis. Nucleic Acids Res *49*, 10046-10060.
Gamper, H.B., Masuda, I., Frenkel-Morgenstern, M., and Hou, Y.M. (2015). Maintenance of protein synthesis reading frame by EF-P and m(1)G37-tRNA. Nat Commun *6*, 7226.
Gao, N., Zavialov, A.V., Li, W., Sengupta, J., Valle, M., Gursky, R.P., Ehrenberg, M., and Frank, J. (2005). Mechanism for the disassembly of the posttermination complex inferred from cryo-EM studies. Mol Cell *18*, 663-674.
Gao, Y.G., Selmer, M., Dunham, C.M., Weixlbaumer, A., Kelley, A.C., and Ramakrishnan, V. (2009). The structure of the ribosome with elongation factor G trapped in the posttranslocational state. Science *326*, 694-699.
Gaspar, C., Jannatipour, M., Dion, P., Laganiere, J., Sequeiros, J., Brais, B., and Rouleau, G.A. (2000). CAG tract of MJD-1 may be prone to frameshifts causing polyalanine accumulation. Hum Mol Genet *9*, 1957-1966.
Geggier, P., Dave, R., Feldman, M.B., Terry, D.S., Altman, R.B., Munro, J.B., and Blanchard, S.C. (2010). Conformational sampling of aminoacyl-tRNA during selection on the bacterial ribosome. J Mol Biol *399*, 576-595.
Giedroc, D.P., and Cornish, P.V. (2009). Frameshifting RNA pseudoknots: structure and mechanism. Virus Res *139*, 193-208.
Giovane, A., Balestrieri, C., Quagliuolo, L., and Servillo, L. (1985). 1-N6-Etheno-ADP-ribosylation of elongation factor-2 by diphtheria toxin. FEBS Lett *191*, 191-194.
Girstmair, H., Saffert, P., Rode, S., Czech, A., Holland, G., Bannert, N., and Ignatova, Z. (2013). Depletion of cognate charged transfer RNA causes translational frameshifting within the expanded CAG stretch in huntingtin. Cell Rep *3*, 148-159.
Goyal, A., Belardinelli, R., Maracci, C., Milon, P., and Rodnina, M.V. (2015). Directional transition from initiation to elongation in bacterial translation. Nucleic Acids Res *43*, 10700-10712.

Grigoriadou, C., Marzi, S., Kirillov, S., Gualerzi, C.O., and Cooperman, B.S. (2007). A quantitative kinetic scheme for 70 S translation initiation complex formation. J Mol Biol *373*, 562-572.
Gromadski, K.B., Wieden, H.J., and Rodnina, M.V. (2002). Kinetic mechanism of elongation factor Ts-catalyzed nucleotide exchange in elongation factor Tu. Biochemistry *41*, 162-169.
Gualerzi, C.O., and Pon, C.L. (2015). Initiation of mRNA translation in bacteria: structural and dynamic aspects. Cell Mol Life Sci *72*, 4341-4367.
Guo, Z., and Noller, H.F. (2012). Rotation of the head of the 30S ribosomal subunit during mRNA translocation. Proceedings of the National Academy of Sciences of the United States of America *109*, 20391-20394.
Gupta, P., Kannan, K., Mankin, A.S., and Vazquez-Laslop, N. (2013). Regulation of gene expression by macrolide-induced ribosomal frameshifting. Mol Cell *52*, 629-642.
Gurvich, O.L., Baranov, P.V., Zhou, J., Hammer, A.W., Gesteland, R.F., and Atkins, J.F. (2003). Sequences that direct significant levels of frameshifting are frequent in coding regions of Escherichia coli. EMBO J *22*, 5941-5950.
Ha, T., Rasnik, I., Cheng, W., Babcock, H.P., Gauss, G.H., Lohman, T.M., and Chu, S. (2002). Initiation and re-initiation of DNA unwinding by the Escherichia coli Rep helicase. Nature *419*, 638-641.
Hawer, H., Utkur, K., Arend, M., Mayer, K., Adrian, L., Brinkmann, U., and Schaffrath, R. (2018). Importance of diphthamide modified EF2 for translational accuracy and competitive cell growth in yeast. PLoS One *13*, e0205870.
Hiller, D.A., Singh, V., Zhong, M., and Strobel, S.A. (2011). A two-step chemical mechanism for ribosome-catalysed peptide bond formation. Nature *476*, 236-239.
Hoffer, E.D., Hong, S., Sunita, S., Maehigashi, T., Gonzalez, R.L.J., Whitford, P.C., and Dunham, C.M. (2020). Structural insights into mRNA reading frame regulation by tRNA modification and slippery codon-anticodon pairing. Elife *9*.
Holtkamp, W., Cunha, C.E., Peske, F., Konevega, A.L., Wintermeyer, W., and Rodnina, M.V. (2014). GTP hydrolysis by EF-G synchronizes tRNA movement on small and large ribosomal subunits. EMBO J *33*, 1073-1085.
Huter, P., Arenz, S., Bock, L.V., Graf, M., Frister, J.O., Heuer, A., Peil, L., Starosta, A.L., Wohlgemuth, I., Peske, F.*, et al.* (2017). Structural Basis for Polyproline-Mediated Ribosome Stalling and Rescue by the Translation Elongation Factor EF-P. Mol Cell *68*, 515-527 e516.
Imai, H., Uchiumi, T., and Kodera, N. (2020). Direct visualization of translational GTPase factor pool formed around the archaeal ribosomal P-stalk by high-speed AFM. Proc Natl Acad Sci U S A *117*, 32386-32394.
Jacks, T., Power, M.D., Masiarz, F.R., Luciw, P.A., Barr, P.J., and Varmus, H.E. (1988). Characterization of ribosomal frameshifting in HIV-1 gag-pol expression. Nature *331*, 280-283.
Jacobs, J.L., Belew, A.T., Rakauskaite, R., and Dinman, J.D. (2007). Identification of functional, endogenous programmed -1 ribosomal frameshift signals in the genome of Saccharomyces cerevisiae. Nucleic Acids Res *35*, 165-174.
Jenner, L., Romby, P., Rees, B., Schulze-Briese, C., Springer, M., Ehresmann, C., Ehresmann, B., Moras, D., Yusupova, G., and Yusupov, M. (2005). Translational operator of mRNA on the ribosome: how repressor proteins exclude ribosome binding. Science *308*, 120-123.
Jenner, L.B., Demeshkina, N., Yusupova, G., and Yusupov, M. (2010). Structural aspects of messenger RNA reading frame maintenance by the ribosome. Nature structural & molecular biology *17*, 555-560.
Jorgensen, F., and Kurland, C.G. (1990). Processivity errors of gene expression in Escherichia coli. J Mol Biol *215*, 511-521.
Jorgensen, R., Merrill, A.R., Yates, S.P., Marquez, V.E., Schwan, A.L., Boesen, T., and Andersen, G.R. (2005). Exotoxin A-eEF2 complex structure indicates ADP ribosylation by ribosome mimicry. Nature *436*, 979-984.

Jorgensen, R., Purdy, A.E., Fieldhouse, R.J., Kimber, M.S., Bartlett, D.H., and Merrill, A.R. (2008). Cholix toxin, a novel ADP-ribosylating factor from Vibrio cholerae. J Biol Chem *283*, 10671-10678.
Julian, P., Konevega, A.L., Scheres, S.H., Lazaro, M., Gil, D., Wintermeyer, W., Rodnina, M.V., and Valle, M. (2008). Structure of ratcheted ribosomes with tRNAs in hybrid states. Proc Natl Acad Sci U S A *105*, 16924-16927.
Julian, P., Milon, P., Agirrezabala, X., Lasso, G., Gil, D., Rodnina, M.V., and Valle, M. (2011). The Cryo-EM structure of a complete 30S translation initiation complex from Escherichia coli. PLoS Biol *9*, e1001095.
Kaledhonkar, S., Fu, Z., Caban, K., Li, W., Chen, B., Sun, M., Gonzalez, R.L., Jr., and Frank, J. (2019). Late steps in bacterial translation initiation visualized using time-resolved cryo-EM. Nature *570*, 400-404.
Kapur, M., and Ackerman, S.L. (2018). mRNA Translation Gone Awry: Translation Fidelity and Neurological Disease. Trends Genet *34*, 218-231.
Katunin, V.I., Savelsbergh, A., Rodnina, M.V., and Wintermeyer, W. (2002). Coupling of GTP hydrolysis by elongation factor G to translocation and factor recycling on the ribosome. Biochemistry *41*, 12806-12812.
Kelly, J.A., Olson, A.N., Neupane, K., Munshi, S., San Emeterio, J., Pollack, L., Woodside, M.T., and Dinman, J.D. (2020). Structural and functional conservation of the programmed -1 ribosomal frameshift signal of SARS coronavirus 2 (SARS-CoV-2). J Biol Chem *295*, 10741-10748.
Kendra, J.A., Advani, V.M., Chen, B., Briggs, J.W., Zhu, J., Bress, H.J., Pathy, S.M., and Dinman, J.D. (2018). Functional and structural characterization of the chikungunya virus translational recoding signals. J Biol Chem *293*, 17536-17545.
Kendra, J.A., de la Fuente, C., Brahms, A., Woodson, C., Bell, T.M., Chen, B., Khan, Y.A., Jacobs, J.L., Kehn-Hall, K., and Dinman, J.D. (2017). Ablation of Programmed -1 Ribosomal Frameshifting in Venezuelan Equine Encephalitis Virus Results in Attenuated Neuropathogenicity. J Virol *91*.
Khan, Y.A., Loughran, G., Steckelberg, A.L., Brown, K., Kiniry, S.J., Stewart, H., Baranov, P.V., Kieft, J.S., Firth, A.E., and Atkins, J.F. (2022). Evaluating ribosomal frameshifting in CCR5 mRNA decoding. Nature *604*, E16-E23.
Kim, H.D., Puglisi, J.D., and Chu, S. (2007). Fluctuations of transfer RNAs between classical and hybrid states. Biophysical journal *93*, 3575-3582.
Kim, H.K., Liu, F., Fei, J., Bustamante, C., Gonzalez, R.L., Jr., and Tinoco, I., Jr. (2014). A frameshifting stimulatory stem loop destabilizes the hybrid state and impedes ribosomal translocation. Proceedings of the National Academy of Sciences of the United States of America *111*, 5538-5543.
Kohanski, M.A., Dwyer, D.J., Wierzbowski, J., Cottarel, G., and Collins, J.J. (2008). Mistranslation of membrane proteins and two-component system activation trigger antibiotic-mediated cell death. Cell *135*, 679-690.
Konevega, A.L., Fischer, N., Semenkov, Y.P., Stark, H., Wintermeyer, W., and Rodnina, M.V. (2007). Spontaneous reverse movement of mRNA-bound tRNA through the ribosome. Nat Struct Mol Biol *14*, 318-324.
Korniy, N., Goyal, A., Hoffmann, M., Samatova, E., Peske, F., Pohlmann, S., and Rodnina, M.V. (2019). Modulation of HIV-1 Gag/Gag-Pol frameshifting by tRNA abundance. Nucleic Acids Res *47*, 5210-5222.
Korostelev, A., Trakhanov, S., Asahara, H., Laurberg, M., Lancaster, L., and Noller, H.F. (2007). Interactions and dynamics of the Shine Dalgarno helix in the 70S ribosome. Proc Natl Acad Sci U S A *104*, 16840-16843.

Kubarenko, A., Sergiev, P., Wintermeyer, W., Dontsova, O., and Rodnina, M.V. (2006). Involvement of helix 34 of 16 S rRNA in decoding and translocation on the ribosome. J Biol Chem *281*, 35235-35244.
Kuhle, B., and Ficner, R. (2014). A monovalent cation acts as structural and catalytic cofactor in translational GTPases. EMBO J *33*, 2547-2563.
Kuhlenkoetter, S., Wintermeyer, W., and Rodnina, M.V. (2011). Different substrate-dependent transition states in the active site of the ribosome. Nature *476*, 351-354.
Kurland, C.G. (1992). Translational accuracy and the fitness of bacteria. Annu Rev Genet *26*, 29-50.
Lill, R., Robertson, J.M., and Wintermeyer, W. (1986). Affinities of tRNA binding sites of ribosomes from Escherichia coli. Biochemistry *25*, 3245-3255.
Lin, J., Gagnon, M.G., Bulkley, D., and Steitz, T.A. (2015). Conformational changes of elongation factor G on the ribosome during tRNA translocation. Cell *160*, 219-227.
Liu, S., Bachran, C., Gupta, P., Miller-Randolph, S., Wang, H., Crown, D., Zhang, Y., Wein, A.N., Singh, R., Fattah, R.*, et al.* (2012). Diphthamide modification on eukaryotic elongation factor 2 is needed to assure fidelity of mRNA translation and mouse development. Proc Natl Acad Sci U S A *109*, 13817-13822.
Loveland, A.B., Demo, G., Grigorieff, N., and Korostelev, A.A. (2017). Ensemble cryo-EM elucidates the mechanism of translation fidelity. Nature *546*, 113-117.
Loveland, A.B., Demo, G., and Korostelev, A.A. (2020). Cryo-EM of elongating ribosome with EF-Tu*GTP elucidates tRNA proofreading. Nature *584*, 640-645.
Luthi, K., Moser, M., Ryser, J., and Weber, H. (1990). Evidence for a role of translational frameshifting in the expression of transposition activity of the bacterial insertion element IS1. Gene *88*, 15-20.
Manktelow, E., Shigemoto, K., and Brierley, I. (2005). Characterization of the frameshift signal of Edr, a mammalian example of programmed -1 ribosomal frameshifting. Nucleic Acids Res *33*, 1553-1563.
Manley, J.L. (1978). Synthesis and degradation of termination and premature-termination fragments of beta-galactosidase in vitro and in vivo. J Mol Biol *125*, 407-432.
Maracci, C., and Rodnina, M.V. (2016). Review: Translational GTPases. Biopolymers *105*, 463-475.
Marzouki, A., Sontag, B., Lavergne, J.P., Vidonne, C., Reboud, J.P., and Reboud, A.M. (1991). Effect of ADP-ribosylation and phosphorylation on the interaction of elongation factor 2 with guanylic nucleotides. Biochimie *73*, 1151-1156.
McLoughlin, H.S., Moore, L.R., and Paulson, H.L. (2020). Pathogenesis of SCA3 and implications for other polyglutamine diseases. Neurobiol Dis *134*, 104635.
Merryman, C., Moazed, D., Daubresse, G., and Noller, H.F. (1999). Nucleotides in 23S rRNA protected by the association of 30S and 50S ribosomal subunits. J Mol Biol *285*, 107-113.
Meydan, S., Klepacki, D., Karthikeyan, S., Margus, T., Thomas, P., Jones, J.E., Khan, Y., Briggs, J., Dinman, J.D., Vazquez-Laslop, N.*, et al.* (2017). Programmed Ribosomal Frameshifting Generates a Copper Transporter and a Copper Chaperone from the Same Gene. Molecular cell *65*, 207-219.
Milon, P., Carotti, M., Konevega, A.L., Wintermeyer, W., Rodnina, M.V., and Gualerzi, C.O. (2010). The ribosome-bound initiation factor 2 recruits initiator tRNA to the 30S initiation complex. EMBO Rep *11*, 312-316.
Milon, P., Konevega, A.L., Gualerzi, C.O., and Rodnina, M.V. (2008). Kinetic checkpoint at a late step in translation initiation. Mol Cell *30*, 712-720.
Milon, P., Konevega, A.L., Peske, F., Fabbretti, A., Gualerzi, C.O., and Rodnina, M.V. (2007). Transient kinetics, fluorescence, and FRET in studies of initiation of translation in bacteria. Methods Enzymol *430*, 1-30.

Milon, P., Maracci, C., Filonava, L., Gualerzi, C.O., and Rodnina, M.V. (2012). Real-time assembly landscape of bacterial 30S translation initiation complex. Nat Struct Mol Biol *19*, 609-615.
Milon, P., and Rodnina, M.V. (2012). Kinetic control of translation initiation in bacteria. Crit Rev Biochem Mol Biol *47*, 334-348.
Moazed, D., and Noller, H.F. (1989a). Interaction of tRNA with 23S rRNA in the ribosomal A, P, and E sites. Cell *57*, 585-597.
Moazed, D., and Noller, H.F. (1989b). Intermediate states in the movement of transfer RNA in the ribosome. Nature *342*, 142-148.
Moazed, D., and Noller, H.F. (1991). Sites of interaction of the CCA end of peptidyl-tRNA with 23S rRNA. Proc Natl Acad Sci U S A *88*, 3725-3728.
Moazed, D., Robertson, J.M., and Noller, H.F. (1988). Interaction of elongation factors EF-G and EF-Tu with a conserved loop in 23S RNA. Nature *334*, 362-364.
Mohammad, F., Green, R., and Buskirk, A.R. (2019). A systematically-revised ribosome profiling method for bacteria reveals pauses at single-codon resolution. Elife *8*.
Mohan, S., Donohue, J.P., and Noller, H.F. (2014). Molecular mechanics of 30S subunit head rotation. Proc Natl Acad Sci U S A *111*, 13325-13330.
Mohan, S., and Noller, H.F. (2017). Recurring RNA structural motifs underlie the mechanics of L1 stalk movement. Nat Commun *8*, 14285.
Mohr, D., Wintermeyer, W., and Rodnina, M.V. (2002). GTPase activation of elongation factors Tu and G on the ribosome. Biochemistry *41*, 12520-12528.
Moine, H., and Dahlberg, A.E. (1994). Mutations in helix 34 of Escherichia coli 16 S ribosomal RNA have multiple effects on ribosome function and synthesis. J Mol Biol *243*, 402-412.
Montanaro, L., Sperti, S., Testoni, G., and Mattioli, A. (1976). Effect of elongation factor 2 and of adenosine diphosphate-ribosylated elongation factor 2 on translocation. Biochem J *156*, 15-23.
Moomau, C., Musalgaonkar, S., Khan, Y.A., Jones, J.E., and Dinman, J.D. (2016). Structural and Functional Characterization of Programmed Ribosomal Frameshift Signals in West Nile Virus Strains Reveals High Structural Plasticity Among cis-Acting RNA Elements. J Biol Chem *291*, 15788-15795.
Moore, P.B., and Steitz, T.A. (2002). The involvement of RNA in ribosome function. Nature *418*, 229-235.
Moore, P.B., and Steitz, T.A. (2011). The roles of RNA in the synthesis of protein. Cold Spring Harb Perspect Biol *3*, a003780.
Munro, J.B., Altman, R.B., O'Connor, N., and Blanchard, S.C. (2007). Identification of two distinct hybrid state intermediates on the ribosome. Molecular cell *25*, 505-517.
Munro, J.B., Sanbonmatsu, K.Y., Spahn, C.M., and Blanchard, S.C. (2009). Navigating the ribosome's metastable energy landscape. Trends Biochem Sci *34*, 390-400.
Munro, J.B., Wasserman, M.R., Altman, R.B., Wang, L., and Blanchard, S.C. (2010). Correlated conformational events in EF-G and the ribosome regulate translocation. Nat Struct Mol Biol *17*, 1470-1477.
Murphy, F.V.t., Ramakrishnan, V., Malkiewicz, A., and Agris, P.F. (2004). The role of modifications in codon discrimination by tRNA(Lys)UUU. Nat Struct Mol Biol *11*, 1186-1191.
Namy, O., Moran, S.J., Stuart, D.I., Gilbert, R.J., and Brierley, I. (2006). A mechanical explanation of RNA pseudoknot function in programmed ribosomal frameshifting. Nature *441*, 244-247.
Napthine, S., Bell, S., Hill, C.H., Brierley, I., and Firth, A.E. (2019). Characterization of the stimulators of protein-directed ribosomal frameshifting in Theiler's murine encephalomyelitis virus. Nucleic Acids Res *47*, 8207-8223.

Napthine, S., Hill, C.H., Nugent, H.C.M., and Brierley, I. (2021). Modulation of Viral Programmed Ribosomal Frameshifting and Stop Codon Readthrough by the Host Restriction Factor Shiftless. Viruses *13*.
Nasvall, S.J., Nilsson, K., and Bjork, G.R. (2009). The ribosomal grip of the peptidyl-tRNA is critical for reading frame maintenance. J Mol Biol *385*, 350-367.
Niblett, D., Nelson, C., Leung, C.S., Rexroad, G., Cozy, J., Zhou, J., Lancaster, L., and Noller, H.F. (2021). Mutations in domain IV of elongation factor EF-G confer -1 frameshifting. RNA *27*, 40-53.
Nishima, W., Girodat, D., Holm, M., Rundlet, E.J., Alejo, J.L., Fischer, K., Blanchard, S.C., and Sanbonmatsu, K.Y. (2022). Hyper-swivel head domain motions are required for complete mRNA-tRNA translocation and ribosome resetting. Nucleic Acids Res.
Nissen, P., Hansen, J., Ban, N., Moore, P.B., and Steitz, T.A. (2000). The structural basis of ribosome activity in peptide bond synthesis. Science *289*, 920-930.
Nissen, P., Kjeldgaard, M., Thirup, S., Polekhina, G., Reshetnikova, L., Clark, B.F., and Nyborg, J. (1995). Crystal structure of the ternary complex of Phe-tRNAPhe, EF-Tu, and a GTP analog. Science *270*, 1464-1472.
Noller, H.F., Hoang, L., and Fredrick, K. (2005). The 30S ribosomal P site: a function of 16S rRNA. FEBS Lett *579*, 855-858.
Noller, H.F., Hoffarth, V., and Zimniak, L. (1992). Unusual resistance of peptidyl transferase to protein extraction procedures. Science *256*, 1416-1419.
Nygard, O., and Nilsson, L. (1990). Kinetic determination of the effects of ADP-ribosylation on the interaction of eukaryotic elongation factor 2 with ribosomes. J Biol Chem *265*, 6030-6034.
Ogle, J.M., Brodersen, D.E., Clemons, W.M., Jr., Tarry, M.J., Carter, A.P., and Ramakrishnan, V. (2001). Recognition of cognate transfer RNA by the 30S ribosomal subunit. Science *292*, 897-902.
Ogle, J.M., Carter, A.P., and Ramakrishnan, V. (2003). Insights into the decoding mechanism from recent ribosome structures. Trends in biochemical sciences *28*, 259-266.
Ogle, J.M., Murphy, F.V., Tarry, M.J., and Ramakrishnan, V. (2002). Selection of tRNA by the ribosome requires a transition from an open to a closed form. Cell *111*, 721-732.
Ortiz, P.A., Ulloque, R., Kihara, G.K., Zheng, H., and Kinzy, T.G. (2006). Translation elongation factor 2 anticodon mimicry domain mutants affect fidelity and diphtheria toxin resistance. J Biol Chem *281*, 32639-32648.
Pan, D., Kirillov, S.V., and Cooperman, B.S. (2007). Kinetically competent intermediates in the translocation step of protein synthesis. Mol Cell *25*, 519-529.
Pape, T., Wintermeyer, W., and Rodnina, M. (1999). Induced fit in initial selection and proofreading of aminoacyl-tRNA on the ribosome. EMBO J *18*, 3800-3807.
Pape, T., Wintermeyer, W., and Rodnina, M.V. (1998). Complete kinetic mechanism of elongation factor Tu-dependent binding of aminoacyl-tRNA to the A site of the E. coli ribosome. EMBO J *17*, 7490-7497.
Pellegrino, S., Demeshkina, N., Mancera-Martinez, E., Melnikov, S., Simonetti, A., Myasnikov, A., Yusupov, M., Yusupova, G., and Hashem, Y. (2018). Structural Insights into the Role of Diphthamide on Elongation Factor 2 in mRNA Reading-Frame Maintenance. J Mol Biol *430*, 2677-2687.
Peng, B.Z., Bock, L.V., Belardinelli, R., Peske, F., Grubmuller, H., and Rodnina, M.V. (2019). Active role of elongation factor G in maintaining the mRNA reading frame during translation. Sci Adv *5*, eaax8030.
Peske, F., Savelsbergh, A., Katunin, V.I., Rodnina, M.V., and Wintermeyer, W. (2004). Conformational changes of the small ribosomal subunit during elongation factor G-dependent tRNA-mRNA translocation. J Mol Biol *343*, 1183-1194.
Petropoulos, A.D., and Green, R. (2012). Further in vitro exploration fails to support the allosteric three-site model. J Biol Chem *287*, 11642-11648.

Petrychenko, V., Peng, B.Z., de A. P. Schwarzer, A.C., Peske, F., Rodnina, M.V., and Fischer, N. (2021). Structural mechanism of GTPase-powered ribosome-tRNA movement. Nat Commun *12*, 5933.
Polikanov, Y.S., Steitz, T.A., and Innis, C.A. (2014). A proton wire to couple aminoacyl-tRNA accommodation and peptide-bond formation on the ribosome. Nat Struct Mol Biol *21*, 787-793.
Poulis, P., Patel, A., Rodnina, M.V., and Adio, S. (2022). Altered tRNA dynamics during translocation on slippery mRNA as determinant of spontaneous ribosome frameshifting. Nature communications *13*, 4231.
Poulter, N.S., Pitkeathly, W.T., Smith, P.J., and Rappoport, J.Z. (2015). The physical basis of total internal reflection fluorescence (TIRF) microscopy and its cellular applications. Methods in molecular biology *1251*, 1-23.
Qin, H., Grigoriadou, C., and Cooperman, B.S. (2009). Interaction of IF2 with the ribosomal GTPase-associated center during 70S initiation complex formation. Biochemistry *48*, 4699-4706.
Ramrath, D.J., Lancaster, L., Sprink, T., Mielke, T., Loerke, J., Noller, H.F., and Spahn, C.M. (2013). Visualization of two transfer RNAs trapped in transit during elongation factor G-mediated translocation. Proceedings of the National Academy of Sciences of the United States of America *110*, 20964-20969.
Ranjan, N., and Rodnina, M.V. (2017). Thio-Modification of tRNA at the Wobble Position as Regulator of the Kinetics of Decoding and Translocation on the Ribosome. J Am Chem Soc *139*, 5857-5864.
Ratje, A.H., Loerke, J., Mikolajka, A., Brunner, M., Hildebrand, P.W., Starosta, A.L., Donhofer, A., Connell, S.R., Fucini, P., Mielke, T.*, et al.* (2010). Head swivel on the ribosome facilitates translocation by means of intra-subunit tRNA hybrid sites. Nature *468*, 713-716.
Rettberg, C.C., Prere, M.F., Gesteland, R.F., Atkins, J.F., and Fayet, O. (1999). A three-way junction and constituent stem-loops as the stimulator for programmed -1 frameshifting in bacterial insertion sequence IS911. J Mol Biol *286*, 1365-1378.
Rezgui, V.A., Tyagi, K., Ranjan, N., Konevega, A.L., Mittelstaet, J., Rodnina, M.V., Peter, M., and Pedrioli, P.G. (2013). tRNA tKUUU, tQUUG, and tEUUC wobble position modifications fine-tune protein translation by promoting ribosome A-site binding. Proc Natl Acad Sci U S A *110*, 12289-12294.
Riegger, R.J., and Caliskan, N. (2022). Thinking Outside the Frame: Impacting Genomes Capacity by Programmed Ribosomal Frameshifting. Front Mol Biosci *9*, 842261.
Robertson, J.M., and Wintermeyer, W. (1987). Mechanism of ribosomal translocation. tRNA binds transiently to an exit site before leaving the ribosome during translocation. J Mol Biol *196*, 525-540.
Rodnina, M.V. (2013). The ribosome as a versatile catalyst: reactions at the peptidyl transferase center. Curr Opin Struct Biol *23*, 595-602.
Rodnina, M.V. (2018). Translation in Prokaryotes. Cold Spring Harb Perspect Biol *10*.
Rodnina, M.V., Fischer, N., Maracci, C., and Stark, H. (2017). Ribosome dynamics during decoding. Philos Trans R Soc Lond B Biol Sci *372*.
Rodnina, M.V., Korniy, N., Klimova, M., Karki, P., Peng, B.Z., Senyushkina, T., Belardinelli, R., Maracci, C., Wohlgemuth, I., Samatova, E.*, et al.* (2020). Translational recoding: canonical translation mechanisms reinterpreted. Nucleic Acids Res *48*, 1056-1067.
Rodnina, M.V., Pape, T., Fricke, R., Kuhn, L., and Wintermeyer, W. (1996). Initial binding of the elongation factor Tu.GTP.aminoacyl-tRNA complex preceding codon recognition on the ribosome. J Biol Chem *271*, 646-652.
Rodnina, M.V., Pape, T., Fricke, R., and Wintermeyer, W. (1995). Elongation factor Tu, a GTPase triggered by codon recognition on the ribosome: mechanism and GTP consumption. Biochem Cell Biol *73*, 1221-1227.

Rodnina, M.V., Peske, F., Peng, B.Z., Belardinelli, R., and Wintermeyer, W. (2019). Converting GTP hydrolysis into motion: versatile translational elongation factor G. Biol Chem *401*, 131-142.
Rodnina, M.V., Savelsbergh, A., Katunin, V.I., and Wintermeyer, W. (1997). Hydrolysis of GTP by elongation factor G drives tRNA movement on the ribosome. Nature *385*, 37-41.
Rodnina, M.V., and Wintermeyer, W. (1995). GTP consumption of elongation factor Tu during translation of heteropolymeric mRNAs. Proceedings of the National Academy of Sciences of the United States of America *92*, 1945-1949.
Roy, R., Hohng, S., and Ha, T. (2008). A practical guide to single-molecule FRET. Nature methods *5*, 507-516.
Rozov, A., Demeshkina, N., Khusainov, I., Westhof, E., Yusupov, M., and Yusupova, G. (2016). Novel base-pairing interactions at the tRNA wobble position crucial for accurate reading of the genetic code. Nat Commun *7*, 10457.
Rundlet, E.J., Holm, M., Schacherl, M., Natchiar, S.K., Altman, R.B., Spahn, C.M.T., Myasnikov, A.G., and Blanchard, S.C. (2021). Structural basis of early translocation events on the ribosome. Nature *595*, 741-745.
Salsi, E., Farah, E., Dann, J., and Ermolenko, D.N. (2014). Following movement of domain IV of elongation factor G during ribosomal translocation. Proc Natl Acad Sci U S A *111*, 15060-15065.
Salsi, E., Farah, E., Netter, Z., Dann, J., and Ermolenko, D.N. (2015). Movement of elongation factor G between compact and extended conformations. J Mol Biol *427*, 454-467.
Samatova, E., Daberger, J., Liutkute, M., and Rodnina, M.V. (2020). Translational Control by Ribosome Pausing in Bacteria: How a Non-uniform Pace of Translation Affects Protein Production and Folding. Front Microbiol *11*, 619430.
Sanbonmatsu, K.Y., Joseph, S., and Tung, C.S. (2005). Simulating movement of tRNA into the ribosome during decoding. Proc Natl Acad Sci U S A *102*, 15854-15859.
Sanders, C.L., Lohr, K.J., Gambill, H.L., Curran, R.B., and Curran, J.F. (2008). Anticodon loop mutations perturb reading frame maintenance by the E site tRNA. RNA *14*, 1874-1881.
Savelsbergh, A., Katunin, V.I., Mohr, D., Peske, F., Rodnina, M.V., and Wintermeyer, W. (2003). An elongation factor G-induced ribosome rearrangement precedes tRNA-mRNA translocation. Mol Cell *11*, 1517-1523.
Savelsbergh, A., Matassova, N.B., Rodnina, M.V., and Wintermeyer, W. (2000). Role of domains 4 and 5 in elongation factor G functions on the ribosome. J Mol Biol *300*, 951-961.
Schmeing, T.M., Huang, K.S., Kitchen, D.E., Strobel, S.A., and Steitz, T.A. (2005). Structural insights into the roles of water and the 2' hydroxyl of the P site tRNA in the peptidyl transferase reaction. Mol Cell *20*, 437-448.
Schmeing, T.M., and Ramakrishnan, V. (2009). What recent ribosome structures have revealed about the mechanism of translation. Nature *461*, 1234-1242.
Schmeing, T.M., Voorhees, R.M., Kelley, A.C., Gao, Y.G., Murphy, F.V.t., Weir, J.R., and Ramakrishnan, V. (2009). The crystal structure of the ribosome bound to EF-Tu and aminoacyl-tRNA. Science *326*, 688-694.
Schuette, J.C., Murphy, F.V.t., Kelley, A.C., Weir, J.R., Giesebrecht, J., Connell, S.R., Loerke, J., Mielke, T., Zhang, W., Penczek, P.A*., et al.* (2009). GTPase activation of elongation factor EF-Tu by the ribosome during decoding. EMBO J *28*, 755-765.
Schuwirth, B.S., Borovinskaya, M.A., Hau, C.W., Zhang, W., Vila-Sanjurjo, A., Holton, J.M., and Cate, J.H. (2005). Structures of the bacterial ribosome at 3.5 A resolution. Science *310*, 827-834.
Sekine, Y., Nagasawa, H., and Ohtsubo, E. (1992). Identification of the site of translational frameshifting required for production of the transposase encoded by insertion sequence IS 1. Mol Gen Genet *235*, 317-324.

Sekine, Y., and Ohtsubo, E. (1989). Frameshifting is required for production of the transposase encoded by insertion sequence 1. Proc Natl Acad Sci U S A *86*, 4609-4613.
Seligmann, H., and Pollock, D.D. (2004). The ambush hypothesis: hidden stop codons prevent off-frame gene reading. DNA Cell Biol *23*, 701-705.
Semenkov, Y.P., Rodnina, M.V., and Wintermeyer, W. (1996). The "allosteric three-site model" of elongation cannot be confirmed in a well-defined ribosome system from Escherichia coli. Proceedings of the National Academy of Sciences of the United States of America *93*, 12183-12188.
Semenkov, Y.P., Shapkina, T.G., and Kirillov, S.V. (1992). Puromycin reaction of the A-site bound peptidyl-tRNA. Biochimie *74*, 411-417.
Sergiev, P.V., Lesnyak, D.V., Kiparisov, S.V., Burakovsky, D.E., Leonov, A.A., Bogdanov, A.A., Brimacombe, R., and Dontsova, O.A. (2005). Function of the ribosomal E-site: a mutagenesis study. Nucleic Acids Res *33*, 6048-6056.
Sharma, H., Adio, S., Senyushkina, T., Belardinelli, R., Peske, F., and Rodnina, M.V. (2016). Kinetics of Spontaneous and EF-G-Accelerated Rotation of Ribosomal Subunits. Cell reports *16*, 2187-2196.
Sharma, V., Prere, M.F., Canal, I., Firth, A.E., Atkins, J.F., Baranov, P.V., and Fayet, O. (2014). Analysis of tetra- and hepta-nucleotides motifs promoting -1 ribosomal frameshifting in Escherichia coli. Nucleic Acids Res *42*, 7210-7225.
Shigemoto, K., Brennan, J., Walls, E., Watson, C.J., Stott, D., Rigby, P.W., and Reith, A.D. (2001). Identification and characterisation of a developmentally regulated mammalian gene that utilises -1 programmed ribosomal frameshifting. Nucleic Acids Res *29*, 4079-4088.
Shine, J., and Dalgarno, L. (1975). Determinant of cistron specificity in bacterial ribosomes. Nature *254*, 34-38.
Simonetti, A., Marzi, S., Myasnikov, A.G., Fabbretti, A., Yusupov, M., Gualerzi, C.O., and Klaholz, B.P. (2008). Structure of the 30S translation initiation complex. Nature *455*, 416-420.
Staple, D.W., and Butcher, S.E. (2005). Solution structure and thermodynamic investigation of the HIV-1 frameshift inducing element. J Mol Biol *349*, 1011-1023.
Stark, H., Rodnina, M.V., Rinke-Appel, J., Brimacombe, R., Wintermeyer, W., and van Heel, M. (1997). Visualization of elongation factor Tu on the Escherichia coli ribosome. Nature *389*, 403-406.
Stark, H., Rodnina, M.V., Wieden, H.J., van Heel, M., and Wintermeyer, W. (2000). Large-scale movement of elongation factor G and extensive conformational change of the ribosome during translocation. Cell *100*, 301-309.
Stefani, M., and Dobson, C.M. (2003). Protein aggregation and aggregate toxicity: new insights into protein folding, misfolding diseases and biological evolution. J Mol Med (Berl) *81*, 678-699.
Stochmanski, S.J., Therrien, M., Laganiere, J., Rochefort, D., Laurent, S., Karemera, L., Gaudet, R., Vyboh, K., Van Meyel, D.J., Di Cristo, G.*, et al.* (2012). Expanded ATXN3 frameshifting events are toxic in Drosophila and mammalian neuron models. Hum Mol Genet *21*, 2211-2218.
Stoebel, D.M., Dean, A.M., and Dykhuizen, D.E. (2008). The cost of expression of Escherichia coli lac operon proteins is in the process, not in the products. Genetics *178*, 1653-1660.
Suzuki, T. (2021). The expanding world of tRNA modifications and their disease relevance. Nat Rev Mol Cell Biol *22*, 375-392.
Tabrizi, S.J., Flower, M.D., Ross, C.A., and Wild, E.J. (2020). Huntington disease: new insights into molecular pathogenesis and therapeutic opportunities. Nat Rev Neurol *16*, 529-546.
Takyar, S., Hickerson, R.P., and Noller, H.F. (2005). mRNA helicase activity of the ribosome. Cell *120*, 49-58.
Temperley, R., Richter, R., Dennerlein, S., Lightowlers, R.N., and Chrzanowska-Lightowlers, Z.M. (2010). Hungry codons promote frameshifting in human mitochondrial ribosomes. Science *327*, 301.

Toulouse, A., Au-Yeung, F., Gaspar, C., Roussel, J., Dion, P., and Rouleau, G.A. (2005). Ribosomal frameshifting on MJD-1 transcripts with long CAG tracts. Hum Mol Genet *14*, 2649-2660.
Tsung, K., Inouye, S., and Inouye, M. (1989). Factors affecting the efficiency of protein synthesis in Escherichia coli. Production of a polypeptide of more than 6000 amino acid residues. J Biol Chem *264*, 4428-4433.
Ude, S., Lassak, J., Starosta, A.L., Kraxenberger, T., Wilson, D.N., and Jung, K. (2013). Translation elongation factor EF-P alleviates ribosome stalling at polyproline stretches. Science *339*, 82-85.
Uemura, S., Aitken, C.E., Korlach, J., Flusberg, B.A., Turner, S.W., and Puglisi, J.D. (2010). Real-time tRNA transit on single translating ribosomes at codon resolution. Nature *464*, 1012-1017.
Urbonavicius, J., Qian, Q., Durand, J.M., Hagervall, T.G., and Bjork, G.R. (2001). Improvement of reading frame maintenance is a common function for several tRNA modifications. EMBO J *20*, 4863-4873.
Urbonavicius, J., Stahl, G., Durand, J.M., Ben Salem, S.N., Qian, Q., Farabaugh, P.J., and Bjork, G.R. (2003). Transfer RNA modifications that alter +1 frameshifting in general fail to affect -1 frameshifting. RNA *9*, 760-768.
Voorhees, R.M., Schmeing, T.M., Kelley, A.C., and Ramakrishnan, V. (2010). The mechanism for activation of GTP hydrolysis on the ribosome. Science *330*, 835-838.
Wang, X., Xuan, Y., Han, Y., Ding, X., Ye, K., Yang, F., Gao, P., Goff, S.P., and Gao, G. (2019). Regulation of HIV-1 Gag-Pol Expression by Shiftless, an Inhibitor of Programmed -1 Ribosomal Frameshifting. Cell *176*, 625-635 e614.
Wang, Y., Qin, H., Kudaravalli, R.D., Kirillov, S.V., Dempsey, G.T., Pan, D., Cooperman, B.S., and Goldman, Y.E. (2007). Single-molecule structural dynamics of EF-G--ribosome interaction during translocation. Biochemistry *46*, 10767-10775.
Wasserman, M.R., Alejo, J.L., Altman, R.B., and Blanchard, S.C. (2016). Multiperspective smFRET reveals rate-determining late intermediates of ribosomal translocation. Nature structural & molecular biology *23*, 333-341.
Weixlbaumer, A., Murphy, F.V.t., Dziergowska, A., Malkiewicz, A., Vendeix, F.A., Agris, P.F., and Ramakrishnan, V. (2007). Mechanism for expanding the decoding capacity of transfer RNAs by modification of uridines. Nat Struct Mol Biol *14*, 498-502.
Wilden, B., Savelsbergh, A., Rodnina, M.V., and Wintermeyer, W. (2006). Role and timing of GTP binding and hydrolysis during EF-G-dependent tRNA translocation on the ribosome. Proceedings of the National Academy of Sciences of the United States of America *103*, 13670-13675.
Wills, N.M., Moore, B., Hammer, A., Gesteland, R.F., and Atkins, J.F. (2006). A functional -1 ribosomal frameshift signal in the human paraneoplastic Ma3 gene. J Biol Chem *281*, 7082-7088.
Wimberly, B.T., Brodersen, D.E., Clemons, W.M., Jr., Morgan-Warren, R.J., Carter, A.P., Vonrhein, C., Hartsch, T., and Ramakrishnan, V. (2000). Structure of the 30S ribosomal subunit. Nature *407*, 327-339.
Wohlgemuth, I., Brenner, S., Beringer, M., and Rodnina, M.V. (2008). Modulation of the rate of peptidyl transfer on the ribosome by the nature of substrates. J Biol Chem *283*, 32229-32235.
Wojciechowska, M., Olejniczak, M., Galka-Marciniak, P., Jazurek, M., and Krzyzosiak, W.J. (2014). RAN translation and frameshifting as translational challenges at simple repeats of human neurodegenerative disorders. Nucleic Acids Res *42*, 11849-11864.
Woolstenhulme, C.J., Parajuli, S., Healey, D.W., Valverde, D.P., Petersen, E.N., Starosta, A.L., Guydosh, N.R., Johnson, W.E., Wilson, D.N., and Buskirk, A.R. (2013). Nascent peptides that block protein synthesis in bacteria. Proc Natl Acad Sci U S A *110*, E878-887.

Wright, S.E., Rodriguez, C.M., Monroe, J., Xing, J., Krans, A., Flores, B.N., Barsur, V., Ivanova, M.I., Koutmou, K.S., Barmada, S.J.*, et al.* (2022). CGG repeats trigger translational frameshifts that generate aggregation-prone chimeric proteins. Nucleic Acids Res.
Yan, S., Wen, J.D., Bustamante, C., and Tinoco, I., Jr. (2015). Ribosome excursions during mRNA translocation mediate broad branching of frameshift pathways. Cell *160*, 870-881.
Yusupov, M.M., Yusupova, G.Z., Baucom, A., Lieberman, K., Earnest, T.N., Cate, J.H., and Noller, H.F. (2001). Crystal structure of the ribosome at 5.5 A resolution. Science *292*, 883-896.
Yusupova, G., Jenner, L., Rees, B., Moras, D., and Yusupov, M. (2006). Structural basis for messenger RNA movement on the ribosome. Nature *444*, 391-394.
Yusupova, G.Z., Yusupov, M.M., Cate, J.H., and Noller, H.F. (2001). The path of messenger RNA through the ribosome. Cell *106*, 233-241.
Zhang, H., Quintana, J., Utkur, K., Adrian, L., Hawer, H., Mayer, K., Gong, X., Castanedo, L., Schulten, A., Janina, N.*, et al.* (2022). Translational fidelity and growth of Arabidopsis require stress-sensitive diphthamide biosynthesis. Nature communications *13*, 4009.
Zhang, W., Dunkle, J.A., and Cate, J.H. (2009). Structures of the ribosome in intermediate states of ratcheting. Science *325*, 1014-1017.
Zhou, J., Lancaster, L., Donohue, J.P., and Noller, H.F. (2014). How the ribosome hands the A-site tRNA to the P site during EF-G-catalyzed translocation. Science *345*, 1188-1191.
Zhou, J., Lancaster, L., Donohue, J.P., and Noller, H.F. (2019). Spontaneous ribosomal translocation of mRNA and tRNAs into a chimeric hybrid state. Proceedings of the National Academy of Sciences of the United States of America *116*, 7813-7818.
Zimmer, M.M., Kibe, A., Rand, U., Pekarek, L., Ye, L., Buck, S., Smyth, R.P., Cicin-Sain, L., and Caliskan, N. (2021). The short isoform of the host antiviral protein ZAP acts as an inhibitor of SARS-CoV-2 programmed ribosomal frameshifting. Nat Commun *12*, 7193.

8. Acknowledgements

This project would not have been a success without the contribution of many people. I would like to cordially thank my two supervisors, Prof. Dr. Marina V. Rodnina and Dr. Sarah Adio. Marina is an incredible supervisor and mentor that trusted me with this challenging project and guided me through via technical and scientific expertise of the highest level, a deep knowledge and understanding of the science behind it, as well as a deeply critical and unbiased way of thinking that led to further improvements of the project. She has also been a great mentor that offered advice not only on the scientific part of my PhD, but also opinions on ideas, conferences and future goals. I am also deeply grateful to my co-supervisor, Dr. Sarah Adio. Sarah possesses a deep knowledge and both technical and scientific experience on the single molecule field and has always been supportive, enthusiastic and offering constructive feedback and fruitful discussions on my experiments. She has also enriched my views by offering advice on my ideas and future plans. I believe no words can describe how deeply grateful I am being surrounded by these great scientists and mentors.

A number of people, each one with their own unique expertise, contributed in various ways that were proven catalytic to the project. I thank Dr. F. Peske, Dr. B.-Z. Peng, Dr. R. Belardinelli, Dr. T. Senyushkina, Dr. N. Korniy, Dr. J. C. Thiele, Dr. N. Ranjan, Dr. E. Mercier, A. Patel, M. Zimmermann and O. Geintzer. I also thank all the current and former members of the department of Physical Biochemistry for a friendly and relaxing working atmosphere. I also thank the members of my thesis committee, Prof. Dr. Jörg Enderlein and Dr. Alex Faesen, for showing genuine interest and engaging in fruitful discussions that led to a successful project. I also thank the Coordination Office of the IMPRS Molecular Biology Program, Dr. Steffen Burkhardt and Kerstin Grüniger, who made the life of the IMPRS Molbio students in Göttingen easy and provided organizational, professional and personal support of the highest level.

I would like to thank many people for their endless care, love and support throughout this journey: my friends Konstantina, Katerina, Julio, Dionysis, Sakshi, Debojit, Anubhav, Gaurika, Jenifer, Anuruti and Ninadini; the lunch group: Gantavya, Michele, Celine, Tessa, Sandra, Namit, Vaishali, Sung-Hui and Aki; my partner, Dimitra, for supporting me and tolerating my stress and anxiety throughout my studies. Finally, I would like to thank my parents, Agatha and Costas, my brothers, Andrianos and Marios, and my late dearest grandma for their unconditional love and support. Without them, my PhD studies would not have been such a memorable experience.